UNIVERSITÉ DE STRASBOURG

ÉCOLE DOCTORALE MSII (ED N°269)

laboratoire des sciences de l'ingénieur, de l'informatique

et de l'imagerie (ICUBE)-UMR 7357

THÈSE présentée par :

Kai LI

soutenue le : **24 Févier 2015**

pour obtenir le grade de : **Docteur de l'Université de Strasbourg**

Discipline/ Spécialité : Mécanique/ Génie Civil

MODELISATION DU COMPORTEMENT HYDROMECANIQUE DES SOLS GONFLANTS BASEE SUR LA THEORIE DE L'ETAT LIMITE

THÈSE dirigée par :

M. MIGAULT Bernard	Maître de conférences (HDR), INSA de Strasbourg

RAPPORTEURS :

M. CUI YuJun	Professeur, École des Ponts ParisTech
M. DAOUADJI Ali	Maître de conférences (HDR), Université de Lorraine

---

AUTRES MEMBRES DU JURY :

Mme. MASROURI Farimah	Professeur, ENSG Nancy
M. CHAZALLON Cyrille	Professeur, INSA de Strasbourg
M. NOWAMOOZ Hossein	Maître de conférences, INSA de Strasbourg

UNIVERSITY OF STRASBOURG

Modeling the Hydromechanical Behavior of Swelling Soils Based on Shakedown Concept

by

Kai LI

A thesis submitted in partial fulfillment for the
degree of Doctor of Philosophy

in the

Doctoral School of MSII

February 2015

"I would rather be tied to the soil as a serf ... than be king of all these dead and destroyed."

Homer, Odyssey

Acknowledgements

I am deeply indebted to my thesis advisors, Assoc Prof. Bernard MIGAULT, Prof. Cyrille CHAZALLON and Assoc Prof. Hossein NOWAMOOZ, who provided immense help and encouragement. The research project was conceived by Prof. Cyrille CHAZALLON. Working with him, I enriched my scientific knowledge in general. I am also very grateful to Assoc Prof. Hossein NOWAMOOZ for his critical comments. I learned a lot from him when discussing the unsaturated soil behavior.

I would like to thank my colleagues in the Group of Civil Engineering and Energy at INSA Strasbourg, Assoc Prof. Saida MOUHOUBI and Assoc Prof. Georg KOVAL for their care and hospitality. Special thanks to my fellow Ph.D students, Ba Danh LE, Ioana Maria ARSENIE, Xuan Nam HO, Quoc Tuan TRINH, Andrea THEMLI, Xiao Feng GAO, Peng JING, Lauba SAGNOL for all the great moments we had.

I also give my gratitude to China Scholarship Council (CSC) who provided me with a full scholarship during three and a half years that guaranteed a smooth completeness of my thesis.

Last but not least, I am grateful to my parents, without their love, care and continuous support, this thesis would never be finished.

Contents

List of Figures

List of Tables

Dedicated to my parents

Chapter 1

Introduction

1.1 General

Unsaturated expansive soils contain clay minerals such as smectite with high capacity of water absorption. As the clay minerals absorb water, they expand; conversely, as they lose water, they shrink. The structures constructed on expansive soils are often subjected to severe distress subsequent to construction, as a result of the differential settlements in the soil. These differential settlements can be caused by the variations of climate, the change of the water table, water uptake by vegetation, removal of vegetation or the excessive watering of a lawn.

Damage to the structures caused by expansive soils has been recorded in many countries. In the United States, costs associated with the damage to all types of structures built on expansive soils are estimated to be near $2.3 billion per year. This amount is greater than the combined damage from natural disasters such as floods, hurricanes, earthquakes, and tornadoes. Although expansive soils do not cause loss of life, the economical loss in the United States makes it the most costly natural hazard. About 60 percent of all houses in the United States suffer minor damage from expansive soils and about 10 percent experience significant damage, some beyond repair. In France, Ministère de l'Ecologie, de l'Energie, du Développement Durable et de la Mer (MEEDDM), estimated that the averaged repair cost for individual residence due to expansive soil hazard, is up to 15,000 Euros. Although this cost is variable depending on the damage condition, still a huge spending to deal with soil disasters.

A world wide interest in research on expansive soils in the last four decades has resulted in great progress for the prediction of soil behavior. This prediction of soil behavior are based either on one-dimensional oedometer test results or on direct in-situ measurements[1]. Although several analytical models for the prediction of soil behavior have been already developed, there has been little development of simple or direct method to simulate the complicated response of expansive soils.

Difficulties in modeling hydromechanical behavior of unsaturated expansive soils present several issues. These issues include the characterization of the soil properties that are required for two- or three-dimensional problems and a succinct model with less model parameters that can model complicated hydromechanical behavior of expansive soils. The geotechnical community is still waiting for satisfactory analytical tools to address the expansive soil problems.

1.2 Objectives and scope

The main purpose of this study is to model the hydromechanical behavior of unsaturated expansive soils based on shakedown theory, to provide a reliable prediction of deformations associated with wetting and drying cycles. The following objectives are included in this study:

1. To develop an analytical model for the hydromechanical behavior of expansive soils under wetting and drying cycles based on shakedown theory.

2. To calibrate and validate the proposed shakedown-based model using the results of the cyclic suction-controlled tests on the different initial states of an expansive soil.

3. To propose a finite element framework based on the analytical shakedown model for expansive soils subjected to wetting and drying cycles.

4. To propose a modified shakedown method for heavily dense expansive soils taking into account the mixed hardening plasticity.

This study considers the prediction of deformations and displacements due to changes in matric suction and the applied load. The effects of temperature, osmotic suction changes in the soils are not considered.

1.3 Outline of thesis

This thesis is organized into five chapters as well as a short summary of conclusions and perspectives:

Chapter 1, "Introduction" presents the objectives and scope of this study and the outline of the thesis.

Chapter 2, "Literature review: unsaturated expansive soils", contains four parts. The first part introduces the basic definitions and general agreements in unsaturated soil mechanics. The second part summarizes the nature of expansive soils, factors affecting swelling, damages to structures and the control of the swell-shrink behavior. The third part reviews the typical experimental results on hydromechanical behavior of expansive soils to better understand the soil behavior. In the end, the fourth part examines several representative models of expansive soils, presenting current understandings on expansive soils.

Chapter 3, "Analytical modeling of expansive soils with shakedown concept", first presents shakedown theory and develops an approach based on this theory to model unsaturated expansive soils subjected to wetting and drying cycles under different net mean stresses. The required parameters of the proposed model are calibrated by the oedometer test results carried out on the initially loose and dense samples. Subsequently, the model is validated for the initially intermediate samples by comparing model predictions with experimental results. Meanwhile, a coupling model between suction cycles and mechanical behavior is proposed and the validation for this coupled model is also performed by showing the comparisons

of the model predictions with test results. In the end, the sensitivity analysis of model parameters is carried out to study the influence of model parameters on model response.

Chapter 4, "Finite element modeling of in-situ behavior of expansive soils" presents the finite element framework for an elasto-plastic structure subjected to wetting and drying cycles between extremely dry and wet conditions. The developed model is implemented in a finite element code (CAST3M) and three two-dimensional examples are simulated to study the in-situ behavior of expansive soils at different initial states under a variable vertical stress. To study the influence of the vertical stress, a series of vertical pressures are applied to the studied model in these simulations.

Chapter 5, "Application of shakedown theory to heavily dense expansive soils" contains a modification of classical shakedown theory developed by Zarka for steel structures, with a mixed hardening plasticity including kinematic hardening and isotropic hardening. Then, this modified method is used to model heavily dense expansive soils subjected to wetting and drying cycles. In the end, the modified model is calibrated by comparing the model estimations with the test results.

An additional chapter, "Conclusions and perspectives", contains a summary of the findings of this study and proposes several recommendations related to the shakedown analysis and the potential future studies.

Four Appendices are included to provide supplementary information to the thesis. Appendix A presents the suction-controlled oedometer device used for the cyclic suction tests on expansive soils under a constant vertical stress. Appendix B illustrates the loading programs of oedometer tests on compacted loose, intermediate and dense samples. Appendix C presents the loading programs of oedometer tests performed on heavily dense samples at different vertical stresses. Appendix D presents the calibration results of shakedown model on a mixture of bentonite and sand.

Chapter 2

Literature Review: Unsaturated Expansive Soils

2.1 Introduction

There are three conditions to be respected for developing an elasto-plastic constitutive model on unsaturated expansive soils. Firstly, an understanding of basic definitions and general agreements in unsaturated soil mechanics is required. Secondly, some classic experiments are needed to understand the hydromechanical behavior of unsaturated expansive soils. Thirdly, the typical models developed for expansive soils should be reviewed, representing the current understanding on unsaturated expansive soils. Therefore, a literature review based on these points is presented in this chapter.

2.2 Unsaturated non-expansive soils

Unsaturated non-expansive soil produces small expansion during wetting, relative to unsaturated expansive soil. It is multi-phase materials, containing soil particles, water and air. The presence of pore-air differs soil behavior significantly with the principles and concepts of classical saturated soil mechanics. Consequently, the previously developed theories are not applicable anymore for unsaturated soil mechanics. In the following section, the definition of suction, the consensus on stress state variables, the proposition of shear strength theory as well as the soil water retention curves in unsaturated soil mechanics are reviewed.

2.2.1 Surface tension and suction

To illustrate the effects of the pore-air on soil behaviour, Figure 2.1(a) shows the idealised soil structure and a section of an interface between pore air and pore water. The molecule in the interior of water experiences equal forces in all directions, which means there is no unbalanced force. The water molecule within the air-water interface experiences an unbalanced force towards the interior of the water. For the equilibrium of air-water interface, a tensile pull is generated along the air-water interface. The property of the air-water interface that allows it to exert a tensile pull, called surface tension that causes the air-water interface to behave like an elastic membrane. This membrane can be subjected to different pressures on each side. Therefore, it shows a concave curvature towards the larger pressure and exerts a tension in the membrane in order to be in equilibrium. As illustrated in Figure 2.1(b), the pressure difference across the curved surface Δu can be related to the surface tension T_s and the curvature of the surface R_s as:

$$\Delta u = \frac{T_s}{R_s} \tag{2.1}$$

Equation 2.1 gives the pressure difference across a two-dimensional curved surface with a radius R_s and a surface tension T_s. For a warped or saddle-shaped surface (i.e. three-dimensional membrane), equation 2.1 can be extended by:

$$\Delta u = T_s \left(\frac{1}{R_1} + \frac{1}{R_2} \right) \tag{2.2}$$

where, R_1 and R_2 are radii of curvature of a warped membrane in two orthogonal principal planes.

If the radius of curvature is the same in all directions (i.e. R_1 and R_2 are equal to R_s), equation 2.2 becomes:

$$\Delta u = \frac{2T_s}{R_s} \tag{2.3}$$

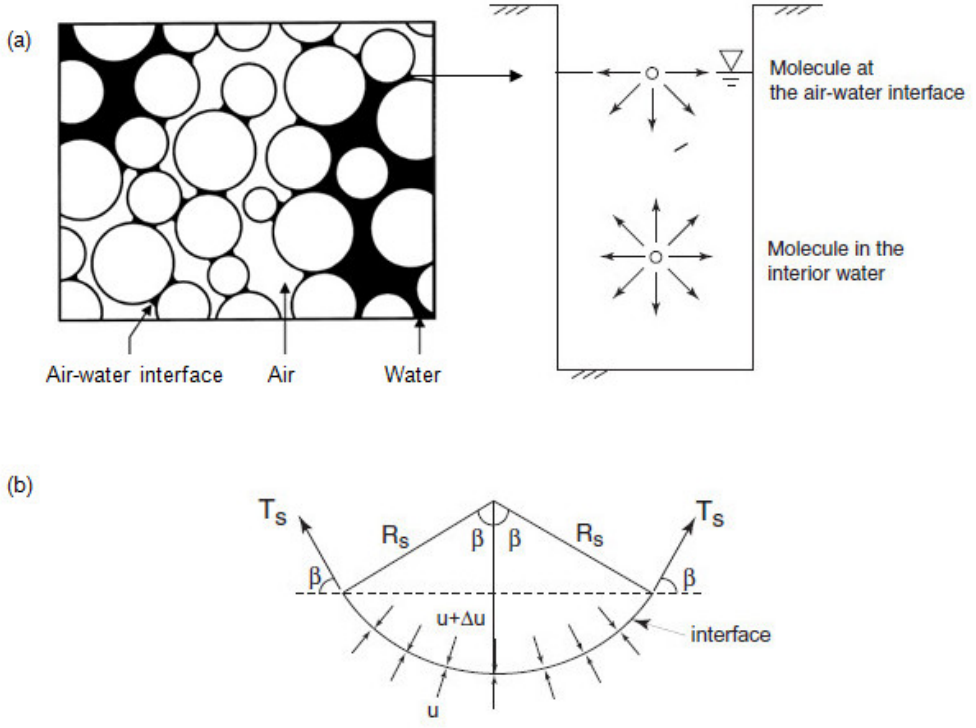

FIGURE 2.1: Surface tension at the air-water interface: (a) intermolecular forces on the interface; (b) pressures and surface tension on a curved interface[1].

In an unsaturated soil, the air-water interface would be subjected to an air pressure u_a, greater than the water pressure u_w. The pressure difference $(u_a - u_w)$, is referred to as matric suction, s. Substitution of $\Delta u = u_a - u_w$ in equation 2.3 gives so-called Kelvin's capillary equation[1]:

$$u_a - u_w = \frac{2T_s}{R_s} \tag{2.4}$$

The above equation suggests that:

- a decrease in the radius of curvature implies an increase of suction. This case corresponds to the drying of soil where water retreats to the smaller and even smaller pores;

- an increase of the radius of curvature suggests a decrease of suction. This case corresponds to the wetting of soil where water invades large pores.

As a matter of fact, the surface tension is dependent on the temperature and the chemical composition of the water. The variation in water chemistry introduces another suction component, known as the osmotic suction. Throughout this thesis the term suction is used to indicate the matric suction only, neglecting any effect of temperature and osmotic suction on the soil behaviour.

2.2.2 Stresses state variables

Fredlund and Morgenstern[2] presented a theoretical stress analysis of an unsaturated soil on the basis of multi-phase continuum mechanics. The soil particles were assumed to be incompressible and the soil was treated as though it were chemically inert. These assumptions are consistent with those used in saturated soil mechanics.

The analysis concluded that any two of three possible normal stress variable $(\sigma - u_a)$, $(\sigma - u_w)$ and $(u_a - u_w)$ would be sufficient to describe the stress state of an unsaturated soil. The first two of these stress state variables $(\sigma - u_a)$ and $(\sigma - u_w)$ are tensor quantities, while the third stress state variable $(u_a - u_w)$ is a scalar quantity. It is therefore sensible to select either $(\sigma - u_a)$ and $(u_a - u_w)$ or $(\sigma - u_w)$ and $(u_a - u_w)$ as the appropriate stress state variables, because the use of two tensor variables $(\sigma - u_a)$ and $(\sigma - u_w)$ would lead to unnecessary complexity and redundant information. The combination of net stress $(\sigma - u_a)$ and matrix suction $(u_a - u_w)$ is usually selected, because u_a is commonly zero, relative to atmospheric pressure. In addition, the pore water pressure in an unsaturated soil is generally negative, which is often difficult to measure accurately. This means that an element of uncertainty will be involved in only one stress state variable if $(\sigma - u_a)$ and $(u_a - u_w)$ are selected, whereas the uncertainty will affect both variables if $(\sigma - u_w)$ and $(u_a - u_w)$ are adopted.

When two independent stress state variables $(\sigma - u_a)$ and $(u_a - u_w)$, are selected to describe the behaviour of unsaturated soils, the mean value of net stress p, the deviator value of net stress q and matrix suction s are defined for the special conditions of the triaxial test $(\sigma_2 = \sigma_3)$ by:

$$p = \frac{1}{3}[(\sigma_1 - u_a) + 2(\sigma_3 - u_a)] = \frac{1}{3}(\sigma_1 + 2\sigma_3) - u_a \tag{2.5}$$

$$q = (\sigma_1 - u_a) - (\sigma_3 - u_a) = \sigma_1 - \sigma_3 \tag{2.6}$$

$$s = u_a - u_w \tag{2.7}$$

where, σ_1 and σ_3 are the axial total stress and the radial total stress, respectively.

2.2.3 Shear strength theory

The shear strength of an unsaturated soil proposed by Fredlund *et al.*[3], can be formulated in terms of two independent stress variables $(\sigma - u_a)$ and $(u_a - u_w)$ and it is expressed as:

$$\tau_{ff} = c' + (\sigma_f - u_a)_f \cdot tan\phi' + (u_a - u_w)_f \cdot tan\phi^b \tag{2.8}$$

where τ_{ff} is the shear stress on the failure plane at failure, c' is the intercept of the extended Mohr-Coulomb failure envelope on the shear stress axis where the net normal stress and the matric suction at failure are equal to zero—it is also referred to as effective cohesion, $(\sigma_f - u_a)_f$ is the net normal stress on the failure plane at failure, ϕ' is the angle of internal friction associated with the net normal stress state variable $(\sigma_f - u_a)_f$, $(u_a - u_w)_f$ is the matric suction on the failure plane at failure, and ϕ^b is the angle indicating the rate of increase in shear strength relative to the matric suction $(u_a - u_w)_f$.

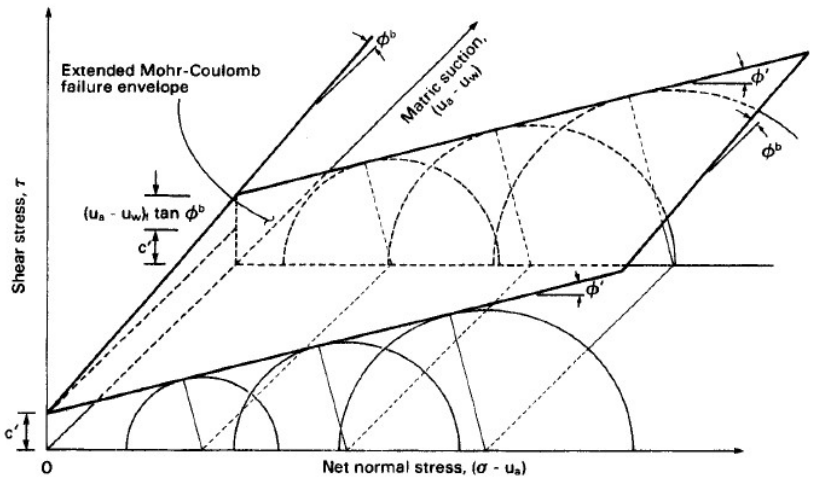

FIGURE 2.2: Extended Mohr-Coulomb failure envelope for unsaturated soils [3].

Figure 2.2 shows an extended Mohr-Coulomb failure envelope for unsaturated soils. The shear strength envelope for unsaturated soils was originally proposed as a planar surface in nature based on a limited set of data available in the literature[3]. Later experimental evidence by several investigators established that the shear strength for unsaturated soils is nonlinear when tested over a large range of suction[4, 5]. The Fredlund *et al.*[3] equation is valid for interpreting data for both linear and nonlinear shear strength envelopes.

2.2.4 Soil water retention curve

A Soil Water Retention Curve (SWRC) describes the amount of water retained in a soil (expressed as water content or degree of saturation) under equilibrium at a given matric potential. The SWRC is an important property of unsaturated soils, related to size and connectedness of pore spaces, strongly affected by soil texture, structure and other constituents including organic matter. Modeling unsaturated soils requires the knowledge of SWRC, therefore it plays a critical role in prediction of the hydromechanical behavior of the soil.

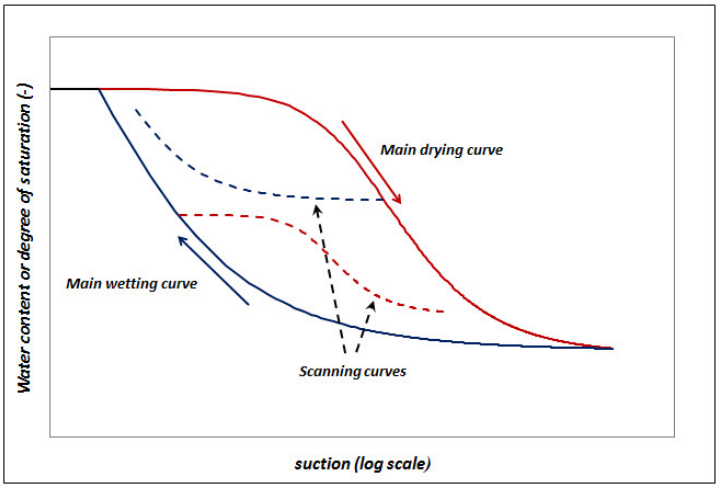

FIGURE 2.3: Idealized soil water retention curve including main, scanning wetting and drying cycles.

Figure 2.3 illustrates the idealized soil water retention curve including main, scanning wetting and drying curves, where the hydraulic hysteresis gives rise to different degrees of saturation in the wetting and drying paths at a given value of suction. The main wetting and drying curves shown in this figure correspond to

wetting from a very dry state and drying from a fully saturated condition respectively. When wetting or drying commences from any other point and follows a previous drying or wetting stage, the new wetting and drying curves lie within the region enclosed by the bounding main wetting and drying curves. Childs[6] termed these new wetting and drying curves as scanning curves. In cycles of wetting and drying performed over a constant range of suction, the response of the soil will gradually approach a stable closed hysteresis loop in the suction - water content (or degree of saturation) plane[7].

The reason for hydraulic hysteresis presented in Figure 2.3 is explained by emptying and flooding of a void with water. During a drying path, the void is about to empty of water that the menisci are at the narrow entry points to the void. This means the radius of curvature R_d is small and therefore according to Equation 2.4, the corresponding suction will be high. In subsequent wetting, the same void is about to be flooded with water. Two sections of menisci will coalesce at locations well inside the narrowest entry points. This means the radius of curvature R_w is greater than the radius R_d and hence the suction is correspondingly lower during wetting than drying. Differences in the contact angles during the wetting and drying processes also contributes to the hydraulic hysteresis[8]. Fredlund and Rahardjo[1] suggested that the entrapped air in the soil might also cause hysteresis.

Considerable empirical equations have been proposed for the soil water retention curve[9–13]. However, it is important to note that the main focus of research pertaining to the soil water retention curve has only been for modeling the inflow or outflow of water to or from unsaturated soils, rather than the mechanical behavior and it is generally assumed that the applied net stresses are negligible and the soil is incompressible. Clearly these assumptions are not appropriate within geotechnical engineering. Although some progress in the empirical equations has been made, the effect of hydraulic hysteresis are not incorporated into generally used constitutive models, mainly to avoid complexity in the models.

2.3 Unsaturated expansive soils

Expansive (or swelling) soils are the soils that experience large volume changes when moisture changes. They swell on wetting and shrink on drying, respectively[14, 15]. These soils are commonly in literature referred to as active clays, swelling clays or volumetrically active soils[16, 17]. In this study, they are called expansive soils.

The high degree of swelling is mainly due to its mineralogical composition. In these soils, important physico-chemical interactions occur in the vicinity of active clays. Proper understanding of these interactions is necessary to explain some of the observed features of soil behavior. Therefore, some fundamental aspects of expansive soils in terms of physico-chemical interactions are firstly reviewed. Then factors affecting the behavior of expansive soils and the different damage forms of the structure are mentioned. To control the cyclic swell-shrink behavior and better use these soils in geotechnical engineering, method of treatment are finally presented in this section.

2.3.1 Nature of expansive soils

The swelling and shrinking phenomena of expansive soils are caused by the presence of clay minerals that have very large specific surface areas, and hence high water absorption capacities. Clay minerals are complex silicates of aluminium, magnesium and iron. The two basic crystalline units, which form the clay minerals are 1) a silicon-oxygen tetrahedral, and 2) an aluminium or magnesium octahedron. The clay minerals are plate-like and very small, being measured in Angstrom (Å) units. However, they have very high specific surface areas. For instance, montmorillonite, an expansive clay mineral, has a specific surface area up to 822 m^2g^{-1}, compared with 1×10^{-2} and 1×10^{-1} m^2g^{-1} for coarse and fine sands, respectively.

Fookes and Parry[18] demonstrated that the volume change depends on the clay particle size and the thickness of the absorbed water. In their study, they noted that the ratio between the absorbed water and the particle thickness was 40 for montmorillonite compared to 0.8 for kaolinite. This indicated a theoretical potential volume change for montmorillonite of about 50 times that of kaolinite from completely dry to fully saturated.

Because the structure of the different clay minerals is complex, the schematic representations have been adopted to simplify the complex structures[19]. Figure 2.4 illustrates the symbolic structures of typical clay minerals. In this figure, it is obvious to observe that the specific surface area of montmorillonite is larger than that of kaolinite, able to absorb more water to increase the volume of soils.

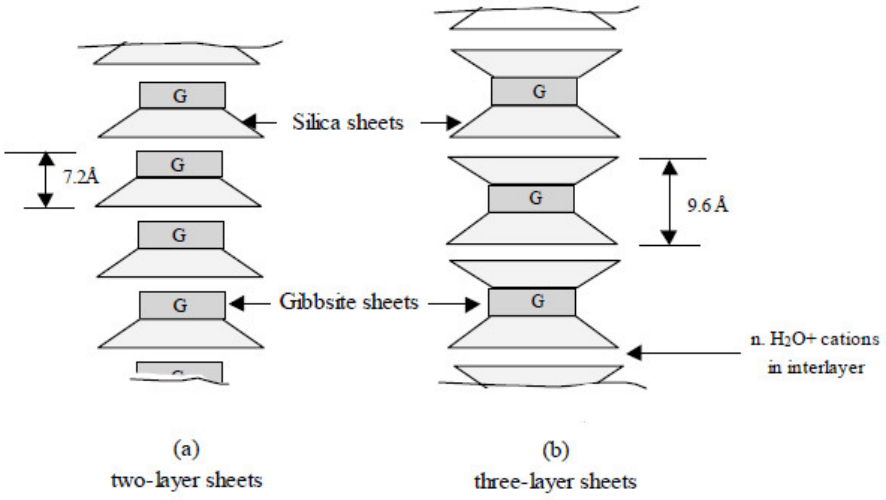

FIGURE 2.4: Symbolic structure of (a) kaolinite and (b) montmorillonite clay minerals[19].

On the other hand, there exists three-layer sheets in montmorillonite clay minerals. These elementary sheets stack together to make particles (platelets or crystals). The particle assemblages are integrated by arrays of elementary particle configurations and they are described as matrices (see Figure 2.5a) or elementary particle arrangements join together to make aggregates resulting in a three-dimensional structure of a granular type (see Figure 2.5b). Figure 2.5 illustrates the sketch of micro-fabric types for expansive soils, made up of montmorillonite clays. In both types of macro-fabric there is a further level of void space, the intra-element pores that separating the clay platelets in the elementary particle arrangements and both micro-fabrics can result in highly volume expansions when wetting the expansive clays[17, 20].

Considering two levels of structure, Gens and Alonso[17] and Alonso *et al.*[21] developed a mechanical model for expansive clays, which combined an existing model for unsaturated soils by linking the macro plasticity with a simple reversible microstructural behavior, using a coupling function. This method is widely employed to model the mechanical behavior of expansive soils and it will be expanded in Section 2.5.1. Many other studies have also been reported concerning the same subject[22–24], but the question of whether or not micro-structural deformations are reversible have not yet been fully addressed.

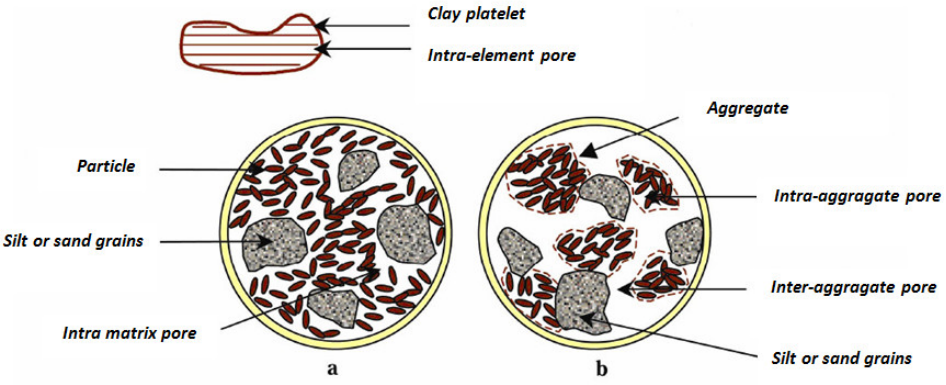

FIGURE 2.5: Fabric types: a) clay matrix predominantly constituted by elementary particle arrangements of clay platelets; b) microfabric of a clay predominantly made up of aggregates of elementary particle arrangements [17].

2.3.2 Factors affecting swelling

Swelling potential refers to the amount of volume increase due to wetting that is possible in a clay body in its natural environment. It is influenced by many factors, some of which have been studied by several authors[16, 25–28]. In this section, the main factors affecting the swelling of clay are summarized as follows:

(1) Soil properties

• Clay Mineralogy: Clay minerals which typically cause soil volume changes are montmorillonites, vermiculates, and some mixed layer minerals. Illites and kaolinites are frequently inexpansive, but can cause volume changes when particle sizes are extremely fine[14–16, 19].

• Soil Water Chemistry: Swelling is repressed by increased cation concentration and increased cation valence. For example, Mg^{2+} cations in the soil water would result in less swelling than Na^{+} cations, because higher valence decreases the thickness of particle layer[29, 30].

• Soil Suction: Soil suction is an independent variable, represented by the negative pore pressure in unsaturated soils. Soil suction is related to saturation, gravity, pore size and shape, surface tension, electrical and chemical characteristics of the soil particles and water [27, 28, 31].

• Plasticity: In general, soils that exhibit plastic behavior over wide ranges of moisture content and have greater potential for swelling and shrinkage. Plasticity is an indicator of swelling potential[28, 32, 33].

• Soil Structure and Fabric: Flocculated clays tend to be more expansive than dispersed clays, and cemented particles reduce swelling. Fabric and structure are altered by compaction at high water content or remolding. Kneading compaction has been shown to create dispersed structures with lower swelling potential than soils statically compacted at lower water contents[27, 34].

• Dry Density: Higher densities usually indicate closer particle spacing, which means greater repulsive forces between particles and larger swelling potential[35].

(2) Environmental variations

• Initial Moisture Content: A desiccated expansive soil will have high affinity for water, which means higher suction, greater potential of swelling. Conversely, a wet soil profile will loose water more readily on exposure to drying influences and shrink more than a relatively dry initial profile. The initial soil suction must be considered in conjunction with the expected range of final suction conditions[27, 28, 31, 36, 37].

• Moisture Variations: Changes in moisture in the active zone near the upper part of the profile primarily define heave. It is in those layers that the widest variation in moisture and volume change will occur[27, 28, 31, 36, 37].

• Climate: Amount and variation of precipitation and evapotranspiration greatly influence the moisture availability and depth of seasonal moisture fluctuation. Greatest seasonal heave occurs in semiarid climates that have short wet periods[27, 28, 31, 36, 37].

• Groundwater: Shallow water tables provide source of moisture and fluctuating water tables contribute to moisture[27, 28, 31, 36, 37].

• Drainage: Surface drainage features, such as ponding around a poorly graded house foundation, provide sources of water at the surface; leaky plumbing can give the soil access to water at greater depth[27, 28, 31, 36, 37].

• Vegetation: Trees, shrubs, and grasses deplete moisture from the soil through transpiration, and cause the soil to be differentially wetted in areas of varying vegetation[38, 39].

• Permeability: Soils with higher permeability, particularly due to fissures and cracks in the field soil mass, allow faster migration of water and promote faster rates of swelling[27, 28].

• Temperature: Increasing temperatures, thermal expansion of soil constituents and mechanical weakening of the contacts between soil aggregates are observed. Nevertheless, it can be concluded that temperature effect on mechanical behavior of swelling soil is small.[40, 41].

(3) Stress conditions

• Stress History: An overconsolidated soil is more expansive than the same soil at the same void ratio, but normally consolidated. Swell pressures (the amount of external stress required to prevent change in volume of soil during wetting) can increase on aging of compacted clays, but the amount of swelling under light loading has been shown to be unaffected by aging. Repeated wetting and drying tend to reduce swelling in laboratory samples, but after a certain number of wetting-drying cycles, swelling is unaffected[7, 21, 42].

• In-situ Conditions: The initial stress state in a soil must be estimated in order to evaluate the possible consequences of loading the soil mass and/or altering the moisture environment therein. The initial effective stresses can be roughly determined through sampling and testing in a laboratory, or by making in-situ measurements and observations[27, 28].

• Loading: Magnitude of surcharge load determines the amount of volume change that will occur for a given moisture content and density. An externally applied load acts to balance inter-particle repulsive forces and reduces swelling[7, 21, 42].

• Soil Profile: The thickness and location of potentially expansive layers in the profile considerably influence potential movements. Greatest movement will occur in profiles that have expansive clays extending from the surface to depths below the active zone. Less movement will occur if expansive soil is overlain by non-expansive material or overlies bedrock at shallow depth[26].

2.3.3 Damage to structures from expansive soils

All structures experience various levels of damages during their lifetime. These damages of the structure may originate from inadequate design, cheap construction materials, poor workmanship, climatic condition or multiple of these factors. For example, the structures especially those made of concrete, a certain degree of cracking is inevitable. Apart from aforementioned damages, the presence of expansive soil at the construction site also can cause significant damage.

The general way that expansive soils damage structures is by differential heave as they swell with moisture increases. The most obvious identifications of these damages of buildings are doors and windows that get jammed, uneven floors, or cracks in masonry walls and ceilings. Moreover, different crack patterns mean different causes for different construction materials.

In most cases, cracks due to swell-shrink behavior of expansive soils usually run from corner towards adjacent opening and are uniform in width or v-shape, wider at the top than the foundation wall[43]. This pattern of cracks happens when the moisture movement is from the perimeter to the centre of the house. Figure 2.6 shows the typical crack pattern on a building due to centre heaving of expansive soils.

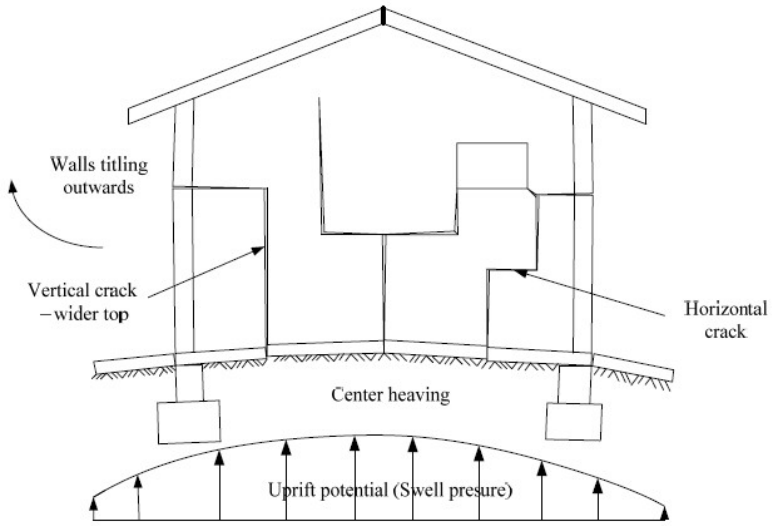

FIGURE 2.6: Typical crack pattern on a building due to centre heave[43].

On the contrary, the cracks are wider in some cases at the bottom than the top due to the dishing of the structure centre. This happens when the moisture moves from centre to the perimeter resulting into the "saucer effect"[43]. In the case of "saucer effect", the cracks are wider bottom than top because of the inwards tilt (see Figure 2.7).

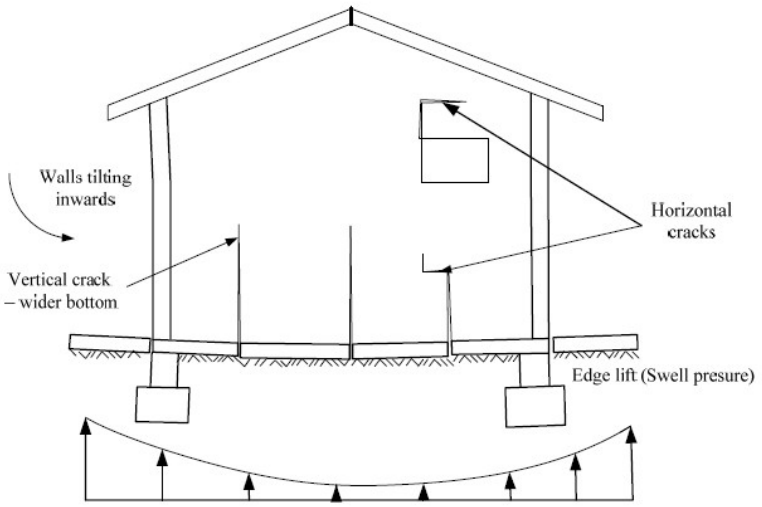

FIGURE 2.7: Typical crack pattern on a building due to centre dishing[43].

2.3.4 Methods of treatment

Based on the economics and practicality of the operation, there are a number of methods which can be used to minimize heave in expansive soils. These methods may include replacement, compaction, ponding, moisture barriers and chemical stabilization. Any of these techniques may be applicable depending on the soil conditions, material, type of construction and accessibility of equipment at the construction site. The success of any stabilization method depends upon the consideration of all conditions and an understanding of application and limits of that particular method. The general treatment methods in engineering, excerpted from the work of Ahmad[44] and Lucian[45] are summarised below:

• Replacement: This process involves replacing the original top expansive soil with compacted non-expansive backfill to a depth below which the seasonal moisture content will tend to remain constant. The idea behind is to capitalize on constant specific volume maintained by non-expansive soil when the water contents change. However, soil replacement is only economical for reasonable thickness of the expansive soil. Thus, if the expansive stratum extends to a great depth to remove, then other treatments should be economically sought.

• Compaction: One of the most practical and economical methods of controlling heave of swelling soils is compaction. Compaction is used in conjunction with replacement or alone to control expansive and shrinkage of near-surface soils. In general, compactive effort should be bounded in order to limit the suction but should be high enough to maintain adequate bearing pressures that develop in

compacted soils. Compacted soils can be placed above moderately expansive clays to serve as a surcharge which will reduce expansion in near-surface soils. Floor slabs, and in some cases, lightly loaded interior footings can then be placed in the fill. Gromko[16] recommended compaction at 2-5% above optimum moisture content.

• Ponding: Covering a construction site with water prior to construction is known as ponding or prewetting. The purpose of ponding is to allow desiccated foundation soils to swell prior to placement of structure. This method has been successful in a few cases. However, wetting the subsoil of foundation by ponding may require many months or even years to increase the water content to the required depths unless the clay contains a fissure system to aid water percolation through the soil. After prewetting, 4% or more of hydrated lime is often mixed with the top layer of clay to reduce its plasticity and make it more workable. As an alternative, the application of a 10-15 cm thick layer of coarse gravel, sand or granular soil on top of the area will aid considerably in providing a good working surface during and after prewetting. This layer has advantages in reducing evaporation, providing a minor surcharge, as well as making a level uniform subgrade.

• Moisture barriers: Moisture barriers may be constructed around the perimeters of slabs-on-grade to minimize moisture variations beneath the slab's perimeter. The field studies showed that movements on similar foundation without barriers were somewhat higher but were far variable around the perimeter.

• Chemical stabilization: Chemical stabilization can improve the properties of expansive soils considerably. Possible materials for the stabilization could include lime, pozzolana, lime-pozzolana mixture, cement, resins of fly ash. The choice of a material or a combination of materials depends on the size and importance of the building (risk/damage acceptable) and economic consideration of the client. However, the need to strike a proper balance between quality and cost should not be overlooked.

2.4 Hydromechanical behavior of expansive soils

The volume change behavior of unsaturated expansive soils, due to the variations of mechanical loadings and suction, has been studied during last four decades. These experimental data treat different aspects: stiffness of expansive soil, shear strength, cyclic swell-shrinkage behavior as well as influence of suction cycles on

soil mechanical behavior. The most important observations of such studies will be illustrated in the following sections.

2.4.1 Compression test under constant suction

Loading-unloading behavior under constant suction is typically studied in one-dimensional compression tests (oedometer condition) or by using suction-controlled triaxial tests. A sketch of stress path is added to Figure 2.8, which presents a typical result of isotropic loading-unloading under constant suction on an expansive soil (80% bentonite and 20% sand). It shows that the elasto-plastic behavior of an expansive soil resembles very much that of a fully saturated soil. The similarity appears in the reversible elastic behavior during unloading-reloading and the existence of a yield point, where the soil shows a sudden reduction in stiffness with irreversible plastic deformations.

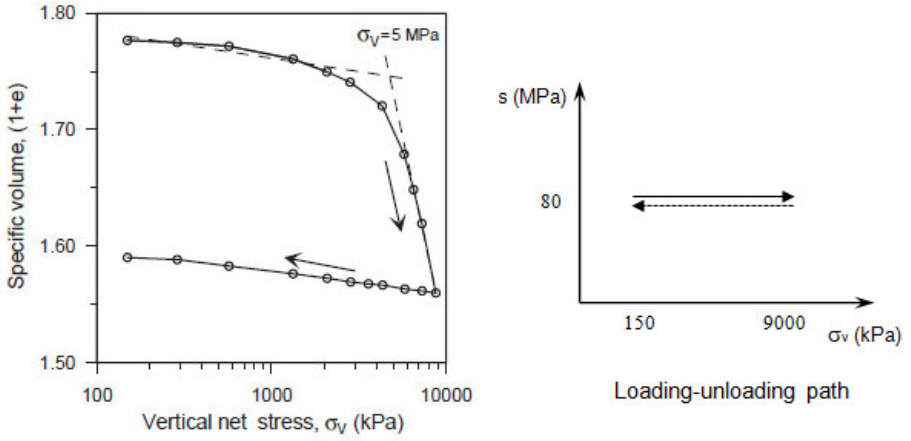

FIGURE 2.8: Loading-unloading test at constant suction[46].

Cuisinier and Masrouri[47] performed isotropic loading tests at the different suction values on an artificially prepared mixture of bentonite and silt. The results are shown in Figure 2.9. According to these results, suction affects both the yield stress and post yielding stiffness. Similar observations have reported by Wheeler and Sivakumar[48].

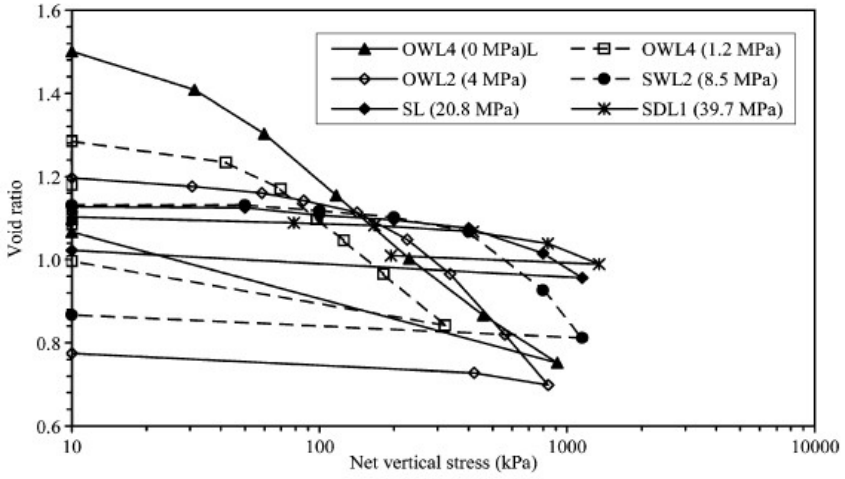

FIGURE 2.9: Isotropic loading-unloading test under different constant suctions[47].

It is widely accepted that suction variation has little influence on soil stiffness in the elastic range. This indicates that the unloading-reloading index can be considered as suction independent[46, 48]. For primary loading there are many discussions about suction effects on plastic compression index. The majority of researchers have observed that plastic compression index decreases with increasing suction, which means increasing stiffness with suction increase[49–51]. However, the contradictory conclusions that plastic compression index increases with suction increase were given by Futai *et al.*[52]. Besides, Kogho *et al.*[53] proposed the empirical expressions for the plastic compression index varying with suctions of different soils.

2.4.2 Shear test under constant suction

Experimental techniques to measure the strength of unsaturated soil are suction-controlled direct shear tests or suction-controlled triaxial shear tests. Figure 2.10 contains typical results of a direct shear test on natural expansive specimens reported by Zhan *et al.*[54]. It shows that unsaturated shear strength increases with suction. The same observations have also been reported by other researchers[1, 55].

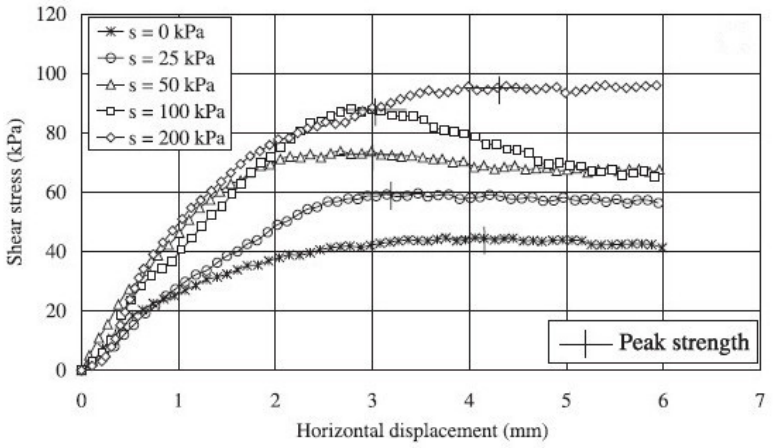

FIGURE 2.10: Direct shear tests on unsaturated natural specimens[54].

To study the effect of suction on shear strength, Zhan *et al.*[54] have performed a series of tests to measure the shear strength of different expansive soils (see Figure 2.11). The effect of suction on shear strength is explained by the authors via two different mechanisms, the capillary force of the interparticle and the suction for the soil dilatancy.

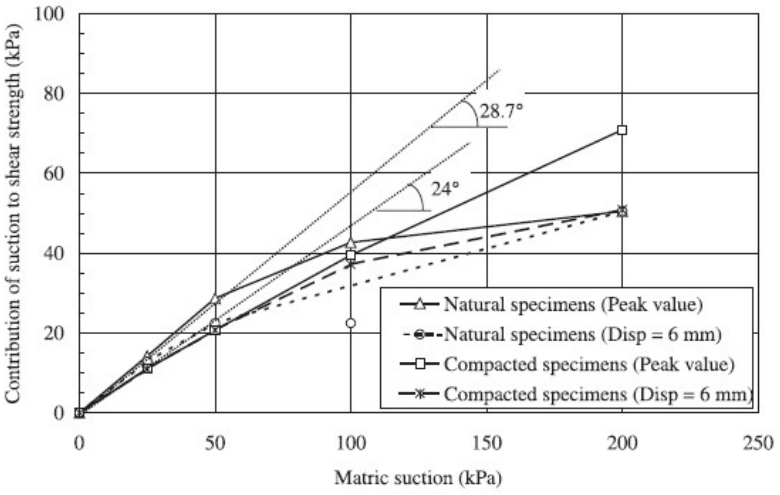

FIGURE 2.11: Contribution of suction to shear strength for natural and compacted specimens[54].

The majority of experimental results show that suction has little influence on the friction angle, as it is clear in Figure 2.12. However, suction causes a significant increase in soil cohesion and consequently improves the shear strength. A series of unsaturated triaxial shear tests conducted by Ye *et al.*[56] on weakly expansive soils

have confirmed the same observations as other authors. The unsaturated shear strength increases linearly with suction and the friction angle is almost constant with suction, equal to 17.6°.

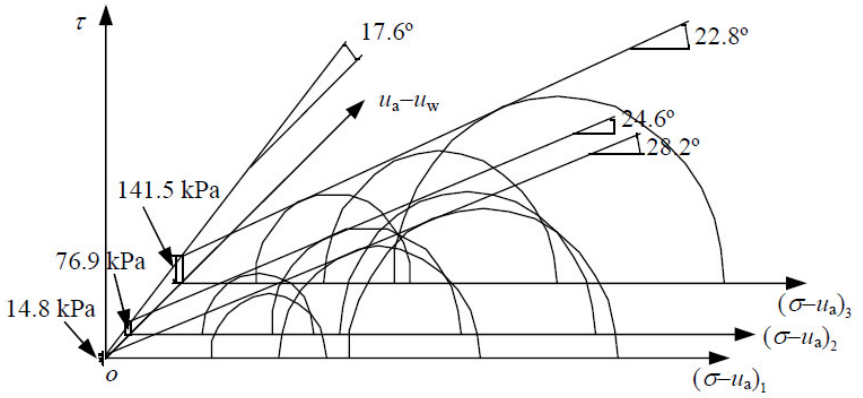

FIGURE 2.12: Mohr-Coulomb's failure envelopes of the weakly expansive soil[56].

2.4.3 Cyclic swell-shrink behavior

Many cyclic suction-controlled oedometer tests on unsaturated expansive soils have been performed to study their hydromechancial behavior[35, 46, 57–64]. All these tests suggest that after the swelling and shrinkage strain accumulations during the wetting and drying cycles under constant vertical stresses, an equilibrium state is reached where the soil behavior is reversible.

Pousada[58] performed cyclic suction-controlled oedometer tests on a compacted expansive clay from Madrid, Spain under different vertical applied stresses. The variation of volumetric strain with suction at the vertical stress of 0.1 MPa is shown in Figure 2.13a. In the first cycle, irreversible vertical compression strain develops during the drying stage and additional irreversible swelling strain during the wetting stage. As the cycles go on, the strain accumulation reduces. At the end of the tests, a net swelling strain of 1.3% was measured. On the other hand, Dif and Bluemel[59] presented results on Hoheneggelsen clay in which a global shrinkage of the material is observed when the sample is successively soaked and air-dried under a vertical stress of 200 kPa. The evolution of the axial deformation measured during the tests and the schematic associated strain-suction path are depicted in Figure 2.13b. These results also show a convergence towards the

reversible equilibrium state at the end of several suction cycles.

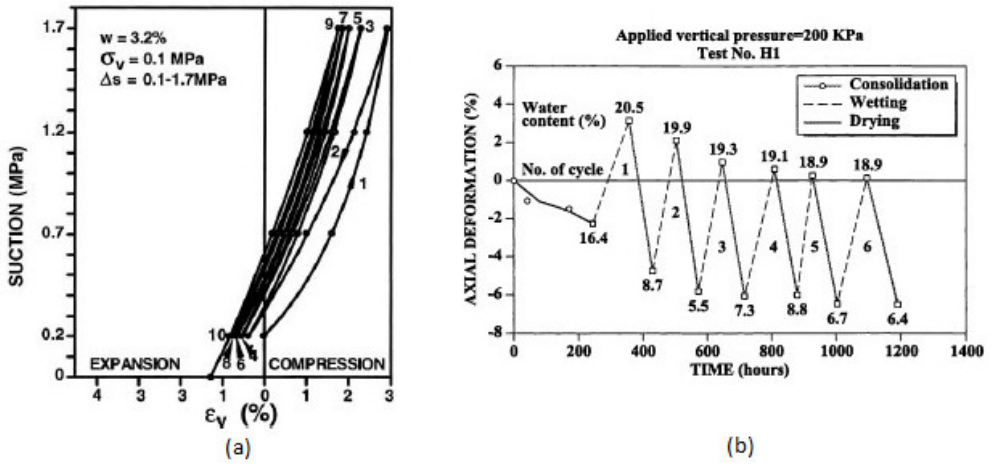

FIGURE 2.13: Strain accumulation during suction cycles: (a) Poudada *et al.*[58]; (b) Dif *et al.*[59].

Alonso *et al.*[46] studied the mechanical behavior of a bentonite/sand mixture during wetting and drying cycles under different vertical stresses. The wetting-drying cycles between 140 and 4 MPa under three constant net vertical stresses of 98, 196 and 396 kPa were applied to the mixture. Figure 2.14 presents the volumetric strains in cyclic suction-controlled tests for the different vertical stresses. The stress path is also plotted in Figure 2.14 to show that the applied vertical stresses were in all cases lower than the yield stress for saturated conditions, preventing the collapse mechanism during the wetting and drying cycles. The results show that the differences between two successive wetting and drying paths become smaller as the number of cycles increases and eventually the shrinkage strain is accumulated during the suction cycles, depending on the stress levels. Clearly, the soil tends towards an equilibrium state at the end of suction cycles.

Besides, Nowamooz and Masrouri[65] published the results on the cyclic swell-shrink behavior of loosely and densely compacted bentonite/silt mixtures. Figure 2.15 shows the void ratio variations versus the suction for both loosely and densely compacted samples during several wetting and drying cycles between 0 and 20 MPa. The loose samples present a shrinkage strain accumulation while a swelling strain accumulation can be observed for dense samples before reaching a unique equilibrium state at the end of the wetting and drying cycles, regardless of the initial dry density of these expansive soil samples. In other words, the loose and

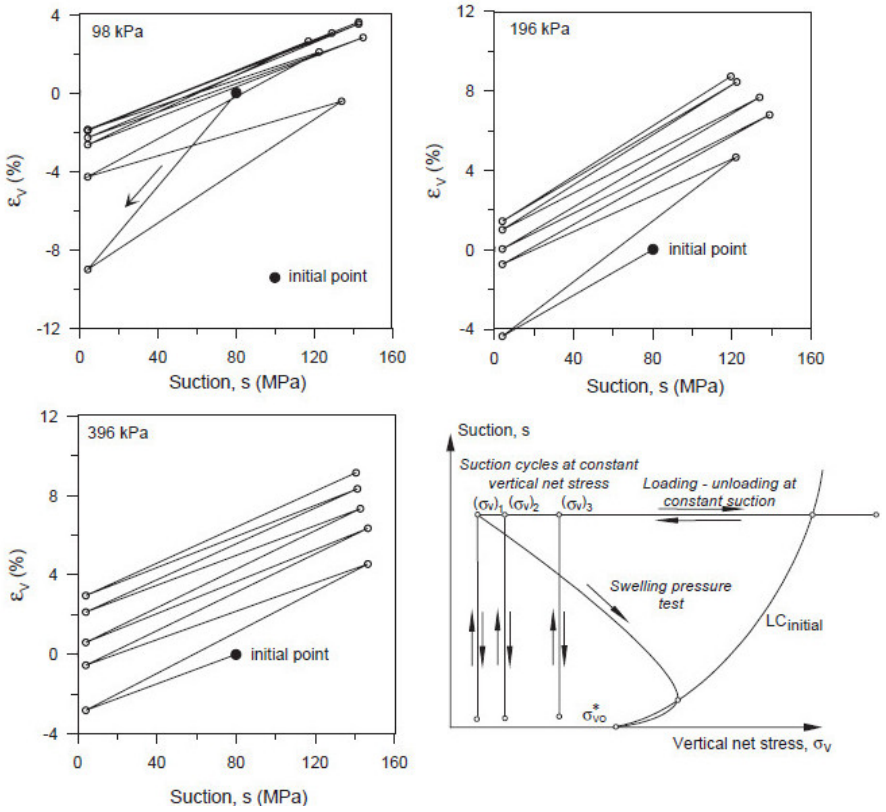

FIGURE 2.14: Volumetric strains in cyclic suction-controlled tests under different vertical pressures[46].

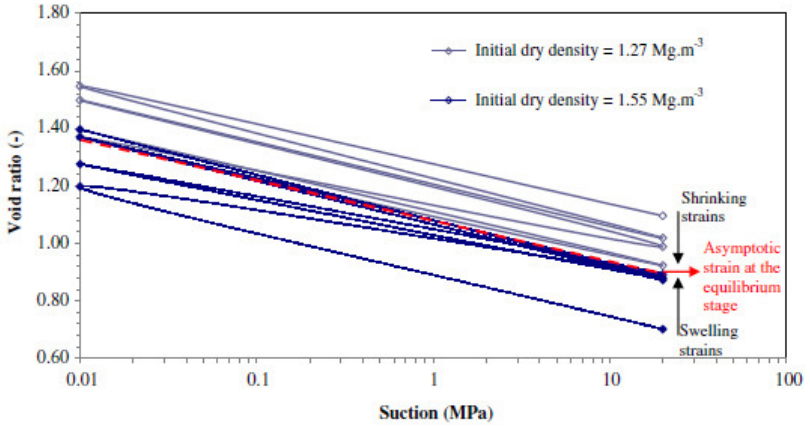

FIGURE 2.15: Variation of void ratio in cyclic suction-controlled paths at a null vertical stress for the densely and loosely compacted bentonite and silt mixtures[65].

dense samples will achieve a unique final state after several wetting and drying cycles.

2.4.4 Influence of suction cycles on mechanical behavior

Different authors highlighted the appearance of reversible deformation at the end of the wetting and drying cycles, but the coupling between these hydraulic cycles and the mechanical behavior has been rarely studied. For example, Wheeler *et al.*[42] demonstrated the effect of a wetting and drying cycle on the mechanical behavior of a bentonite-kaolin sample. In Figure 2.16, an isotropic loading-unloading cycle a-b-c performed at a constant suction of 200 kPa, was followed by a wetting-drying cycle c-d-e (not shown in the figure) and then another isotropic reloading and unloading e-f-g at a suction of 200 kPa. A significant increase in the degree of saturation occurred during the wetting-drying cycle c-d-e (see Figure 2.16b), as a consequence of hydraulic hysteresis. During the second isotropic loading stage e-f, yield occurred at a net mean stress lower than the previously applied value of 100 kPa.

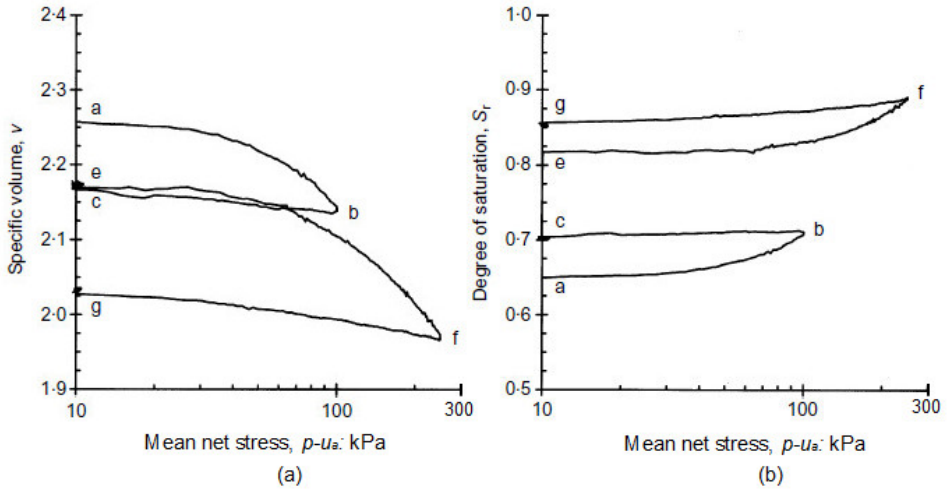

FIGURE 2.16: Influence of wetting-drying cycle on subsequent behavior during isotropic loading [42]: (a) Specific volume; (b) degree of saturation.

In the same way, Chen *et al.*[66] performed a series of tests to study the effect of a wetting-drying cycle on the mechanical behavior of an unsaturated compacted clay. A wetting-drying cycle followed by an isotropic compression at different suctions were performed on three different samples: UW4 and UW5 were respectively

wetted to a suction of 25kPa and 50kPa under a net confining stress of 20kPa while UI14 was a reference sample wetted to a constant suction 100 kPa from initial state. The samples UW4 and UW5 were subsequently dried to a suction of 100kPa and all the specimens UW4, UW5, UI14 were then subjected to an isotropic compression up to 350kPa at a constant suction of 100 kPa. The volume changes of different samples are presented in Figure 2.17, where a wetting-drying cycle results in a smaller pre-consolidation stress in UW4 and UW5 by 48% and 29%, respectively. The significant reduction in pre-consolidation stress is also likely attributed to the irreversible swelling resulting from the wetting and drying cycles. The irreversible swelling reduces the soil resistance and softens the soil. A larger irreversible swelling generally results in a larger reduction in the pre-consolidation stress.

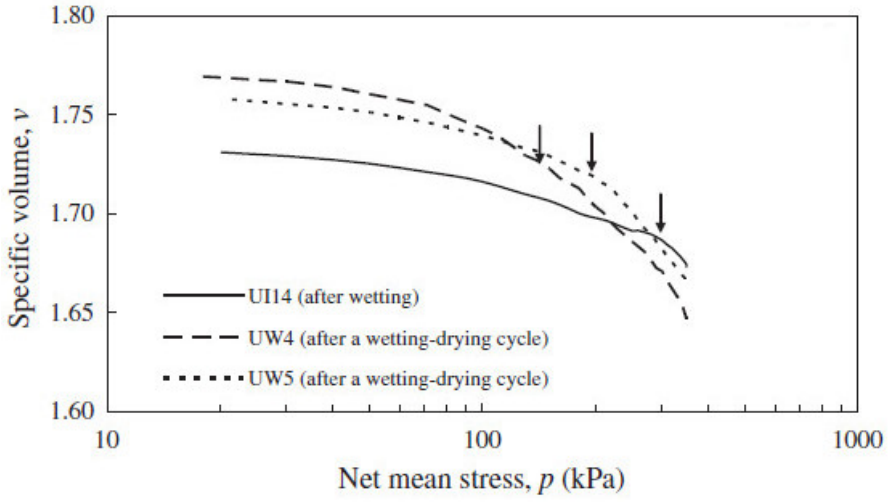

FIGURE 2.17: Effect of a wetting and drying cycle on volume changes[66].

Nowamooz and Masrouri[35, 67] studied the effect of several wetting and drying cycles on the mechanical behavior of an expansive soil compacted at loose and dense initial states. For the higher stresses, the compression curves (for both initial states) with and without the suction cycles at the suctions of 0, 2 MPa gradually converge towards the normally consolidated curve (NCC). However, this convergence is not observed for loose sample, the compression curve without suction cycles at the suction of 8 MPa (see Figure 2.18). With the application of suction cycles, the same loading/unloading curve at the suction of 8 MPa also converges to the NCC. Additionally, the authors pointed out that there is an obvious increase of preconsolidation stress at different suctions for loose samples because the wetting and drying cycles stiffen the loose samples. On the other hand, a decrease

of preconsolidation stress for dense samples can be observed because the suction cycles soften these materials.

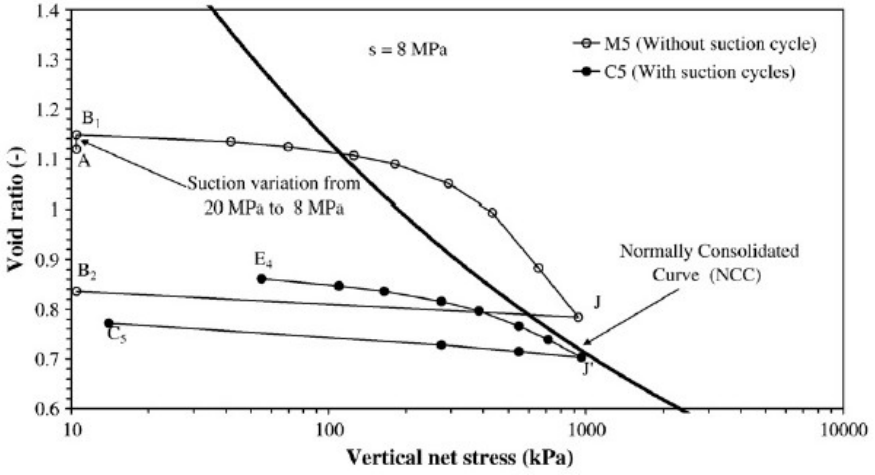

FIGURE 2.18: Loading and unloading tests with and without the application of suction cycles at constant suction s=8 MPa [67].

2.5 Elasto-plastic constitutive modeling

Generalised elasto-plastic models incorporating volumetric behavior and shear strength have been well established for saturated soils. With the development of unsaturated soil mechanics, this type of approach have been extended to model unsaturated soils which can be divided into two groups according to different selections of stress state variables. This section starts with the basic model using total stress concept, and then follows by the representative models with the concept of effective stress.

2.5.1 Model with total stress concept

The first successful use of total stress as an independent state variable was initially presented based on the elasto-plasticity theory (Alonso *et al.*, 1987)[49]. A fully developed mathematical formulation in the form of a critical state model for non-expansive unsaturated soils was presented in the space (p:q:s) by Alonso *et al.*[68], known as BBM (Barcelona Basic Model). Due to the limitations of BBM in modeling the behavior of more expansive soils, particularly, the swelling plastic strain during wetting, an enhanced model BExM (Barcelona Expansive Model),

was proposed by Alonso *et al.*[21] with the consideration of two levels of structures of expansive soils. The mathematical descriptions of the above models are presented in the following:

• Barcelona Basic Model

- General expressions for isotropic stress state

The SI (Suction Increase) and LC (Loading Collapse) curve are proposed to bound the elastic region, and these boundaries can be expressed as:

$$s = s_0 \tag{2.9}$$

$$p_0 = p_c \cdot \left(\frac{p_0^*}{p_c}\right)^{\frac{\lambda(0)-\kappa}{\lambda(s)-\kappa}} \tag{2.10}$$

where,

$$\lambda(s) = \lambda(\infty) - [\lambda(\infty) - \lambda(0)] \cdot e^{-\beta \cdot s} \tag{2.11}$$

In these equations, s_0 has the meaning of the maximum past suction ever experienced by the soil and bounds the transition from the elastic state to the virgin range when suction is increased, p_0^* the preconsolidation stress for saturated state, p_c the reference pressure, κ elastic stiffness parameter for changes in net mean stress and $\lambda(s)$ stiffness parameter for changes in net mean stress. Additionally, $\lambda(\infty)$ represents soil stiffness at very high level of suction and β is a factor controlling the rate of stiffness increase with suction. Eventually, the graphical representation of yield surfaces are illustrated in Figure 2.19.

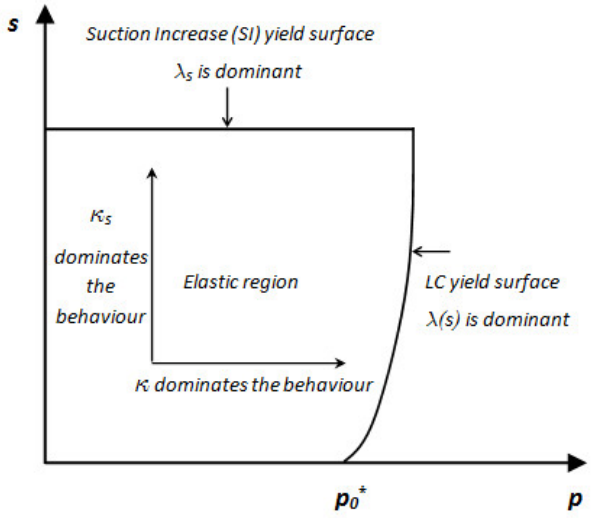

FIGURE 2.19: Loading-collapse (LC) and suction increase (SI) yield surfaces.

For the general case of isotropic loading-unloading, the change of elastic volumetric strain is related to the net mean stress and the suction as:

$$d\epsilon_v^e = \frac{\kappa}{v} \cdot \frac{dp}{p} + \frac{\kappa_s}{v} \cdot \frac{ds}{s + p_{at}} \tag{2.12}$$

where, v is the specific volume, p_{at} is the atmospheric pressure, κ is the elastic stiffness parameter for changes in net mean stress and κ_s is the elastic stiffness parameter for changes in suction.

Once the loading of suction and net mean stress reaches the yield surface, the variation of total volumetric strain and plastic volumetric strain are proposed as:

$$d\epsilon_v = \frac{\lambda(s)}{v} \cdot \frac{dp_0}{p_0} + \frac{\lambda_s}{v} \cdot \frac{ds_0}{s_0 + p_{at}} \tag{2.13}$$

$$d\epsilon_v^p = \frac{\lambda(s) - \kappa}{v} \cdot \frac{dp_0}{p_0} + \frac{\lambda_s - \kappa_s}{v} \cdot \frac{ds_0}{s_0 + p_{at}} \tag{2.14}$$

where, λ_s is the stiffness parameter for changes in suction.

Additionally, this model presents a simple way to couple suction increase with loading-collapse behavior. A suction increase across the yield locus has been shown to affect the response of the soil loading along p axis. On the other hand, a coupling between the motion of the LC surface and an eventual translation of the SI surface is also possible. However, experimental evidence is not available in this case and the model will be kept simple by specifying the position of the SI surface at the maximum past suction ever experienced by the soil.

- Model formulations for triaxial stress state

The modified Cam-clay model as a critical state theory corresponding to the saturated case is incorporated in Barcelona Basic Model. Consequently, extension of the model to deviatoric stress states resulted in elliptical yield surface in the q:p plane for each value of suction. A linear increase of cohesion with suction is assumed in Barcelona Basic Model and finally the three-dimensional view of the yield surfaces presented in p:q:s space is illustrated in Figure 2.20.

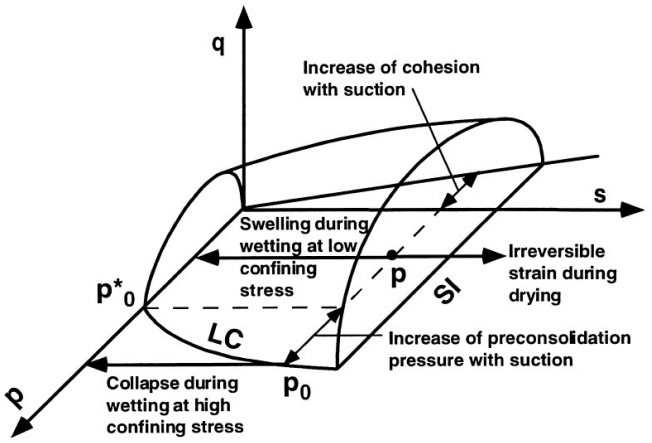

FIGURE 2.20: Three-dimensional view of the yield surfaces in p:q:s space[68].

• Barcelona Expansive Model

- Microstructural and macrostructural behavior

Two distinct levels are distinguished: the microstructural level at which swelling of active minerals takes place and the macrostructural level responsible for major structural rearrangement. The following assumptions are adopted:

1) the microstructural level is mainly saturated and its behavior is elastic, volumetric;
2) mechanical, hydraulic and chemical equilibrium exists between microstructure and macrostructure.

With these assumptions, several yield surfaces are proposed. Suction Increase (SI) and Suction Decrease (SD) lines define the onset of macrostructural volumetric plastic strain due to microstructural shrinkage and swelling. LC yield surface defines the set of yield preconsolidation stress for each associated suction, the same mathematical description as BBM (see Figure 2.21).

Two alternative constitutive laws are considered for the microstructural volumetric elastic strain:

$$d\epsilon_{vm}^{e} = \frac{d(p+s)}{K_m} \tag{2.15}$$

$$K_m = \frac{e^{-\alpha_m(p+s)}}{\beta_m} \quad \text{or} \quad K_m = \frac{(1+e_m)\cdot(p+s)}{\kappa_m} \tag{2.16}$$

depending on the type of expansion to model. In this equation, α_m, β_m, and κ_m are the constant model parameters and e_m is the void ratio of microstructure.

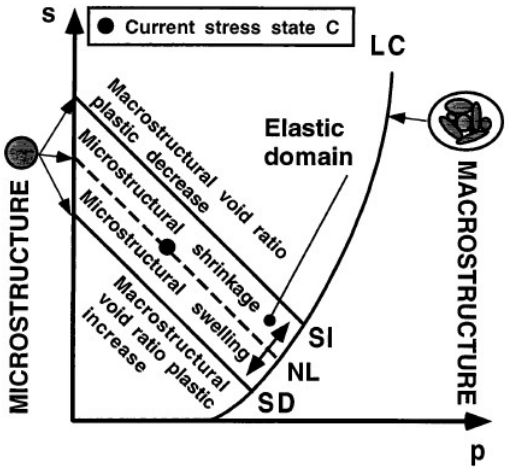

FIGURE 2.21: BExM yield loci in p-s plane [21].

The macrostructural volumetric elastic strain is expressed as a function of net mean stress and suction, the same as BBM:

$$d\epsilon^e_{vM} = \frac{dp}{K_t} + \frac{ds}{K_s} \tag{2.17}$$

$$K_t = \frac{(1+e_M)\cdot p}{\kappa} \tag{2.18}$$

$$K_s = \frac{(1+e_M)\cdot (s+p_{at})}{\kappa_s} \tag{2.19}$$

where, e_M is the void ratio of macrostructure and other parameters are the same definitions of BBM.

- Coupling between micro- and macrostructure

The micro-macrostructural coupling functions f_I and f_D are proposed in BExM (see Figure 2.22), to define the increment of the volumetric macrostructural plastic strain due to microstructural swelling/shrinkage:

$$d\epsilon^p_{vM} = f_I \cdot d\epsilon^e_{vm} \quad \text{when SI is activated;} \tag{2.20}$$

$$d\epsilon^p_{vM} = f_D \cdot d\epsilon^e_{vm} \quad \text{when SD is activated.} \tag{2.21}$$

where f_I, f_D depend on the ratio of p over p_0. Several coupling functions have been developed to model different materials in the literature[21, 46, 69].

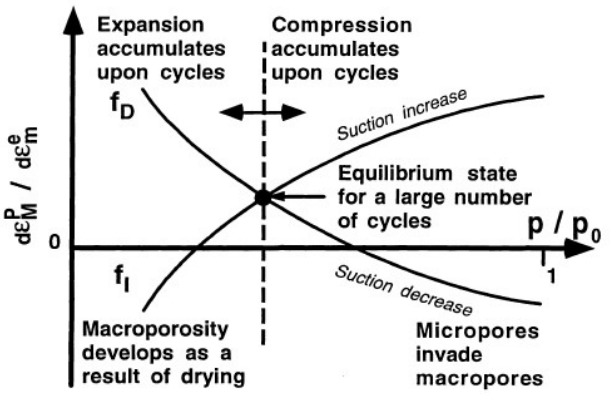

FIGURE 2.22: Interaction mechanism of micro-macrostructure [21].

By this simple approach, global expansion of the material during application of suction cycles at low confining stress, global contraction of the material during application of suction cycles at high confining stress and decrease of volume changes with the progression of the cycles can be represented.

The evolution of yield surfaces, controlled by two hardening parameters p_0^* and s_0, is defined by:

$$ds_i = \frac{(1+e_m)\cdot(p+s)}{\kappa_m \cdot f}(d\epsilon^p_{vSI} + d\epsilon^p_{vSD}) = ds_0 \tag{2.22}$$

$$\frac{dp_0^*}{p_0^*} = \frac{v}{\lambda(0)-\kappa}(d\epsilon^p_{vSI} + d\epsilon^p_{vSD} + d\epsilon^p_{vLC}) \tag{2.23}$$

where the function f corresponds the micro-macrostructural coupling function in use, that is $f = f_I$ if SI is active and $f = f_D$ if SD is active. Additionally, ϵ^p_{vSI}, ϵ^p_{vSD}, ϵ^p_{vLC} are the volumetric plastic strains due to activation of respectively SI, SD and LC.

- Simplification of the model BExM

The complex mathematical expressions of coupling function makes it difficult to adopt a simple systematic procedure to determine model parameters. Accordingly, Alonso *et al.*[46] have decided to introduce some simplifications even if some model capabilities are reduced. The following simplifying assumptions were introduced:

1) The assumption of a fully saturated microstructure eliminates the need to introduce the water retention curve and the relative parameter;
2) Suction-induced elastic deformations are considered only as microstructural deformations, i.e. any suction-induced macrostructural elastic deformations are ignored;

3) It will be assumed that the SI and SD yield surfaces are always activated as suction changes during the application of drying-wetting cycles. In other words, the elastic region bounded by SI and SD is assumed to be negligible. This assumption facilitates the computation of plastic strains.

- Limitations of the model BExM

The deformations of double-structure (microstructure and macrostructure) of expansive soils are considered in BExM and the mechanical behavior of macrostructure follows the framework of BBM. This model is able to simulate the basic behavior of unsaturated expansive soil, including the strain fatigue phenomenon during drying-wetting cycles and the prediction of final equilibrium state at the end of the suction cycles. However, this model presents the following limitations:

1) A large number of model parameters should be determined. The calibration of these parameters needs several experimental tests which lead to a time-consuming procedure to characterize their hydro-mechanical behaviors.
2) Certain parameters such as the coupling functions for micro- and macrostructural strains are difficult to quantify.
3) Time dependent effects are not taken into account in the present model, that can be interpreted as no coupling between soil behavior and water retention phenomenon.

2.5.2 Model with effective stress concept

In order to identify the hydromechanical behavior of unsaturated soils properly, effective stress is selected as one stress state variable to model unsaturated soil behavior. This idea is mainly originated from classic saturated soil mechanics that has already been well established by soil researchers. At the beginning of this section, previous attempts to effective stress are reviewed, and then a representative framework based on effective stress concept (Wheeler's model) is presented.

• Previous attempts to effective stress

It would be helpful to first note the basic concept behind effective stress. Terzaghi [70] described the stress state variable controlling the behaviour of saturated soils as follows:

" ... all the measurable effects of a change in stress, such as compression, distortion and a change in shearing resistance are exclusively due to changes in the effective stress".

The effective stress σ' is mathematically expressed as:

$$\sigma' = \sigma - u_w \tag{2.24}$$

where, σ is the total normal stress and u_w is the pore-water pressure.

The definition of this stress state variable has been well examined and experimentally verified for saturated soils[71–74]. There have been attempts to extend this effective stress equation to unsaturated soils. Bishop[75] suggested a tentative expression for effective stress which has gained widespread reference:

$$\sigma' = (\sigma - u_a) + \chi(u_a - u_w) \tag{2.25}$$

where, u_a is the pore-air pressure and χ is the parameter related to the degree of saturation of soils (called Bishop's parameter). The Bishop's parameter can be replaced by the degree of saturation S_r, equal to 1 for saturated soils and zero for dry soils, then the Bishop's effective stress is described as:

$$\sigma' = \sigma - S_r u_w - (1 - S_r)u_a \tag{2.26}$$

Aitchison and Jennings [76, 77] have proposed different effective stress equations, the similar form as Bishop's effective stress. However, Bishop's effective stress has been questioned by several researchers. It was suggested that Bishop's equation did not provide an adequate relationship between volume change and effective stress for many soils, particularly those below a critical degree of saturation[78].

Many other effective stress equations have been proposed for unsaturated soils[76, 77, 79, 80]. All these equations incorporate a complicated soil parameter in order to form the effective stress, a single-value stress state variable.

For the sake of simplicity, Bishop effective stress σ' is usually selected as a stress state variable, the second stress state variable can be chosen on the basis of the work (Houlsby, 1997)[81] that proved the increment of work input dW, per unit volume of unsaturated soil for the isotropic state can be written as:

$$dW = p' d\epsilon_v - s' dS_r \tag{2.27}$$

where, ϵ_v is the volumetric strain, S_r is the degree of saturation and s' is the modified suction, a product of porosity and suction, $n \cdot (u_a - u_w)$.

In this equation, p' is the mean Bishop's stress, defined by

$$p' = p - S_r u_w - (1 - S_r)u_a \tag{2.28}$$

where p is the net mean stress.

Therefore, the proposed stress state variables for the isotropic stress state are p', s' and the corresponding conjugate strain increment variables are $d\epsilon_v$, $-dS_r$ respectively. The proposed stress state variables are clearly more complex than the traditional variables of net mean stress and suction. In particular, the expression for p' includes the degree of saturation and the expression for s' includes the porosity. If the use of the proposed stress variables is to be justified, this must produce significant improvements in modeling capability or in the simplicity of the resulting stress-strain relations.

• Wheeler's model

Consideration of the different roles of pore air pressure, pore water pressure within bulk water and pore water pressure within meniscus water suggests that the degree of saturation has a significant influence on the the stress-strain behavior of an unsaturated soil, in addition to any influence of suction. However, the BExM model is unable to represent accurately the soil behavior during stress-suction variations where hydraulic hysteresis is significant. In light of this, a new elasto-plastic model for unsaturated soils is proposed by Wheeler *et al.*[42], involving coupling of hydraulic hysteresis and mechanical behavior. In the following, the constitutive relation for isotropic stress state is presented.

A rectangular yield surface is proposed in the model, bounded by s'_I, s'_D and p'_0, and these yield surfaces are illustrated in the following figure.

Elastic volumetric strain increments are given by:

$$d\epsilon_v^e = \frac{\kappa dp'}{vp'} \tag{2.29}$$

where κ is the slope of an elastic line for saturated state. When yielding on only the LC curve, plastic volumetric strain increments are given by:

$$d\epsilon_v^p = \frac{(\lambda - \kappa)dp'_0}{vp'_0} \tag{2.30}$$

where λ is the slope of the normal compression line for saturated state.

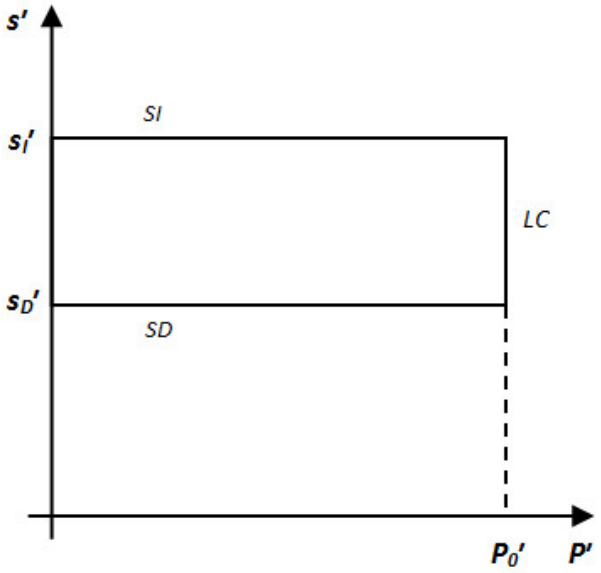

FIGURE 2.23: LC, SI and SD yield curves for isotropic stress states[42].

Elastic increments of degree of saturation are given by:

$$dS_r^e = -\frac{\kappa_s ds'}{s'} \tag{2.31}$$

where κ_s is an additional elastic constant. When yielding only on the SI or SD yield surface, plastic changes of S_r are given by:

$$dS_r^p = -(\lambda_s - \kappa_s)\frac{ds_I'}{s_I'} = -(\lambda_s - \kappa_s)\frac{ds_D'}{s_D'} \tag{2.32}$$

where λ_s is a plastic constant. Figure 2.24 shows the form of water retention behavior predicted by equation 2.31 and 2.32. In a plot of S_r against lns', the main drying and wetting curves have a gradient λ_s and elastic paths have a gradient κ_s. The modelling of the water retention behavior shown in Figure 2.24 is relatively crude and future refinement may be desirable.

When yielding only on the SI or SD curve, coupled movements of the LC yield curve are given by:

$$\frac{dp_0'}{p_0'} = k_1\frac{ds_I'}{s_I'} = k_1\frac{ds_D'}{s_D'} \tag{2.33}$$

where, k_1 is the first coupling parameter.

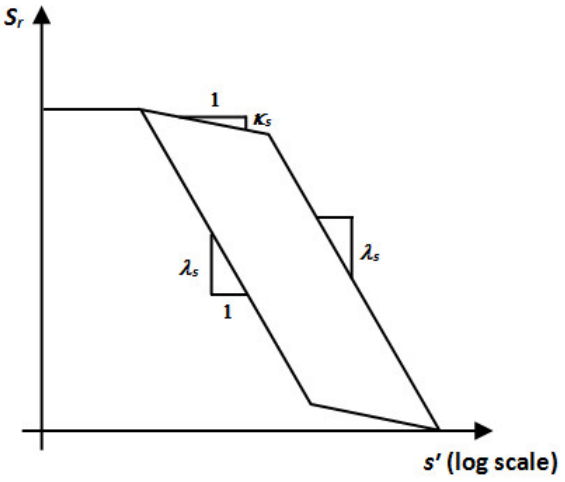

FIGURE 2.24: Model for water retention behavior[42].

When yielding on only LC curve, coupled movements of the SI and SD curves are given by:

$$\frac{ds'_I}{s'_I} = \frac{ds'_D}{s'_D} = k_2 \frac{dp'_0}{p'_0} \tag{2.34}$$

where, k_2 is the second coupling parameter.

In general, the overall movement of the LC yield curve is given by the sum of any direct movement caused by yielding on the LC curve itself and any coupled movement produced by the yielding on the SI or SD curve:

$$\frac{dp'_0}{p'_0} = \frac{v d\epsilon^p_v}{\lambda - \kappa} - \frac{k_1 dS^p_r}{\lambda_s - \kappa_s} \tag{2.35}$$

Similarly, overall movements of the SI or SD curves are given by the sum of any direct movements caused by yielding on the SI or SD curve and any coupled movements produced by yielding on the LC curve:

$$\frac{ds'_I}{s'_I} = \frac{ds'_D}{s'_D} = -\frac{dS^p_r}{\lambda_s - \kappa_s} + \frac{k_2 v d\epsilon^p_v}{\lambda - \kappa} \tag{2.36}$$

Eventually, this elasto-plastic framework can be extended to anisotropic stress states, with the critical state theory.

It is clear, to summarise this section, that any adequate set of work-conjugate stresses and strains can be used for constitutive modelling of unsaturated soils. The choice of net stress and suction is convenient and precise, while the use of effective stress concept introduces a complex nonlinear parameter χ, but it leads to

a simpler stress-strain relation. In the models by e.g. Alonso and Gens[68], Cui *et al.*[82], Wheeler and Sivakumar[48], Alonso *et al.*[21], Romero and Vaunat[83] and Buisson and Wheeler[84], the net stresses and the suction are used as the stress variable, meanwhile the soil skeleton strain and the hydraulic strain are their work-conjugate strains, respectively. In the models by e.g. Jommi and Di Prisco[85], Abou-bekr[86], Bolzon *et al.* [87] and Sun *et al.*[88], the average skeleton stress (effective stress) and the suction are used as the stress variables, then the soil skeleton strain and the degree of saturation are the work-conjugate strain variables. Note that some of the earlier models do not use the complete work-conjugate stresses and strains, the selection of stress variables in these models, therefore, needs more discussions and further justifications.

In this study, the net stress and the suction are selected as two independent variables to model the behavior of expansive soils, because of their simplicity and accessibility. With more experimental results, a single effective stress equation could be used in future modeling of expansive soils.

2.6 Conclusion

The experimental results on expansive soils are many and varied, but efforts in this chapter have directly reviewed those classical and representative tests to identify the hydromechanical behavior of expansive soils. The experimental results show that loose samples present a shrinkage strain accumulation while dense samples present a swelling strain accumulation during wetting and drying cycles. However, all these tests show that a stable equilibrium state can be reached after several wetting and drying cycles.

The generally accepted models of unsaturated soils examined in this chapter need a large number of parameters and a time-consuming calculation during wetting and drying cycles. This leads to the fact that the absence of a simple and straightforward model for the expansive soils. In our proposed framework, we try to consider these points to simplify the modeling.

Therefore, shakedown theory will be used to model the hydromechanical behavior of expansive soils. The idea of shakedown is widely accepted by civil engineers and researchers that can be applied to the sophisticated materials and structures using non-incremental analysis to facilitate designs and calculations. In the following chapter, the classic shakedown theory is first reviewed. Then, an analytical

shakedown model for expansive soils is developed. Finally, the shakedown model is validated by comparing model predictions with test results.

Chapter 3

Analytical Modeling of Expansive Soils with Shakedown Concept

3.1 Introduction

A review of literature suggests that the generally accepted model for expansive soils (i.e. BExM) presents a large number of parameters, such as the coupling functions for micro- and macrostructural strains. The calibration of these parameters needs several tests leading to a time-consuming procedure to characterise their hydro-mechanical behaviors. On the other hand, swell-shrink behavior of expansive soils with an increasing number of wetting and drying cycles have been shown to reach an equilibrium state where the soil sample nearly behaves in a reversible manner in terms of volumetric deformations. This equilibrium state presents the shakedown behavior of expansive soils during wetting and drying cycles, but no study has been conducted in the past about the modeling of expansive soils with shakedown theory.

Therefore, this chapter presents an approach based on shakedown theory to improve the modeling of expansive soils subjected to wetting and drying cycles under different vertical stresses. The required parameters of the shakedown model are calibrated by the suction-controlled oedometer tests obtained for an expansive soil compacted at loose and dense initial states, and then validated for the same soil compacted at intermediate initial state by comparing the model predictions with the experimental results. In the following section, shakedown theory and its further extension are first presented.

3.2 The theory of shakedown

When an elasto-plastic structure is subjected to a variable loading between given extreme values, its behavior may fall into one of the following stages (as illustrated in Figure 3.1):

(a) purely elastic. The applied repeated load is sufficiently small that no element of the material achieves any yield condition. From the first type of loading, all deformations are fully recovered and the response is purely elastic;

(b) elastic shakedown. The applied force is slightly less than the limit to produce plastic shakedown. The material response is plastic while the ultimate response is purely elastic. The material is said to have "shaken down" and the maximum stress level is defined as "elastic shakedown limit".

(c) plastic shakedown. The applied cyclic force is slightly less than the limit to produce collapse after the incremental accumulation of permanent strain. The material achieves a long term steady state response, i.e. no further accumulation of permanent strain and each response is hysteretic. This implies that the material absorbs a finite amount of energy during cyclic loading. Once a steady closed loop has been obtained, the material is said, once again, to have "shaken down" and the maximum stress is termed by "plastic shakedown limit".

(d) incremental collapse or ratchetting. The applied cyclic load is relatively large. The stresses applied cause the material to reach and exceed the yield condition. The permanent strains then accumulated rapidly with failure occurring in a relatively short time.

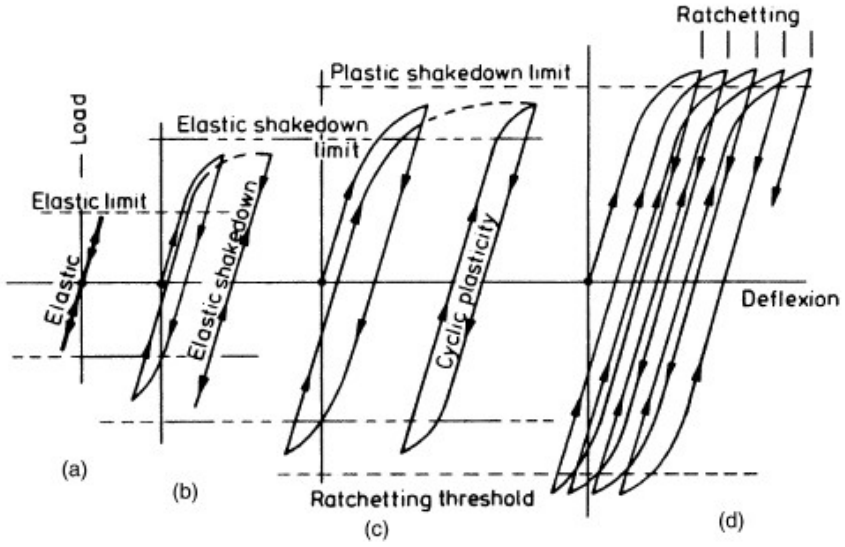

FIGURE 3.1: Material response under cyclic tension and compression.

In light of the above discussion, it is important to determine whether an elasto-plastic structure will shakedown for given extreme load values. Its direct solution is difficult but has been helped greatly by two theorems developed by Melan[89] and Koiter[90]. Like the lower and upper bound theorems of limit state, these two basic shakedown theorems can also be used to obtain a lower bound and an upper bound for the shakedown load limits under which the structure will shakedown.

For simplicity, the discussion of the basic shakedown theorems will be restricted to the most important case where the prescribed surface displacements are zero. Therefore, elasto-plastic structures will be subjected to some surface loads that vary between extreme values.

3.2.1 Principles of shakedown

• Melan's lower bound theorems

Melan's lower bound shakedown theorem can be stated as follows:

> *An elastic-perfectly plastic structure will shakedown for given extreme load values if and only if there exists a state of time-independent self-stress (i.e. residual stress) that nowhere violates the yield criterion when it is superimposed on the state of elastic stresses of the structure caused by the extreme load values.*

where the state of self-stress or residual stresses is in equilibrium with zero external load. The state of elastic stresses, is superimposed on the state of self-stress, determined from the external loads by assuming that the structure is made of an elastic material. For simplicity, it assumes that the loading is applied sufficiently slow so that the effect of inertia may be small and therefore ignored.

Melan's theorem considers an elastic-perfectly plastic structure that has already shakedown under a loading path that varies in time within a certain range of the surface tractions. At the state of shakedown, the plastic strain field remains constant with time and defines a time-independent self-stress or residual stress field. This residual stress field R_{ij}, combined with the elastic stress field $\lambda\sigma^e_{ij}$, does not violate the yield criterion throughout the structure:

$$f(\sigma_{ij}) = f(\lambda\sigma^e_{ij} + R_{ij}) \leq 0 \tag{3.1}$$

where, λ is a factor. The greatest value λ_{SD} which satisfies the theorem is called shakedown-factor.

The static shakedown theorem is formulated in terms of stresses and gives a lower bound to λ_{SD}. This leads to the mathematical optimization problem:

$$\begin{aligned} &max\ \lambda \\ &such\ that: \frac{\partial R_{ij}}{\partial x_j} + b_i = 0 \quad in\ \Omega \\ &\qquad\qquad R_{ij}n_j = p_i \quad on\ \Gamma_F \\ &\qquad\qquad f(\lambda\sigma^e_{ij} + R_{ij}) \leq 0 \quad in\ \Omega \end{aligned} \tag{3.2}$$

where, b_i is the body force vector in structure volume Ω, n_j is an arbitrary direction vector and p_i is surface force vector on structure boundary Γ_F.

• Koiter's upper bound theorems

Koiter's upper bound shakedown theorem can be stated as follows:

> *If any kinematically admissible mechanism of plastic collapse can be found in which the rate of work done by elastic stresses due to the load exceeds the rate of plastic dissipation, then incremental collapse will take place. The ratio of the work done by the elastic stresses to the plastic dissipation has a maximum in the "true" mechanism of collapse, so that any other mechanism gives an upper bound to the shakedown limit. That is, shakedown may happen if the*

following inequality is satisfied:

$$\lambda \int_0^T dt \int_\Omega \sigma_{ij}^e \dot{\epsilon}_{ij}^p d\Omega \leq \int_0^T dt \int_\Omega D^p(\dot{\epsilon}_{ij}^p) d\Omega \tag{3.3}$$

where, $D^p(\dot{\epsilon}_{ij}^p)$ is the rate of plastic dissipation.

The lowest value λ_{SD} which satisfies the theorem is called shakedown-factor in this case. The kinematic shakedown theorem is formulated in terms of strain rates and gives a upper bound to λ_{SD}. This leads to the mathematical optimization problem:

$$\begin{aligned} min\ \lambda &= \frac{\int_0^T dt \int_\Omega D^p(\dot{\epsilon}_{ij}^p) d\Omega}{\int_0^T dt \int_\Omega \sigma_{ij}^e \dot{\epsilon}_{ij}^p d\Omega} \\ such\ that : \Delta\epsilon_{ij}^p &= \int_0^T \dot{\epsilon}_{ij}^p dt\ in\ \Omega \\ \Delta\epsilon_{ij}^p &= \frac{1}{2}\left(\frac{\partial \Delta u_i}{\partial x_j} + \frac{\partial \Delta u_j}{\partial x_i}\right)\ in\ \Omega \\ \Delta u_i &= 0\ on\ \Gamma_u \end{aligned} \tag{3.4}$$

where, u_i is the displacement and Γ_u is the displacement boundary of the structure volume Ω.

3.2.2 Historical remarks and further extension

The lower bound shakedown theorem for structures under variable loads was first established by Bleich[91] for simple indeterminate structures. This work was later generalised by Melan to a general three-dimensional elastic-perfectly plastic structure. It is noted that Melan's original proof was rather complex and considerable simplifications of Melan's proof were achieved by Symonds[92] and Koiter (1960)[90]. Meanwhile, the upper bound shakedown theorem was proposed by Koiter and this theorem bears some resemblance to the earlier method of Symonds and Neal[93]. The notable feature of Melan and Koiter theorems is path-independence: these theorems ensure the structure is safe with a time-independent boundary in loading space, regardless of particular loading histories. In other words, it is not necessary to follow an exact loading paths to solve shakedown problem by classical step-by-step analysis, that simplifies the work and saves the time.

Many attempts have been made to extend the theorems of Melan and Koiter to cover various complicated materials. The majority of papers on shakedown problems

are restricted to elastic-perfectly plastic material behavior, although some fundamental results for material hardening were given by Melan[89] and later Neal[94], Maier[95] and Ponter[96], which treat the case of linear and unlimited hardening, allowable for the translation of individual active yield planes. Alternatively, König[97, 98] extended Melan's concept to general linear hardening material and emphasized that the usual assumption of unlimited kinematic hardening makes it impossible to predict failure because there is no bounds for the motion of the yield surface in the stress space. More precisely, the assuming unlimited kinematic hardening gives sufficient criteria for shakedown load, instead of failure predictions. Ponter[96], Zarka and Casier[99] come independently to a similar conclusion.

Although numerous shakedown approaches have been extended from the theorems of Melan and Koiter, the accumulation of plastic strain and displacement which occurs during the history of loading is not known. The displacement bounding theorem proposed by Zarka and Casier[99], also known as Zarka simplified method, provides the calculation of accumulated plastic strain and displacement during the state of shakedown. For this simplified method, Zarka introduces the transformed internal variables to characterize the mechanical system, then a local geometrical construction in transformed internal parameter plane is performed to estimate the stabilized limit state and the associated deformation components. This simplified shakedown analysis has been applied to metallic structures with the linear kinematic hardening and associated flow rule with Von Mises yield criterion.

Apart from the great progress in theoretical work based on shakedown concept, engineering practice for pavement analysis using shakedown approach has already been carried out since 1980s. Sharp and Booker[100] introduced the shakedown theorem for the first time to pavement structures which defined shakedown load as the key design load. This work was followed by Raad *et al.*[101, 102], Radovsky and Murashina[103], Yu and Hossain[104], Shiau and Yu[105], Yu[106] and Yu and Wang[107]. They modelled the pavement structures through lower bound approach and the Mohr-Coulomb yield criterion was used to compute the shakedown limit. On the other hand, Collins and Cliffe[108], Collins and Boulbibane[109], Chen and Ponter[110], and Li and Yu[111]employed the upper bound theorem to analyses the shakedown state of pavement. From their computation results, they concluded that the shakedown analysis using the upper bound theorem provides a rational limit load to pavement structures.

At the same time, Habiballah and Chazallon[112], Allou *et al.*[113], Chazallon *et al.*[114] and Chazallon *et al.*[115] have developed a shakedown model, based

on Zarka simplified method, for unbound granular materials subjected to cyclic traffic loadings. This model uses Druker-Prager yield surface and Von Mises plastic potential. The parameters of the proposed model are calibrated by repeated load triaxial tests and the finite element calculation of 2D and 3D pavements have been performed to determine the rut depth during cyclic loading. All these calculations underline the capacities of the shakedown-based model to take into account the cyclic behavior of unbound materials.

3.3 Shakedown modeling of expansive soils

In this section, we first present the analytical formulation of Zarka shakedown method. Subsequently, it is used to model the hydromechanical behavior of expansive soils subjected to successive wetting and drying cycles. Finally, the coupling function between suction cycles and mechanical behavior is developed to study the influence of wetting and drying cycles on the following mechanical behavior of expansive soils.

3.3.1 Principles of Zarka method

Zarka method, being a direct method of shakedown analysis, has been examined to be efficient instead of involving time-consuming incremental approach. This inelastic analysis is previously applied to model kinematic hardening materials by introducing a group of internal variables to characterize the local behavior of the material and the transformed internal parameter plane is used to estimate the limit state during cyclic loadings. Eventually, the plastic deformations during cyclic loadings can be determined from elastic shakedown theory (or plastic shakedown theory) depending on the positions of the initial yield surface and the final yield surface in the transformed internal parameter plane.

In the case of one-dimensional elasto-plastic problem, the elastic behavior of the material can be supposed linear, independent of temperature. Thus, the mechanical problem can be solved as follows:

$$\epsilon(x,t) = \frac{1}{E} \cdot \sigma(x,t) + \epsilon^p(x,t) + \epsilon^I(x,t) \tag{3.5}$$

in which, E is the elastic modulus, $\sigma(x,t)$ is the stress, $\epsilon(x,t)$ the total strain, $\epsilon^p(x,t)$ the plastic strain, and $\epsilon^I(x,t)$ the initial strain.

The yield surface equation with a linear kinematic hardening can be written as:

$$f = |\sigma - y_\alpha| - \sigma_\alpha \tag{3.6}$$

where, σ_α is the yield stress and y_α the kinematic hardening variable is related to the plastic strain,

$$y_\alpha = h \cdot \epsilon^p \tag{3.7}$$

where, h is the kinematic hardening modulus.

When $f = 0$, the yield surface equation can be written as:

$$\sigma = \sigma_\alpha + y_\alpha \tag{3.8}$$

In this stress plane, the normality law of plasticity can be written with the Moreau's notation (Moreau, 1971)[116]:

$$\dot{\epsilon}^p \in \partial\phi_{C(y_\alpha)}(\sigma) \text{ with } \sigma \in C(y_\alpha) \tag{3.9}$$

$\partial\phi_{C(y_\alpha)}(\sigma)$ is the subdifferential to the convex $C(y_\alpha)$, where the plastic strain rate is an external normal to the convex $C(y_\alpha)$ (see Figure 3.2a).

The yield surface equation can also be written as (when $f = 0$):

$$y_\alpha = \sigma - \sigma_\alpha \tag{3.10}$$

here, y_α represents the transformed internal parameter and this equation indicates that the yield surface centered in the applied stress σ with a radius of σ_α, translates in the transformed internal parameter y_α plane. In this transformed internal parameter y_α plane, the normality law of plasticity becomes:

$$\dot{\epsilon}^p \in -\partial\phi_{C(\sigma)}(y_\alpha) \text{ with } y_\alpha \in C(\sigma) \tag{3.11}$$

$-\partial\phi_{C(\sigma)}(y_\alpha)$ is the subdifferential to the convex $C(\sigma)$, where the plastic strain rate is an internal normal to the plasticity convex (see Figure 3.2c).

The main idea of Zarka shakedown method is to study the material response through the transformed internal parameter plane. Two cases exist according to the loading amplitude in the transformed internal parameter plane:

- Elastic shakedown

When the extreme positions of the convex centered in σ_{min} and σ_{max} have a common part, elastic shakedown occurs (see Figure 3.2d). In this case, the response of material becomes purely elastic after a certain number of cycles, and plastic strain fields tend towards constant fields depending on the initial state of the material. For this, the accumulated plastic strains during cyclic loadings can be computed by the following equation,

$$\Delta\epsilon^p = \frac{\Delta(\sigma - \sigma_\alpha)}{h} \tag{3.12}$$

where, σ is the applied stress.

• Plastic shakedown

When the loading amplitude is large, the extreme positions of the convex have no common part and in this case, plastic shakedown occurs (see Figure 3.2e). For plastic shakedown, the response of material becomes periodic during cycles with a periodic plastic strain field where a closed elastic-plastic loop is obtained, treated as a steady state with no additional accumulation of plastic deformation.

In the case of plastic shakedown, the maximum plastic strain and the minimum plastic strain between σ_{max} and σ_{min} can be defined in the transformed internal parameter plane:

$$\epsilon^p_{max} = \frac{1}{h} \cdot \left(y_{moy} + \frac{1}{2} \cdot \Delta y_\alpha \right) \tag{3.13}$$

$$\epsilon^p_{min} = \frac{1}{h} \cdot \left(y_{moy} - \frac{1}{2} \cdot \Delta y_\alpha \right) \tag{3.14}$$

where, y_{moy} is presented in Figure 3.2e, equal to $(\sigma_{max} + \sigma_{min})/2$.

The above Zarka shakedown method is based on Melan static theorem and it defines the lower bounds of the shakedown behavior. It should be added that the collapse phenomenon is not considered for this method, because of the unlimited kinematic hardening. Although Zarka simplified method can not predict the collapse of material, it provides sufficient estimations of the deformation and the displacement at the shakedown stage.

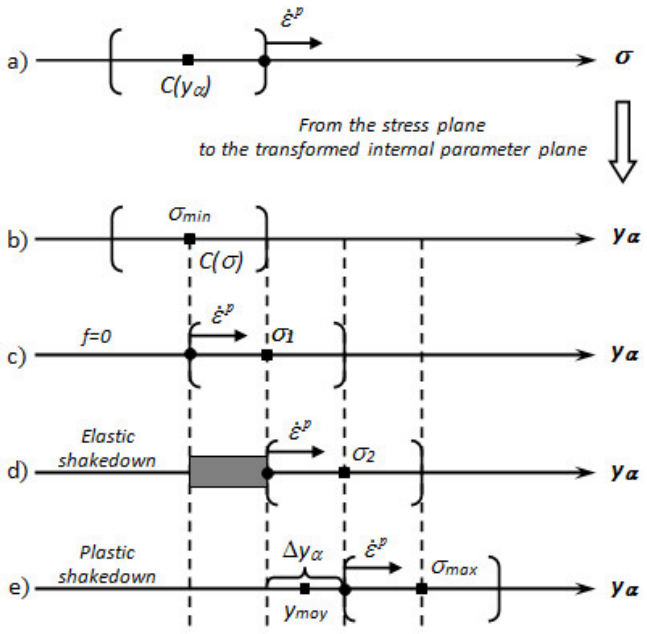

FIGURE 3.2: Transformed internal parameter plane for elastic shakedown and plastic shakedown.

3.3.2 Simplified model for isotropic stress states

It is generally accepted that a unique plane (net mean stress–suction) is sufficient to describe the hydro-mechanical behavior of unsaturated soils. In this section, the net mean stress was taken equal to the applied vertical pressure because of one-dimensional loading. Figure 3.3 shows in this plane a rectangular yield surface representing the elastic domain. The equations of the different boundaries can be given by:

$$s = s_I \tag{3.15}$$

$$s = s_D \tag{3.16}$$

$$p = p_0 \tag{3.17}$$

where, s_I is the Suction Increase limit, s_D is the Suction Decrease limit and p_0 is the Preconsolidation Stress. In this study, we suppose that the s_I and s_D yield surfaces are always activated as the suction changes and this simplification can facilitate the following shakedown modeling.

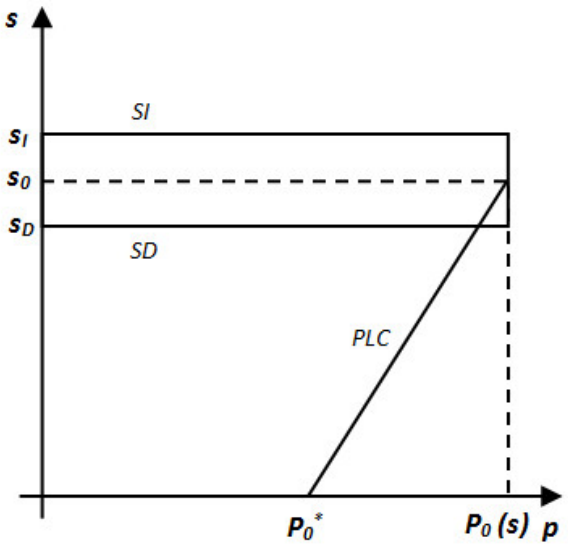

FIGURE 3.3: Rectangular shape for the yield surfaces in (suction - preconsolidation stress) plane.

For the sake of simplicity, we take into account the following hypotheses for the yield surfaces:

(1) the width of the elastic domain is small and is not changing with suction cycles.

The suction variation within the rectangular will result in the elastic volumetric strain:

$$d\epsilon_{vs}^{e} = \frac{\kappa_s}{v} \cdot \frac{ds}{s + p_{at}} \tag{3.18}$$

where v is the specific volume, equal to $(1 + e_0)$ in which e_0 is the initial void ratio of the sample.

And if the boundaries $s = s_I$ and $s = s_D$ (denoted as $s = s_0$) are activated, the following total and plastic volumetric strain will be generated,

$$d\epsilon_{vs} = \frac{\lambda_s}{v} \cdot \frac{ds_0}{s_0 + p_{at}} \tag{3.19}$$

$$d\epsilon_{vs}^{p} = \frac{\lambda_s - \kappa_s}{v} \cdot \frac{ds_0}{s_0 + p_{at}} \tag{3.20}$$

in which, κ_s and λ_s are elastic stiffness index and elastoplastic stiffness index for suction variation, respectively.

(2) the length of the rectangular depends on the suction level.

Based on this hypothesis, we define a Pseudo Loading Collapse (PLC) curve, with a linear relation between the preconsolidation stress and the suction level. This relation can be given by:

$$p_0(s) = A \cdot s + B \tag{3.21}$$

where, A and B can be determined by the isotropic compression tests at different suctions.

Parameter A, controlling the slope of PLC curves, is constant during suction cycles since these curves are only activated along p-axis.

Parameter B can be given by:

$$B = p_0^*(\gamma_d) \tag{3.22}$$

where, $p_0^*(\gamma_d)$ is the preconsolidation stress for saturated state, changing with the initial state of soils (loose or dense state).

The increase of the net mean stress within the rectangular will generate the elastic volumetric strain:

$$d\epsilon_{vp}^e = \frac{\kappa}{v} \cdot \frac{dp}{p} \tag{3.23}$$

and if the boundary $p = p_0(s)$ is reached, the following total and plastic volumetric strain will be given by,

$$d\epsilon_{vp} = \frac{\lambda(s)}{v} \cdot \frac{dp_0}{p_0} \tag{3.24}$$

$$d\epsilon_{vp}^p = \frac{\lambda(s) - \kappa}{v} \cdot \frac{dp_0}{p_0} \tag{3.25}$$

in which, κ and $\lambda(s)$ are elastic stiffness index and elastoplastic stiffness index for loading variation, respectively.

The above simplified model for isotropic stress state is used to the subsequent shakedown modeling, instead of step-by-step calculation of material deformations, although it has a similar formulation as BBM model. To facilitate the shakedown modeling in the transformed internal parameter plane, a simple shape of yield surface (i.e. rectangle) is taken into account in this study and it will be employed in the next section of shakedown modeling.

3.3.3 Plastic shakedown during suction cycles

• Water retention curves during suction cycles

Water retention curve is one of the essential parameters required for hydromechanical modeling in unsaturated expansive soils. Figure 3.4 shows the conceptual evolution of water retention curve during suction cycles.

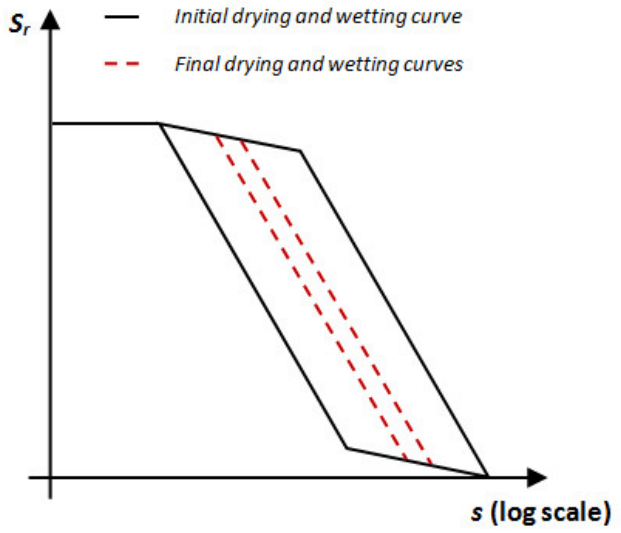

FIGURE 3.4: Evolution of the water retention curves with suction cycles.

In this figure, there is an evident hysteresis phenomenon before suction cycles. The hysteresis becomes smaller with the following suction cycles. However, it can not be completely eliminated even though the equilibrium state is reached after several suction cycles. This hydraulic behavior indicates that plastic shakedown occurs during suction cycles. In other words, plastic shakedown should be used to model hydromechanical behavior of expansive soils when wetting and drying cycles are applied.

• Plastic shakedown modeling

The proposed yield surface with a kinematic hardening for suction variations can be written as:

$$f = |s - y_\alpha| - s_\alpha \tag{3.26}$$

where, s_α is the threshold value of elastic limit for suction variation.

The kinematic hardening variable y_α can be related to the plastic strain,

$$y_\alpha = h \cdot \epsilon^p \tag{3.27}$$

where, h is the kinematic hardening modulus,

To perform shakedown modeling, the proposed yield surface is presented in the transformed internal parameter y_α as well as the preconsolidation stress p plane (see Figure 3.5). In this $y_\alpha - p$ plane, the rectangular yield surface that characterises the behavior of the expansive soil, translated between the minimum suction s_{min} position and the maximum suction s_{max} position during the wetting and drying cycles.

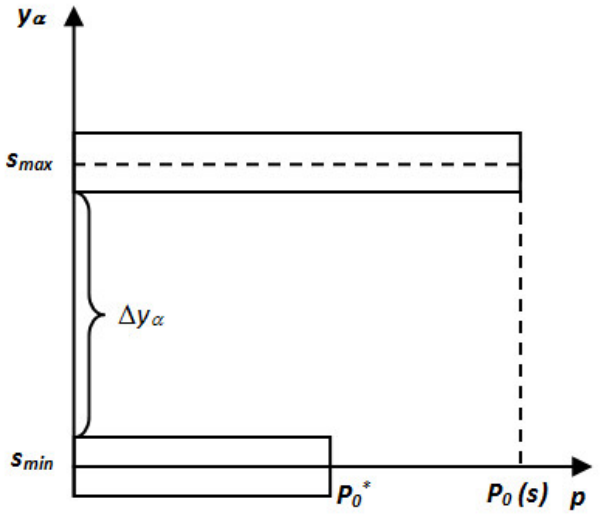

FIGURE 3.5: $y_\alpha - p$ (transformed internal parameter - preconsolidation stress) plane for plastic shakedown.

When the extreme positions of the two convex have no common part on the transformed internal parameter axis, plastic shakedown occurs. Therefore, the variation of the volumetric plastic deformation $\Delta\epsilon^p_{vs}$ during wetting and drying cycles can be computed by:

$$\Delta\epsilon^p_{vs} = \frac{1}{h} \cdot \Delta y_\alpha \tag{3.28}$$

where, h the kinematic hardening modulus, is a constant material parameter at the given net mean stress, (more discussions are presented in section 3.4.3). Additionally, Δy_α can be determined in the transformed internal parameter plane when the minimum suction and maximum suction are given.

3.3.4 Elastic behavior at the equilibrium state

With the application of wetting and drying cycles, the equilibrium state can be obtained at the end of the suction cycles in the volumetric strain-suction plane (see Figure 3.6) where no additional plastic strain accumulation can be observed. Because we have far too few experimental points at the equilibrium state, the hysteresis phenomenon can not be described precisely. Consequently, a linear variation of the elastic strain with the suction is supposed at the equilibrium state.

It can be written as:

$$\Delta\epsilon^{e}_{vs} = \frac{\kappa_s}{v} \cdot \frac{\Delta s}{s + p_{at}} \tag{3.29}$$

where, κ_s is the elastic stiffness index for suction variation.

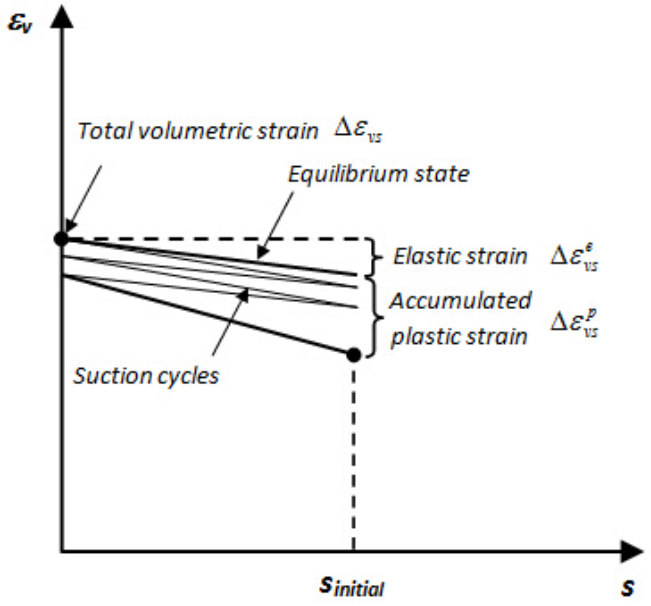

FIGURE 3.6: Variation of the volumetric strain with suction during the suction cycles.

Here, the resilient modulus E_r is defined and the above equation becomes:

$$\Delta\epsilon^{e}_{vs} = \frac{1}{E_r} \cdot \Delta s \tag{3.30}$$

with

$$\frac{1}{E_r} = \frac{\kappa_s}{v} \cdot \frac{1}{s + p_{at}} \tag{3.31}$$

where, E_r can be calibrated from the elastic equilibrium state of suction-controlled odometer tests. In this study, the resilient modulus E_r changes with the net mean

stresses, independent of initial suction state. Its evolution law will be presented in the section 3.4.2 and this parameter will be used to determine the elastic deformation at the equilibrium state.

3.3.5 Coupling between suction cycles and mechanical behavior

Gens and Alonso (1992) stated that the fatigue of swelling associated with suction cycles under a vertical pressure is due to the macrostructural softening induced by microstructural expansion. In this case, the loading collapse yield surface (called PLC curve in this study) presented in the net mean stress-suction plane shifts to the left of the initial PLC yield surface (see Figure 3.7). On the other hand, an increase in shrinkage deformation causes the shifting of the loading collapse yield surface to the right of the initial PLC yield surface accompanied by macrostructural hardening behavior.

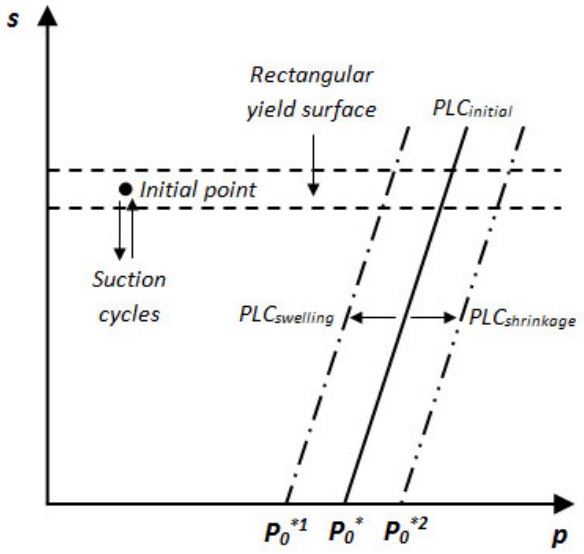

FIGURE 3.7: Evolution of the initial yield surface with suction cycles for expansive soils in (suction- preconsolidation stress) plane.

Experimental evidence shows a strong dependency of the preconsolidation stress on the macrostructural plastic strain during wetting and drying cycles. For simplicity, we assume that the increment of preconsolidation stress is proportional to the variation of volumetric plastic strain due to suction cycles, the same equation as BBM (or BExM):

$$\frac{\Delta p_0^*}{p_0^*} = \frac{1+e_0}{\lambda(0)-\kappa} \cdot \Delta\epsilon_{vs}^p \tag{3.32}$$

where, $\lambda(0)$ is stiffness parameters for changes in net mean stress at the saturated states and κ is elastic stiffness parameter for changes in net mean stress.

Based on this equation, the volumetric plastic deformation ϵ_{vs}^{p} estimated by shakedown analysis (see section 3.3.3), can be used to determine the preconsolidation stress for the saturated state p_0^*. Thereafter, this saturated preconsolidation stress p_0^* is used in Equation 3.21, to find the preconsolidation stress $p_0(s)$ as well as the final position of the PLC yield surface. Finally, the coupling law between the suction cycles and subsequent mechanical behavior is developed.

3.4 Calibration and validation of the proposed model

In the following section, the parameters of the proposed shakedown-based model as well as the coupling model between suction cycles and the mechanical behavior are firstly calibrated and then validated using the oedometer experimental results.

3.4.1 Test description

This part presents an experimental study performed on a bentonite/silt mixture using the suction-controlled oedometer device. Several cycles of the suctions ranging between 8 and 0 MPa at different constant loads are firstly applied, then at the end of these wetting and drying cycles, a loading/unloading cycle at the three indicated suctions is applied. All these tests were performed by Dr. Nowamooz at University of Nancy[117] and these test results will be used to model the hydromechanical behavior of expansive soils.

• Tested materials

The tests were performed on an artificially prepared mixture of 40% silt and 60% bentonite. The mineralogical composition of the material was determined by X-ray diffraction. The silt contains 60% quartz, 20% calcium montmorillonite, 11% feldspar and the remaining component was comprised of kaolinite and mica. The bentonite was composed of more than 90% of calcium montmorillonite.

The size of the particles used to prepare the samples was less than 400 μm (obtained by sieving). The materials were mixed together and wetted up to a gravimetric water content of 15%±0.3% (dry side of optimum). Then the mixtures were statically compacted under the selected vertical pressures: 1000, 2000 and 3000kPa

and three dry densities were formed: 1.27, 1.48 and 1.55 $Mg{\cdot}m^{-3}$, corresponding to loose (L), intermediate (I) and dense (D) soils, respectively.

Under these conditions, the initial suction of the samples, measured by the filter paper method (ASTM, 1995), was about 20±1 MPa. As the suction value can be considered independent of the mechanical loading for the samples compacted on the dry side of optimum, the initial suction of all the compacted samples is regarded as 20 MPa at the initial water content of 15%.[118**?**]

• Hydraulic tests during a wetting and drying path

The variation in the degree of saturation relative to the suction within a single wetting and drying cycle is presented in Figure 3.8 for the loosely and densely compacted mixtures. Points A and A′ in this figure indicate the initial state of the loose and dense samples, corresponding to an initial suction of 20 MPa with an initial water content of 15%. A wide range of suctions between 0 and 287.9 MPa was applied to the samples, producing a wetting path for the suctions between 20 and 0 MPa and a drying path for the suctions between 20 and 287.9 MPa. All of the saturated samples were finally dried again with a maximum suction of 287.9 MPa.

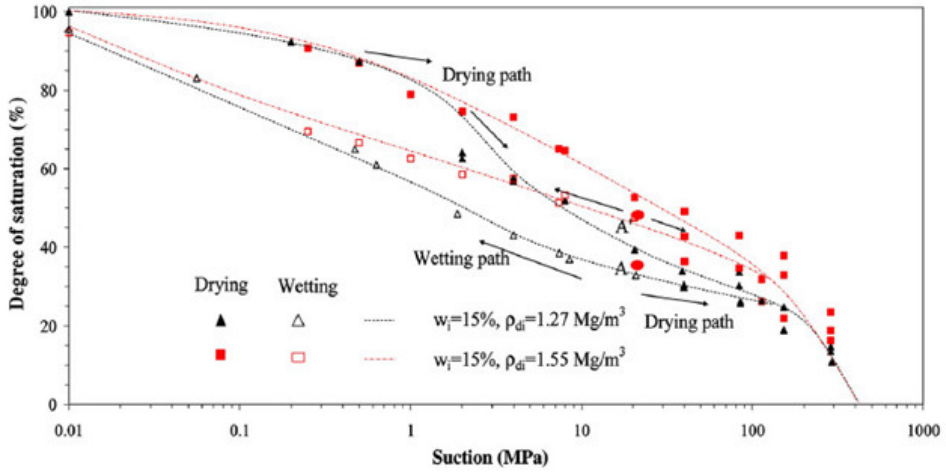

FIGURE 3.8: Void ratio variation of densely and loosely compacted bentonite and silt mixtures during a single wetting and drying cycle (Nowamooz and Masrouri, 2011).

This test shows an obvious retention behavior for both loose samples and dense samples. Because of a large variation of pore size distribution for loose samples, its retention loop is greater than that of dense samples. Experimental evidence demonstrates that the retention loop decreases with the number of suction cycles,

but the hysteresis behavior can not be eliminated at the end of wetting and drying cycles even though the equilibrium state is reached for these samples. This point will be proved in the following cyclic suction-controlled test, where a small loop is obtained for dense samples after wetting and drying cycles. Eventually, plastic shakedown occurs for the studied materials during wetting and drying cycles.

• Cyclic suction-controlled tests

A schematic representation of oedometer device used for the cyclic suction-controlled test is presented in Appendix 1 and the loading program for the loose, intermediate and dense expansive soils is presented in Appendix 2. Figure 3.9 shows the void ratio variation versus suction of the loose, intermediate and dense samples for different applied stresses: 15, 30 and 60 kPa. For all tests, the first wetting path produced the swelling strains. During the following suction cycles, the loose samples present a shrinkage strain accumulation while a swelling strain accumulation is obtained for dense samples before reaching a unique equilibrium state at the end of the wetting and drying cycles. The swelling strain accumulation can also be observed for intermediate samples during suction cycles and at the end of the cycles, the intermediate samples reach the same equilibrium state as the loose and the dense samples. This final equilibrium state is considered to be independent of the initial dry density of expansive soil samples. Additionally, we note that less suction cycles are needed for intermediate samples to reach the unique equilibrium state, because its initial state is not too far from this equilibrium state.

• Compression tests after suction cycles

A loading/unloading cycle was applied at three constant suctions after having reached the equilibrium state at the end of successive wetting and drying cycles. These applied suctions were 0 MPa for L1, I1, D1 tests, 2 MPa for L2, I2, D2 tests and 8 MPa for L3, I3, D3 tests (see Appendix 2). The test results were plotted in Figure 3.10. In these figures, the compression curves with the application of suction cycles at the different constant suctions gradually converge towards the normally consolidated curve (NCC). Besides, it is also noted that the wetting and drying cycles stiffen the loose initial state samples while these cycles soften the dense initial state samples. For the intermediate initial state samples, small softening due to the wetting and drying cycles can be observed, because this state is close to the equilibrium state.

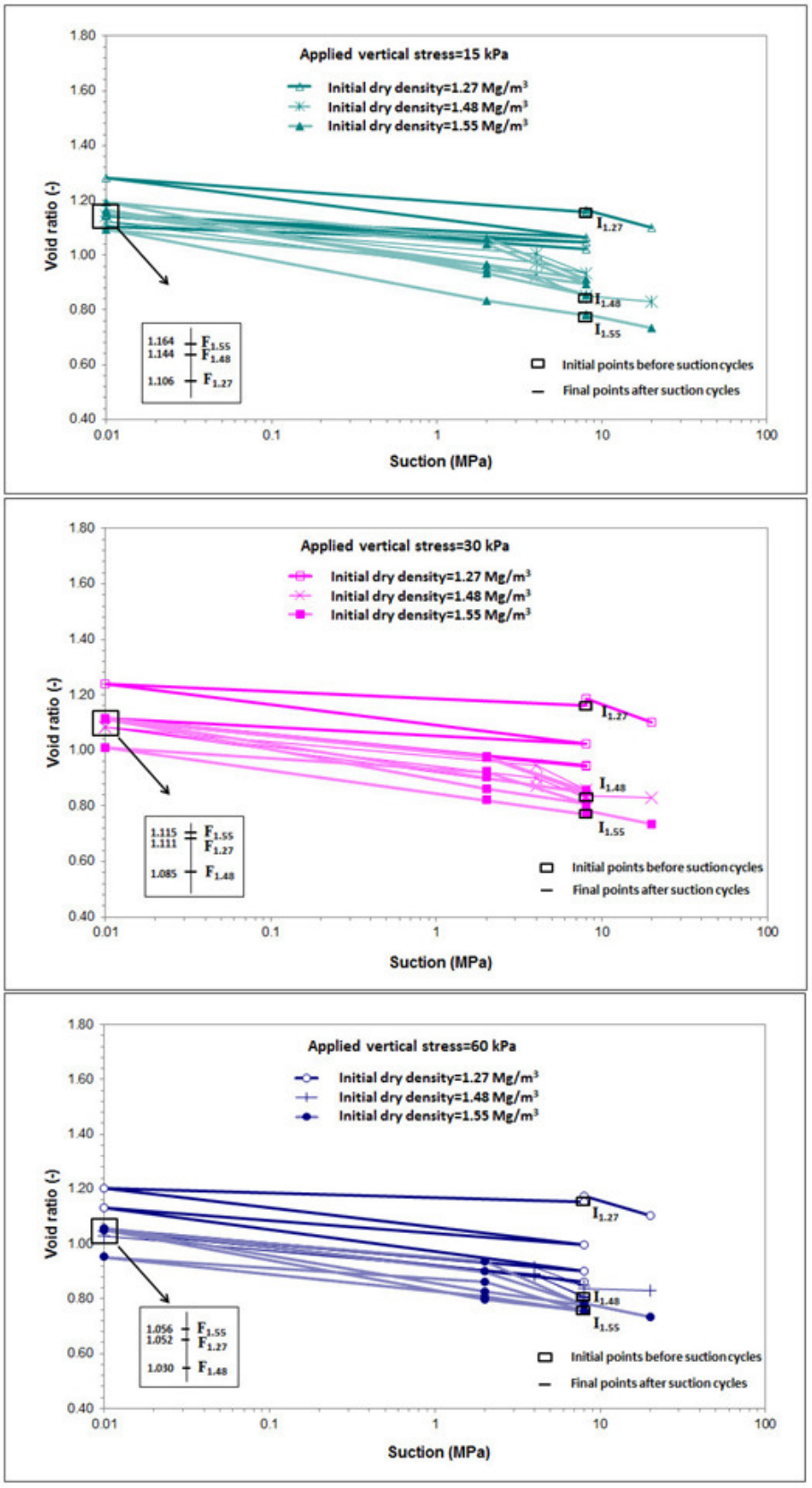

FIGURE 3.9: Cyclic oedometer tests on loose, intermediate and dense expansive soils at the constant vertical pressure of 15, 30, 60 kPa

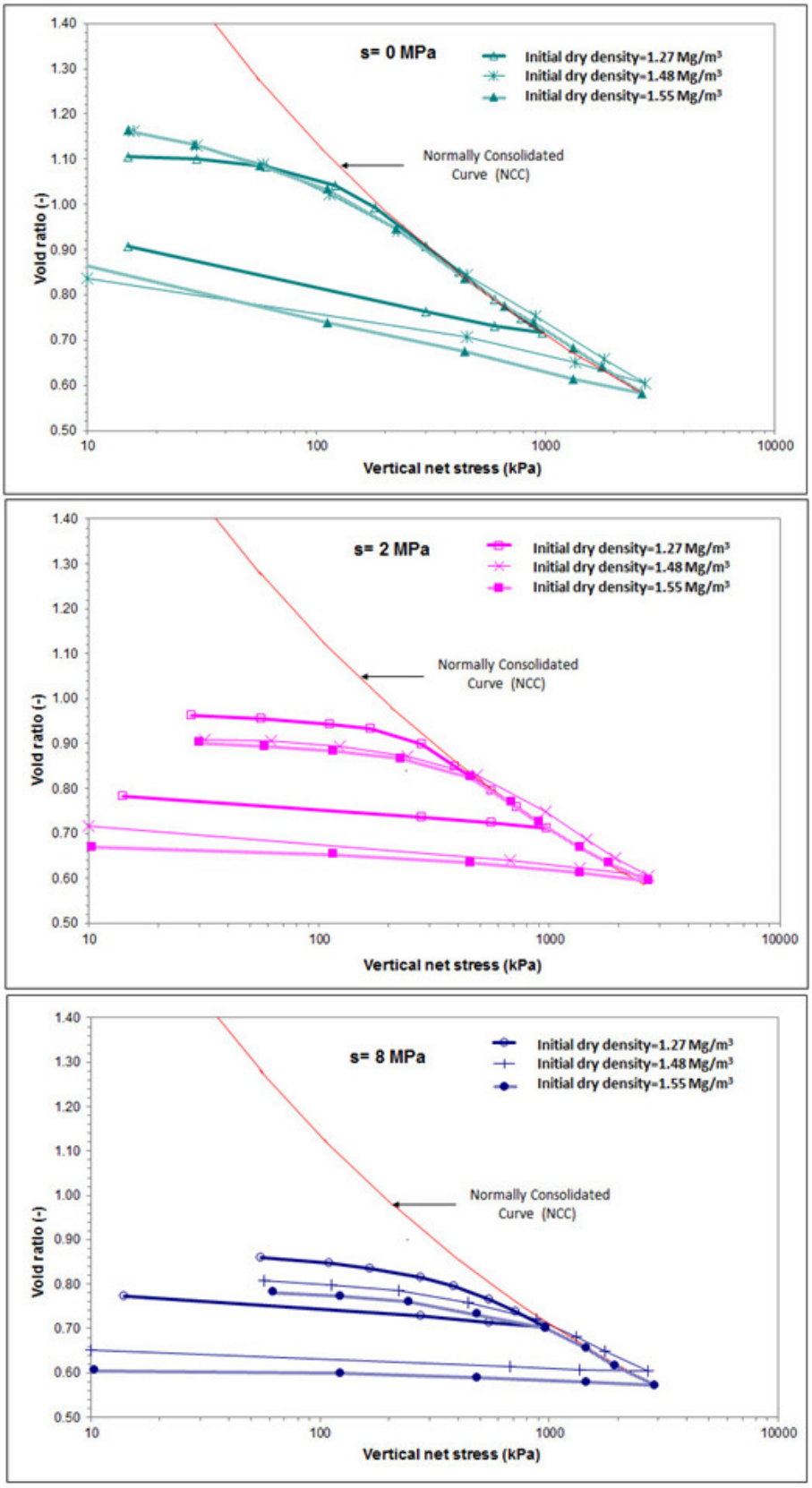

FIGURE 3.10: Loading/unloading tests with the application of suction cycles at the constant suction of 0, 2 and 8 MPa

3.4.2 Elasticity parameters

The elasticity parameter (E_r) can be calibrated by the elastic equilibrium state of suction-controlled tests reached after several wetting and drying cycles. Tables 3.1 summarizes the E_r value of loose and dense samples for the different net mean stresses 15, 30 and 60 kPa. In Figure 3.11, we propose a linear variation of the inverse of the elasticity parameter ($1/E_r$) with the net mean stress (p):

$$1/E_r = C \cdot p + D \tag{3.33}$$

where, C and D are constant parameters related to the initial dry density of expansive soil, given in Table 3.2 for the loose and dense samples.

TABLE 3.1: Calibrated resilient modulus for the loose and dense initial states

Net mean stress (kPa)	15	30	60
E_r value for loose sample (MPa)	204	103	90
E_r value for dense sample (MPa)	53	55	51

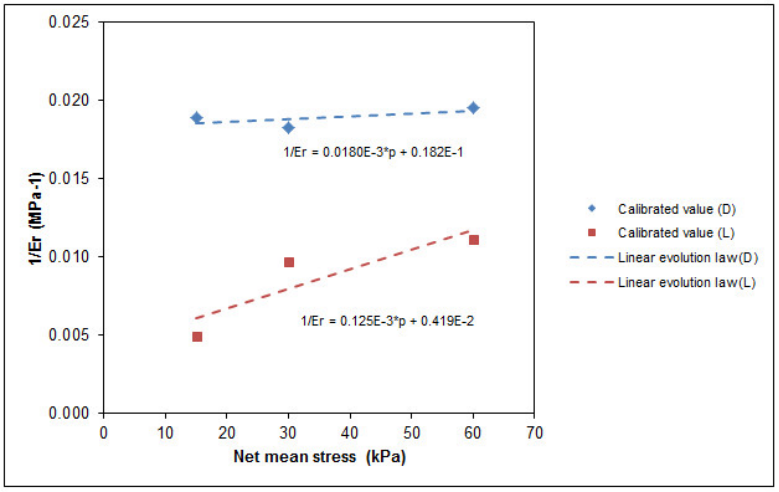

FIGURE 3.11: Evolution of the inverse of the resilient modulus with net mean stress for the loose and dense samples.

TABLE 3.2: Variations of the parameters C and D for the loose and dense initial states

Parameters	C(MPa^{-2})	D(MPa^{-1})
Loose(γ_d=1.27 Mg·m^{-3})	0.125	0.419E-2
Dense(γ_d=1.55 Mg·m^{-3})	0.180E-1	0.182E-1

3.4.3 Plasticity parameters

For the application of Zarka shakedown theory on expansive soils, the threshold value of elastic limit for suction variation (s_α) may be considered very small and therefore it is neglected in this work.

Since we know the accumulated plastic deformation ($\Delta\epsilon_{vs}^{p}$) as well as the transformed internal parameter (Δy_α) at a given net mean stress, the hardening modulus (h) can be deduced according to Equation 3.28. Because of the volumetric shrinkage strains for the loose samples during the suction cycles, a positive sign was attributed to h values. On the other hand, a negative sign was used for the dense samples because of the swelling strains. Tables 3.3 summarizes these calibrated parameters of loose and dense samples.

TABLE 3.3: Calibrated hardening modulus for the loose and dense initial states

Net mean stress (kPa)	15	30	60
h value for loose sample (MPa)	126	79	60
h value for dense sample (MPa)	-125	-163	-540

Figure 3.12 illustrates the evolution of the inverse of the hardening modulus ($1/h$) with the net mean stress (p). The larger the applied vertical pressure, the larger the inverse of the hardening modulus ($1/h$). In other words, the accumulated plastic deformation increases with an increase of the net mean stress. We propose additionally a linear variation of the inverse of the hardening modulus ($1/h$) with the net mean stress (p):

$$1/h = E \cdot p + F \tag{3.34}$$

where, E and F are constant parameters, also related to the initial dry density of expansive soils, given in Table 3.4 for the loose and dense samples.

TABLE 3.4: Variations of the parameters E and F for the loose and dense initial states

Parameters	E(MPa^{-2})	F(MPa^{-1})
Loose(γ_d=1.27 Mg·m^{-3})	0.188	0.589E-2
Dense(γ_d=1.55 Mg·m^{-3})	0.138	-0.101E-1

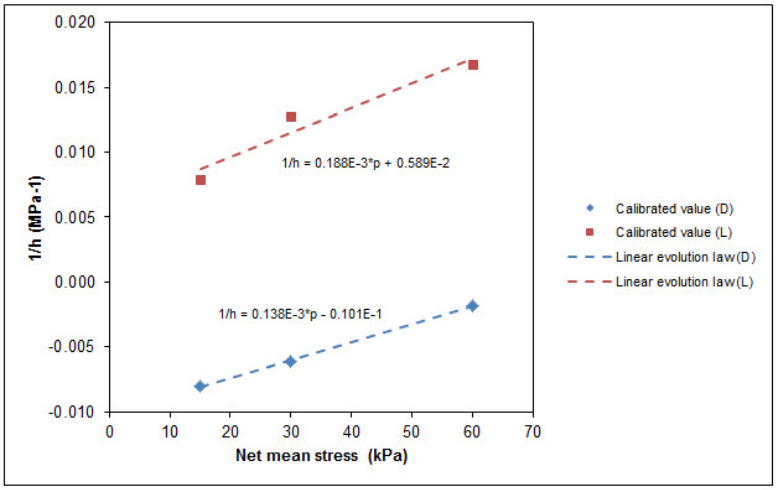

FIGURE 3.12: Evolution of the inverse of the hardening modulus with net mean stress for loose and dense samples.

Figure 3.13 and 3.14 present the model calibrations compared with the experimental results for the loose and dense samples at the net mean stresses of 15, 30 and 60 kPa. It can be observed that the wetting and drying cycles generate the shrinkage strain accumulation for the loose samples and the swelling strain accumulation for the dense samples. It also can be noted that model estimations produce a good agreement with the test results at the different net mean stresses.

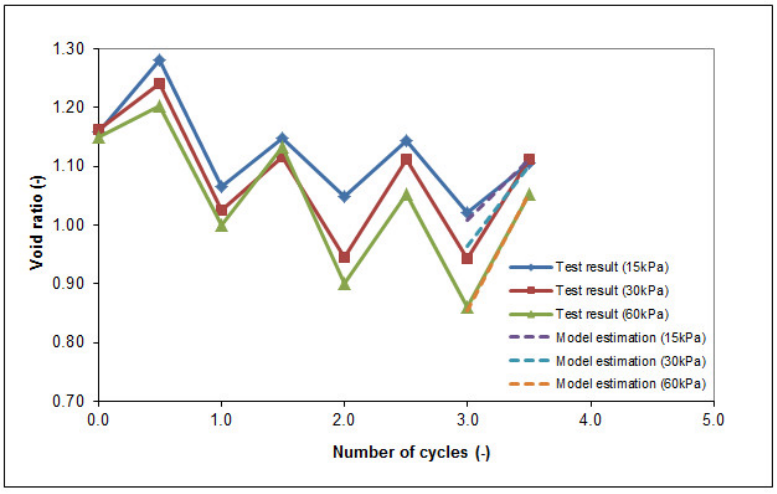

FIGURE 3.13: Comparison of test results with model calibrations for the loose samples at different net mean stresses.

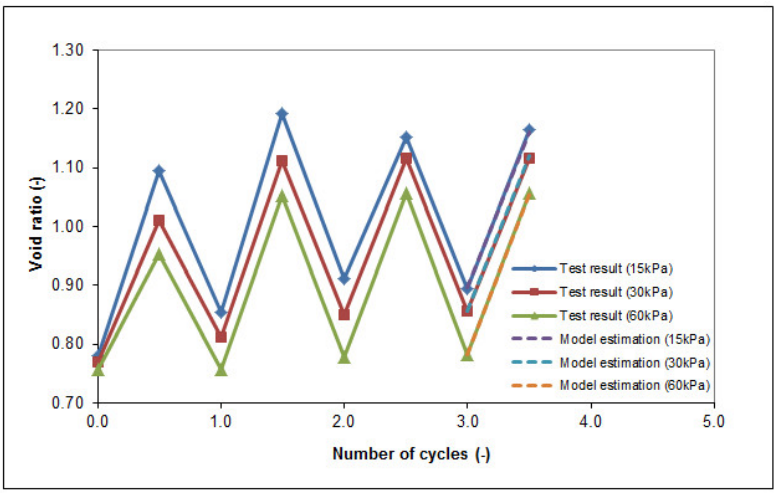

FIGURE 3.14: Comparison of test results with model calibrations for the dense samples at different net mean stresses.

3.4.4 Model validation of shakedown-based model

The validation of the model is carried out with the test results obtained for the samples compacted at the intermediate initial state. The linear variation of the inverse of the elasticity parameter $(1/Er)$ as well as the hardening modulus $(1/h)$ with the net mean stresses is interpolated in Figures 3.15 and 3.16 for the intermediate samples. The predicted parameters C, D, E and F in Equations 3.33 and 3.34 are presented in Table 3.5 and 3.6. For intermediate samples, the threshold value of elastic limit for suction variation (s_α) is also considered negligible.

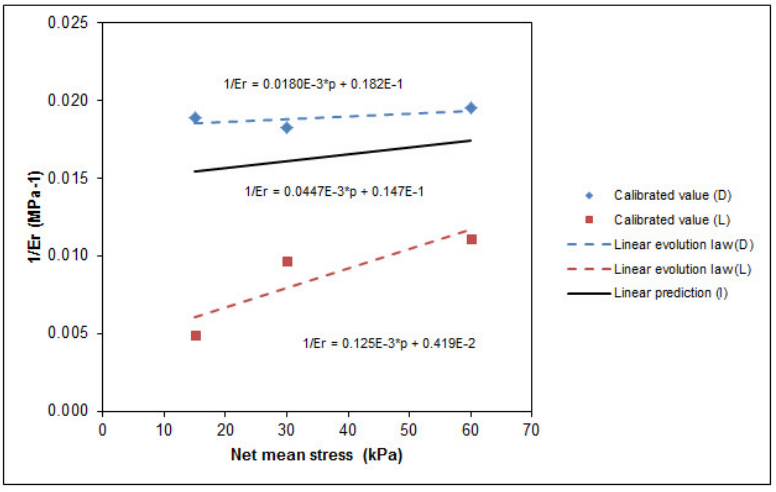

FIGURE 3.15: Prediction of the inverse of the resilient modulus $(1/E_r)$ with net mean stress for intermediate samples based on the estimated parameters (C and D) of the loose and dense samples.

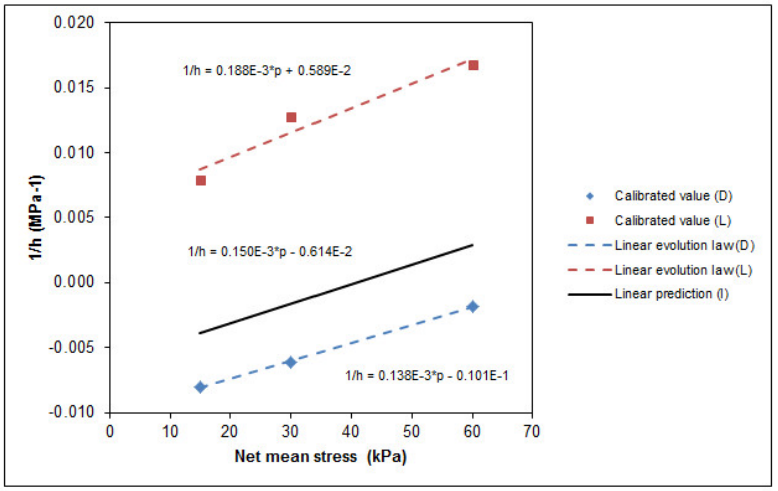

FIGURE 3.16: Prediction of the inverse of the hardening modulus ($1/h$) with net mean stress for intermediate samples based on the estimated parameters (E and F) of the loose and dense samples.

TABLE 3.5: Model parameters C and D for the intermediate initial states

Parameters	$C(\text{MPa}^{-2})$	$D(\text{MPa}^{-1})$
Intermediate(γ_d=1.48 Mg·m^{-3})	0.447E-1	0.147E-1

TABLE 3.6: Model parameters E and F for the intermediate initial states

Parameters	$E(\text{MPa}^{-2})$	$F(\text{MPa}^{-1})$
Intermediate(γ_d=1.48 Mg·m^{-3})	0.150	-0.614E-2

Based on these predicted model parameters, the model validation is conducted for the intermediate samples. Figure 3.17 represents the comparison between the test results and the model predictions at the different net mean stresses. For these samples, the initial state is close to the reversible line, which means that less suction cycles are needed to obtain the equilibrium state. The relative error varies between 5% and 8% confirming the capacity of the proposed model to predict the accumulated plastic strains.

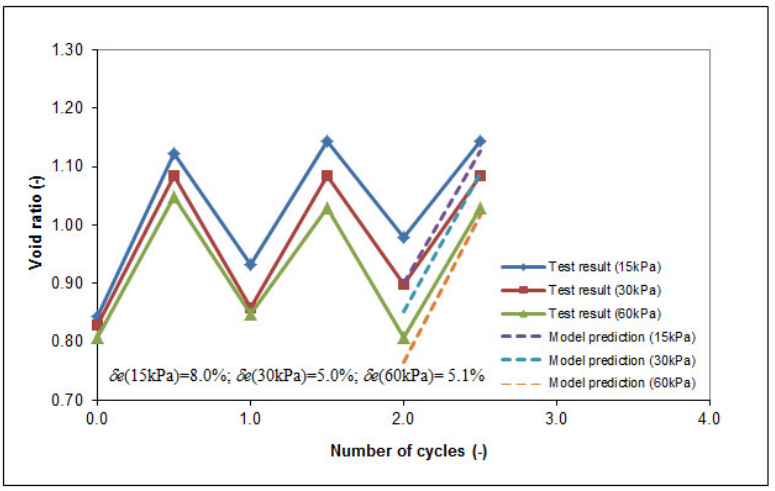

FIGURE 3.17: Comparisons of test results with model predictions for intermediate sample at the different net mean stresses.

The model calibration and validation of shakedown-based model present a good agreement with the experimental results. This simplified shakedown model is able to simulate the behavior of expansive soils with less model parameters, including the accumulated plastic strains during suction cycles and the prediction of final equilibrium state at the end of suction cycles. However, this model also presents some limitations:

- Only the deformation at the stabilised limit state can be determined, which indicates that the proposed shakedown model is not able to predict the deformation at the intermediate state between suction cycles;
- Because two supposed linear evolution laws for elasticity parameter and plasticity parameter are used in this model, more experimental results of expansive soils should be used to validate the shakedown model to check its capacity;
- The assumption that SI and SD yield surfaces are always activated during suction cycles (i.e. s_α is negligible) facilitates the computation of accumulated plastic strains, but the model capacity is also reduced that the elastic strain during small wetting or drying can not be determined.

3.4.5 Model validation of coupling behaviors

In this section, the coupling hydromechanical parameters of the proposed model are first determined from the equilibrium state of loading/unloading tests on the studied samples after suction cycles. Then, these calibrated parameters were

used to predict the preconsolidation stresses at different suctions for the loose, intermediate and dense samples without the suction cycles.

Table 3.7 introduces the required coupling parameters (A, B, $\lambda(0)$ and κ) at the equilibrium state for the studied materials. Parameters A and B (Equation 3.21) can be determined from loading/unloading tests at the end of suction cycles[119, 120] to illustrate the final PLC curve for the studied samples. The final PLC is unique for all the studied samples in this study. For the sake of simplicity, a linear variation of preconsolidation stress with suction is proposed in Equation 3.21. We suppose the same slope of PLC curve for the different initial states of expansive soils without and with suction cycles. It is considered that κ (the elastic stiffness parameter for changes in net mean stress) is independent of the suction state. Nowamooz[117] suggests that the compression curves of an expansive soils compacted at different initial states after several suction cycles converge towards the unique normally consolidated curve, which means that a constant value $\lambda(0)$ can be used for all different initial states of the expansive soil.

TABLE 3.7: Parameters of the coupling model at the equilibrium state

Parameters	A(-)	B(kPa)	$\lambda(0)$	κ
Equilibrium state	0.061	120	0.22	0.02

After the calibration of the coupling parameters, the saturated preconsolidation stress variation (Δp_0^*) in Equation 3.32 is known because the accumulated plastic strain during suction cycles ($\Delta \epsilon_{vs}^p$) can be derived by the shakedown-based model presented in section 3.3.3. Figure 3.18 plots the PLC before suction cycles, the PLC after suction cycles as well as the experimental values of preconsolidation stress before and after suction cycles for loose and dense samples. A hardening plasticity occurs for the loose samples because of the shrinkage strain accumulations during suction cycles, while a softening plasticity is observed for dense samples due to the accumulated swelling strain during cycles.

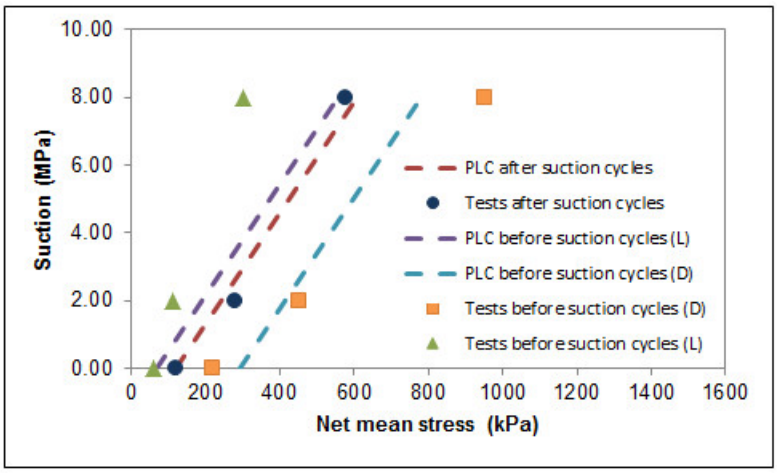

FIGURE 3.18: Initial PLC, final PLC, the test values of preconsolidation stress before and after suction cycles for loose and dense samples.

The coupling parameters are then used to predict the initial preconsolidation stress without suction cycles for the intermediate samples. The required coupling parameters for the intermediate samples are presented in Table 3.7. Figure 3.19 compares the model prediction for the intermediate samples with the experimental results. It shows that our proposed method is able to predict the mechanical behavior during wetting and drying cycles. A softening plasticity can be observed the same as the dense samples, but the value is very small because the initial intermediate state is close to the finial equilibrium state.

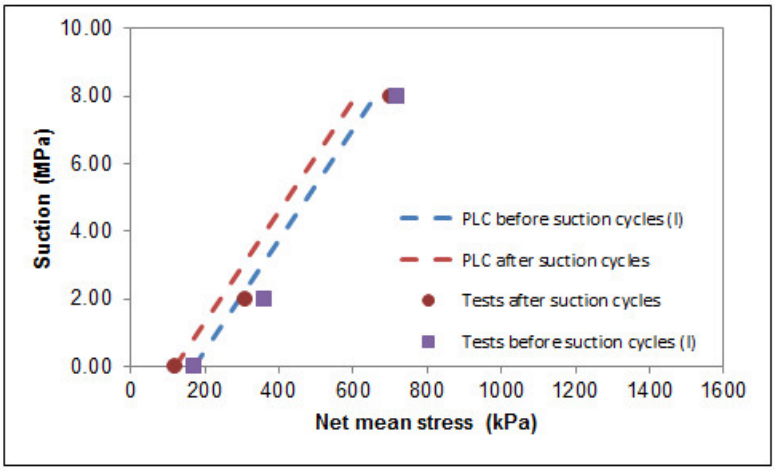

FIGURE 3.19: Initial PLC, final PLC, the test values of preconsolidation stress before and after suction cycles for intermediate soils.

One point should be mentioned that the predicted value of preconsolidation stress

at a higher suction does not correspond well with the experimental values (the preconsolidation stress is overestimated for the loose sample and underestimated for the dense samples), only because a simple linear variation of preconsolidation stress with the suction is used in this study. A non-linear variation (i.e. LC curve defined in BBM or BExM) can be used to improve the model simulation in the future modeling.

3.5 Sensitivity analysis of model parameters

The purpose of this section is to develop a sensitivity analysis of the parameters characterizing the model. Our sensitivity analysis only focuses on the shakedown-based model and the simplest sensitivity analysis (one-at-a-time method) is employed to isolate the most influential model parameters.

As we have seen, the proposed shakedown model requires five parameters to be defined: parameters C and D for the linear evolution law of elasticity parameters $(1/E_r)$ determined from the equilibrium state at the end of the wetting and drying cycles; parameters E and F for the linear evolution law of hardening modulus $(1/h)$ calibrated from the accumulated plastic strains during wetting and drying cycles; and the threshold value of elastic limit for suction variation (s_α), taken zero for the sake of simplification.

Our application of the one-at-a-time sensitivity analysis consists in four steps: (i) defining the acceptable variation ranges of the input parameters; (ii) implementing the one-at-a-time methodology to calculate the model outputs based on the previously defined input ranges; (iii) presenting these model outputs in the same coordinate plane, convenient to distinguish the different influences of model parameters; (iv) isolating the most influential input parameters from other model parameters to finish the one-at-a-time sensitivity analysis.

The input ranges ($\mp 10\%$ of the model parameters C, D, E and F) are selected in this study as the acceptable input ranges to analyze the parameter sensitivity. Because the model parameter s_α is considered negligible, the 5% and 10% increments relative to the reference value of s_α are chosen to tell its influence on the model response.

In this section, we only present the sensitivity analysis for the loose samples, because the same procedure can be used for other initial states of the studied expansive soils. Figure 3.20 $\sim$ 3.22 illustrate the sensitivity analysis of the plasticity

parameters in the shakedown model. From these figures, we can observe that the most influential parameters on plasticity are E and F, compared with s_α whose influence can be taken negligible (only 2.5% variation of model outputs due to 10% variation of parameter inputs). Parameter E shows less influence than parameter F on the plastic deformation at lower level of the stress. With the increase of stress, the influence of parameter E on the plasticity becomes dominate, while the influence of parameter F on plastic deformation is relatively stable in Figure 3.21. Additionally, the maximum influences of both parameters on model outputs are less than 6.8% when 10% variation of parameter inputs are applied.

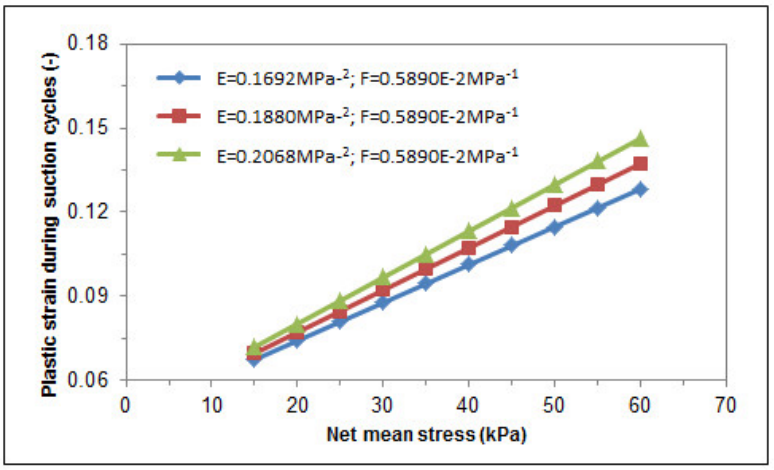

FIGURE 3.20: The influence of parameter E on the response of shakedown model.

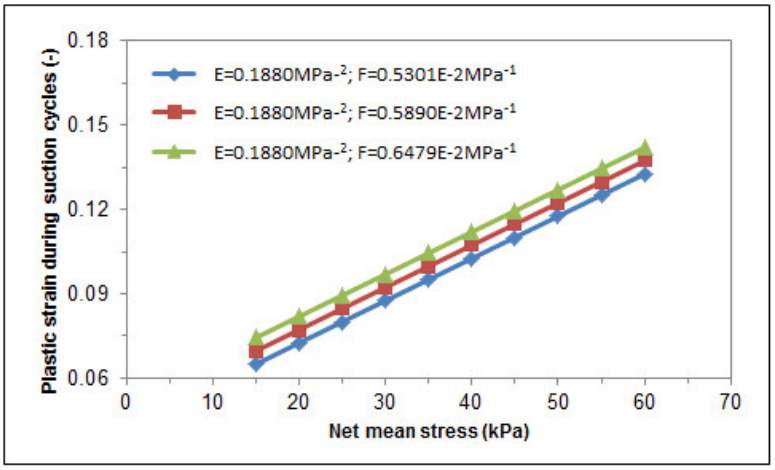

FIGURE 3.21: The influence of parameter F on the response of shakedown model.

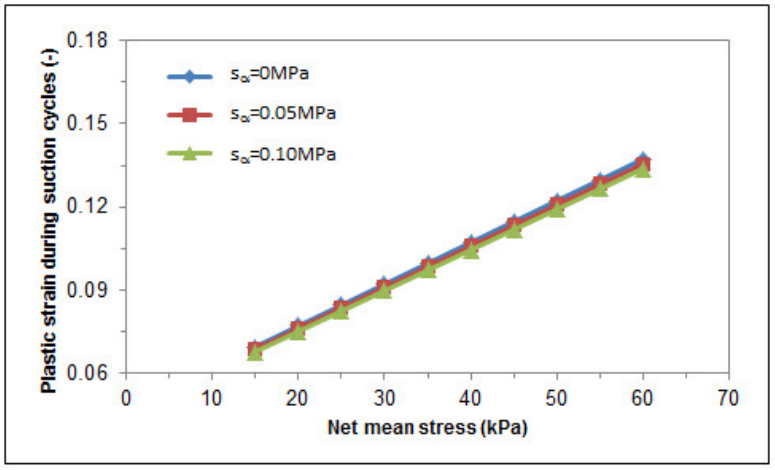

FIGURE 3.22: The influence of parameter s_α on the response of shakedown model.

Owing to the same methodology of the sensitivity analysis being used on elasticity parameters C and D, the results of this sensitivity study are directly presented in Figure 3.23 and 3.24. From these figures, the same observations for elasticity parameters are obtained, as the plasticity parameters E and F, because they have a similarly linear evolution law, but the model response varies from 3% to 7% due to 10% variation of elasticity parameter inputs.

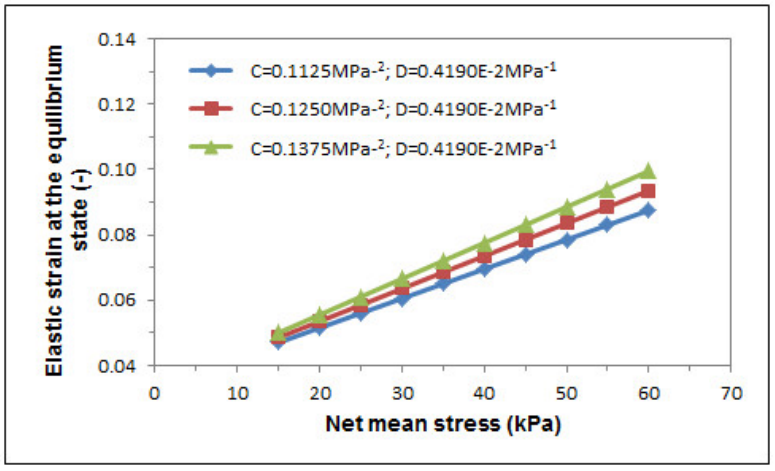

FIGURE 3.23: The influence of parameter C on the response of shakedown model.

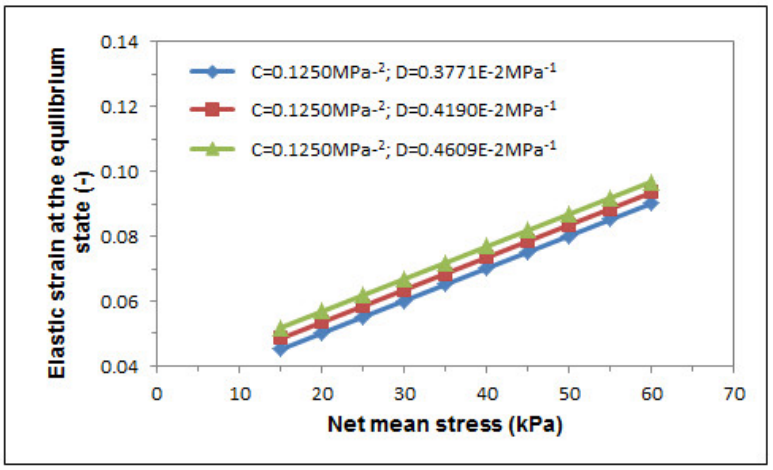

FIGURE 3.24: The influence of parameter D on the response of shakedown model.

3.6 Conclusion

In this chapter, a linear kinematic hardening model is developed to characterize the hydro-mechanical behavior of unsaturated expansive soils. The shakedown behavior is investigated in the plane of transformed internal parameter – net mean stress with a rectangular shape of the yield surface. During wetting and drying cycles, plastic shakedown eventually occurs because there is no intersection between two extreme positions of the convex.

Elasticity parameters and plasticity parameters are required for the proposed shakedown model. Elasticity parameters C and D are determined from the equilibrium state of suction-controlled oedometer tests for the linear change of $(1/E_r)$ with net mean stress. Then the parameters E and F for the linear evolution law of hardening modulus $(1/h)$ are calibrated by the accumulated plastic strains during suction cycles from suction-controlled oedometer tests. The last plasticity parameter is the threshold value of elastic limit for suction variation (s_α), we take it small, equal to 0 MPa in this study.

Apart from the shakedown-based model, the coupling law between the suction cycles and the mechanical behavior is also developed to illustrate the translation of the pseudo loading collapse (PLC) curve. The model parameters of this coupling law are determined from loading/unloading tests of the studied materials. Thereafter, the comparisons of test results with model predictions are carried out to show the capacity of proposed method.

At the end of this chapter, the sensitivity analysis of shakedown model parameters is carried out. From these results, the influence of model parameters D and F on model output is evident at lower vertical stress while model parameters C and E become more influential at the higher vertical stress. Additionally, the influence of parameter s_α on plastic deformation can be considered negligible by comparing all the model responses among different parameter inputs.

Chapter 4

Finite Element Modeling of In-situ Behavior of Expansive Soils

4.1 Introduction

Finite Element Method (FEM) has been developed over the last fifty years as the most powerful and general numerical method for the analysis of engineering problems. Its use and application to geotechanical engineering is now widespread. In this chapter, we will introduce this numerical method to simulate the response of a geotechnical problem when cyclic climate changes and different external loads are applied.

The analytical constitutive model based on shakedown concept presented in the previous chapters has shown in details that it can describe the response of unsaturated expansive soils subjected to wetting and drying cycles. It is also clear from the discussion of key aspects of the shakedown framework in previous sections that the extension of this analytical model to two-dimensional (or three-dimensional) finite element calculations is readily able to be developed.

We start this chapter by presenting a group of governing equations used to model the response of an elasto-plastic engineering structure when wetting and drying cycles are applied. These equations are extended from the proposed shakedown-based constitutive model presented in previous chapters. Then, numerical simulations of an elasto-plastic structure for different initial states of an expansive soils are carried out, to demonstrate that the developed code is able to calculate the plastic strain field and the inelastic displacement field. Additionally, the finite element code CAST3M (http://www-cast3m.cea.fr/)[121] is introduced to implement finite element modeling of the aforementioned structure.

4.2 Global evolution of a structure

In this section, an elasto-plastic structure, made up of an unsaturated expansive soil is considered. Its boundary Γ is subjected to the imposed surface forces $F_i(x)$ on Γ_{F_i} partition and the prescribed surface displacements $U_j(x)$ on Γ_{U_j} partition. The body forces $X_j(x)$ and the initial strain $\epsilon^I_{ij}(x,0)$ are defined in the volume V. Here, $'x'$ is the space coordinate vectors. Moreover, the wetting and drying cycles are also defined in the volume V and these cycles are imposed between extremely dry and wet conditions.

4.2.1 Mechanical analysis

In this study, we suppose that the studied elasto-plastic structure meets the requirements of small deformations.

In-situ stress analysis is firstly performed before shakedown modeling of the structure subjected to wetting and drying cycles. Considering the finite element calculation with the imposed boundary conditions, the stress state can be determined by the linear elasticity:

$$\sigma^M_{ij}(x,t) = D_{ijkl} \cdot [\epsilon^M_{ij}(x,t) - \epsilon^I_{ij}(x,0)] \tag{4.1}$$

in which D_{ijkl} is the matrix of elastic moduli, $\sigma_{ij}^{M}(x,t)$ is the stress tensor and $\epsilon_{ij}^{M}(x,t)$ is the strain tensor. Here, the superscript $'M'$ represents the parameters calculated from mechanical analysis. With this calculation, the net mean stress for each point in the structure can be determined, which will be used in the following shakedown modeling.

4.2.2 Real response of suction variation

In the case of suction variation in structure volume V, the real response of the studied structure can be written as follows:

$$\epsilon_{ij}(x,t) = M_{ijkl} \cdot s_{kl}(x,t) + \epsilon_{ij}^{p}(x,t) + \epsilon_{ij}^{I}(x,0) \tag{4.2}$$

where, the strain tensor $\epsilon_{ij}(x,t)$ is kinematically admissible with $U_j(x,t)$ on Γ_{U_j} and the suction tensor $s_{kl}(x,t)$ is statically admissible with the suction variation in volume V. M_{ijkl} is the compliance elasticity matrix for suction loading and $\epsilon_{ij}^{p}(x,t)$ is the plastic strain tensor.

In this equation, the isotropic suction tensor $s_{kl}(x,t)$ is defined by:

$$s_{kl} = (u_a - u_w) \cdot \delta_{kl} = s \cdot \delta_{kl} \tag{4.3}$$

where, δ_{kl} is Kronecker delta whose value is 1 when $k = l$ and is equal to 0 otherwise.

The general problem can be decomposed into an elastic part and an inelastic part:

- Elastic response of suction variation

  For 1-D problem, the volumetric strain within the elastic limit of suction can be calculated by the following expression:

  $$d\epsilon_{vs}^{el} = d\epsilon^{el} = \frac{\kappa_s}{v} \cdot \frac{ds}{s + p_{at}} \tag{4.4}$$

  where, κ_s is the elastic stiffness for suction variation, v the soil specific volume, p_{at} the atmospheric pressure and ϵ^{el} is the vertical strain.

  Here, the resilient modulus E_r is defined and the above equation becomes:

  $$d\epsilon^{el} = \frac{1}{E_r} \cdot ds \tag{4.5}$$

with

$$\frac{1}{E_r} = \frac{\kappa_s}{v} \cdot \frac{1}{s + p_{at}} \tag{4.6}$$

In this study, the evolution of E_r with the net mean stress is presented in chapter 3 (see Equation 3.33).

Now, we can easily extend 1-D equation to 3-D problem because the suction is an isotropic tensor, and we have:

$$d\epsilon_{ij}^{el} = M_{ijkl} \cdot ds_{kl} \tag{4.7}$$

where, $M_{ijkl} = \frac{1}{E_r} \cdot I_{ijkl}$ and I_{ijkl} is the identity tensor, $I_{ijkl} = 1$ if $i = j = k = l$. E_r is constant under a given stress state and it can be determined from the equilibrium state after suction cycles.

Taking into account the above equation and the initial strain, the elastic response can be determined as follows:

$$\epsilon_{ij}^{el}(x,t) = M_{ijkl} \cdot s_{kl}^{el}(x,t) + \epsilon_{ij}^{I}(x,0) \tag{4.8}$$

where, the strain tensor $\epsilon_{ij}^{el}(x,t)$ is kinematically admissible with $U_j(x,t)$ on Γ_{U_j} and the suction tensor $s_{kl}(x,t)$ is statically admissible with the suction variation in volume V.

Thus, the elasticity fields U_i^{el} and $\epsilon_{ij}^{el}(x,t)$ can be calculated by an elastic analysis with the given boundary conditions and the compliance elasticity matrix of suction M_{ijkl}.

• Inelastic response of suction variation

Because the general problem consists of elastic part and inelastic part, the inelastic strain can be expressed by the following equation:

$$\epsilon_{ij}^{ine}(x,t) = \epsilon_{ij}(x,t) - \epsilon_{ij}^{el}(x,t) \tag{4.9}$$

where, $\epsilon_{ij}^{ine}(x,t)$ is kinematically admissible with 0 on Γ_{U_j}.

Considering Equations 4.2 and 4.8, the above equation can be written as:

$$\epsilon_{ij}^{ine}(x,t) = M_{ijkl} \cdot \rho_{ij}(x,t) + \epsilon_{ij}^{p}(x,t) \tag{4.10}$$

The residual suction field $\rho_{ij}(x,t)$ is obtained by the difference between total suction and elastic suction fields:

$$\rho_{ij}(x,t) = s_{ij}(x,t) - s_{ij}^{el}(x,t) \tag{4.11}$$

where $\rho_{ij}(x,t)$ is statically admissible with 0 in V.

As long as the plastic strain tensor $\epsilon_{ij}^{p}(x,t)$ and the compliance elasticity matrix of suction M_{ijkl} are known, the inelastic problem can be solved with null boundary condition and the inelastic fields $U_i^{ine}(x,t)$ and $\epsilon_{ij}^{ine}(x,t)$ are obtained.

Eventually, the residual suction tensor can be derived from Equation 4.10 as follows:

$$\rho_{ij}(x,t) = M_{ijkl}^{-1}[\epsilon_{ij}^{ine}(x,t) - \epsilon_{ij}^{p}(x,t)] \tag{4.12}$$

In the following section, this proposed method will be generalized to model the response of the full-scale structures.

4.2.3 Structure with kinematic hardening

The yield surface with kinematic hardening can be defined by:

$$f = \sqrt{(s_{ij} - y_{ij}) \cdot (s_{ij} - y_{ij})} - s_{\alpha} \tag{4.13}$$

where, s_{α} is the threshold value of elastic limit for suction variation and y_{ij} is a kinematic hardening tensor which can be related to the plastic strain,

$$y_{ij} = h \cdot \epsilon_{ij}^{p} \tag{4.14}$$

where, h is the kinematic hardening modulus, a critical important parameter in shakedown modeling. The evolution of kinematic hardening modulus with the net mean stress has been developed for unsaturated expansive soils during suction cycles (see chapter 3). In contrast, this modulus is a constant for steels and it depends on the state of stress for unbound granular materials (Chazallon, 2005, 2007, 2009).

By rewriting the Equation 4.11, the suction field can be expressed by:

$$s_{ij}(x,t) = s_{ij}^{el}(x,t) + \rho_{ij}(x,t) \tag{4.15}$$

Here, the field of transformed structural parameters $Y_{ij}(x,t)$ is defined:

$$Y_{ij}(x,t) = y_{ij}(x,t) - \rho_{ij}(x,t) \tag{4.16}$$

Taking into account the above equations, the yield surface can be expressed by:

$$f(s_{ij}^{el} - Y_{ij}) \leq 0 \tag{4.17}$$

This equation indicates that the yield surface centered in s_{ij}^{el}, translates in the transformed structural parameter Y_{ij} plane.

With the transformed structural parameter field (Equations 4.10, 4.14 and 4.16), the inelastic problem can be solved by:

$$\epsilon_{ij}^{ine}(x,t) = M'_{ijkl} \cdot \rho_{kl}(x,t) + \frac{1}{h} \cdot Y_{ij}(x,t) \tag{4.18}$$

where, M'_{ijkl} is the modified elasticity matrix of suction, defined by the following equation:

$$M'_{ijkl} = M_{ijkl} + \frac{1}{h} \cdot I_{ijkl} \tag{4.19}$$

where, I_{ijkl} is the identity tensor, I_{ijkl} if $i = j = k = l$.

Considering equation 4.18, the residual suction tensor of the elastoplastic structure is obtained:

$$\rho_{ij}(x,t) = M'^{-1}_{ijkl} \cdot \left[\epsilon_{ij}^{ine}(x,t) - \frac{1}{h} \cdot Y_{ij}(x,t)\right] \tag{4.20}$$

Finally, the plastic strain field is given by combining Equation 4.14 and 4.16:

$$\epsilon_{ij}^{p}(x,t) = \frac{1}{h} \cdot [Y_{ij}(x,t) + \rho_{ij}(x,t)] \tag{4.21}$$

Consequently, a one-to-one relation exists between the kinematic hardening variable field $y_{ij}(x,t)$ and the transformed structural parameter field $Y_{ij}(x,t)$. At any time t, for a given kinematic hardening variable field $y_{ij}(x,t)$, there is a unique residual suction field $\rho_{ij}(x,t)$, a unique suction field $s_{ij}(x,t)$ as well as a unique transformed structural parameter field $Y_{ij}(x,t)$, and vice versa. Within this framework, the inelastic problem is solved through elastic analysis with null boundary condition and a modified elasticity matrix of suction. Eventually, all unknown fields at the limit state are obtained.

4.2.4 Structure response under wetting and drying cycles

During successive wetting and drying cycles, the elastic suction field can be expressed by:

$$s_{ij}^{el}(x,t) = [1 - \wedge(t)] \cdot s_{ij_{min}}^{el}(x) + \wedge(t) \cdot s_{ij_{max}}^{el}(x) \tag{4.22}$$

where, $s_{ij_{min}}^{el}(x)$ and $s_{ij_{max}}^{el}(x)$ are the minimal and maximal value of cyclic suction, respectively. $\wedge(t)$ is a monotonic periodic function, varying between 0 and 1.

The local suction at the level of the plastic mechanisms are expressed as:

$$\widetilde{s}_{ij}(x,t) = s_{ij}(x,t) - y_{ij}(x,t) \tag{4.23}$$

In the local suction plane, the plasticity convex domain (C_0) is a fixed segment on the isoclinic suction axis. The normality law is written with the Moreau's notation:

$$\dot{\epsilon}_{ij}^{p} \in \partial\phi_{(C_0)}(\widetilde{s}_{ij}) \text{ with } \widetilde{s}_{ij} \in (C_0) \tag{4.24}$$

$\partial\phi_{(C_0)}(\widetilde{s}_{ij})$ is the subdifferential to the convex (C_0) at $\widetilde{s}_{ij}$, where the plastic strain rate is an external normal to the convex (C_0).

At the maximum suction state, the transformed structural parameter at the level of inelastic mechanism is expressed by:

$$Y_{ij} = -\widetilde{s}_{ij} + s_{ij_{max}}^{el} \tag{4.25}$$

with

$$Y_{ij} \in C(s_{ij_{max}}^{el}) \text{ and } C(s_{ij_{max}}^{el}) = (C_0)_{min} + s_{ij_{max}}^{el} \tag{4.26}$$

This equation implies that Y_{ij} belongs to the convex $C(s_{ij_{max}}^{el})$ obtained from $(C_0)_{min}$ with the translation $s_{ij_{max}}^{el}$ (Figure 4.1). The normality law is

$$\dot{\epsilon}_{ij}^{p} \in -\partial\phi_{C(s_{ij_{max}}^{el})}(Y_{ij}) \text{ with } Y_{ij} \in C(s_{ij_{max}}^{el}) \tag{4.27}$$

$-\partial\phi_{C(s_{ij_{max}}^{el})}(Y_{ij})$ is the subdifferential to the convex $C(s_{ij_{max}}^{el})$ at $Y_{ij}(x,t)$, where the plastic strain rate is an internal normal to the convex $C(s_{ij_{max}}^{el})$. This convex is locally built for each plastic mechanism and the yield surface is a segment, centred in $s_{ij_{max}}^{el}$, translating in the transformed structural parameter plane.

A Pseudo Loading Collapse (PLC) yield surface is also presented in Figure 4.1, the same description defined in the chapter 3. It shows an increase of the preconsolidation stress p_{ij} with the suction s_{ij} increase. In this section, no plastic

deformation is generated by the mechanical loading during the wetting and drying cycles because the p_{ij} value was selected less than p_{ij}^* representing the preconsolidation stress at the saturated state (suction= 0).

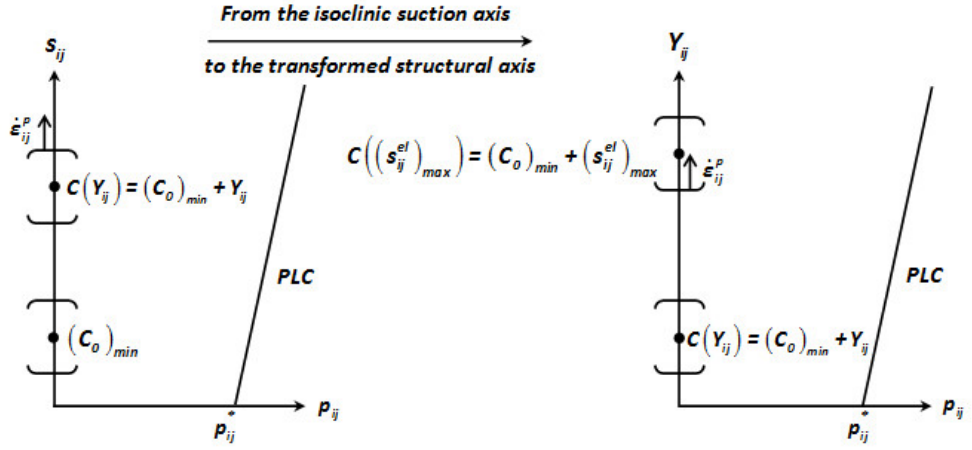

FIGURE 4.1: Evolution of plasticity convex in local suction plane and transformed structural parameter plane.

According to the suction loading amplitude Δs_{ij}^{el}, two cases exist in the transformed structural parameter plane:

- The extreme positions of the convex centred in $s_{ij_{min}}^{el}$ and $s_{ij_{max}}^{el}$ have a common part C_l, in this case, elastic shakedown will occur;
- The extreme positions of the convex have no intersection, in this case, plastic shakedown will occur.

(1) Elastic shakedown

During a cyclic loading, the convex that characterises the behavior of each point of the structure, translates between the extreme suctions. If $(Y_0)_{ij}$ is the initial value of the transformed structural parameters, $(Y_0)_{ij}$ can be transported with the convex during cyclic loadings. Two cases can be obtained in the transformed structural parameter plane (see Figure 4.2):

a) If $(Y_0)_{ij}$ is inside C_l, $(Y_0)_{ij}$ remains immobile and the behavior is purely elastic;

b) If $(Y_0)_{ij}$ is outside C_l, the position variation $(\Delta Y_0)_{ij}$ of the point $(Y_0)_{ij}$ after the first cycle is obtained by projection on the boundary of C_l. After that, the inelastic and plastic strain fields can be solved by Equations 4.18

and 4.21.

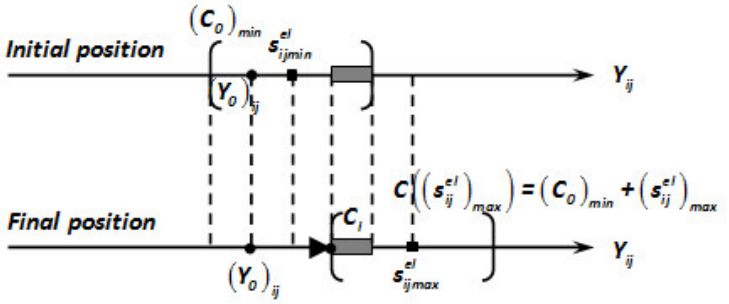

FIGURE 4.2: Transformed structural parameter plane for elastic shakedown.

(2) Plastic shakedown

When the suction loading Δs_{ij}^{el} becomes very large, a stationary state can be reached and plastic shakedown is achieved presented in Figure 4.3. In this case, the distance between two extreme positions of the mobile convex centred in $s_{ij_{min}}^{el}$ and $s_{ij_{max}}^{el}$ in the transformed structural parameter plane can be obtained:

$$\| \Delta Y_{ij} \| = \| s_{ij_{max}}^{el} \| - \| s_{ij_{min}}^{el} \| - 2 \cdot s_{\alpha} \tag{4.28}$$

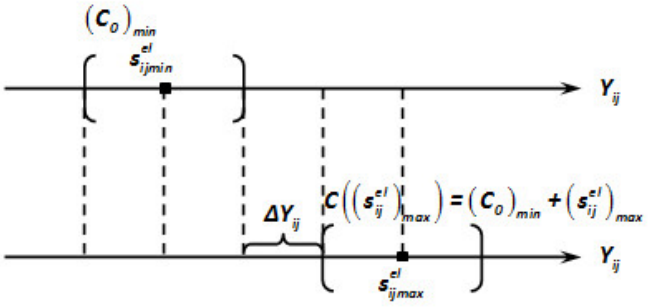

FIGURE 4.3: Transformed structural parameter plane for plastic shakedown.

Finally, the value of ΔY_{ij} can be written as:

$$\Delta Y_{ij} = \left(1 - \frac{2 \cdot s_{\alpha}}{\| \Delta s_{ij}^{el} \|} \right) \cdot \Delta s_{ij}^{el} \tag{4.29}$$

In these two equations, $\| \cdot \|$ is the notation of 2-norm.

4.3 Algorithm of the shakedown model

Zarka procedure defines a very simple way to estimate the asymptotic solution during cyclic loadings, strongly depending on the initial state of the structure. This procedure can solve an inelastic problem using the elastic analysis and generally respect four steps as follows:

First, the cycle has to be "entered", an analysis of the first cycle or of the first half cycle is performed to determine the initial and the final positions of the yield surfaces.

Second, the variations of the transformed structural parameter ΔY_{ij} are determined locally from two extreme positions of the yield surface. According to the amplitude $\parallel \Delta s_{ij}^{el} \parallel$, there are two cases in the transformed structural parameter plane:

i) If $\parallel \Delta s_{ij}^{el} \parallel \leq 2 \cdot s_\alpha$, the initial transformed structural parameter $(Y_0)_{ij}$ is orthogonally projected on the activated plasticity yield surface, giving ΔY_{ij}.

ii) If $\parallel \Delta s_{ij}^{el} \parallel > 2 \cdot s_\alpha$, ΔY_{ij} is decided by the distance between two yield surfaces centered in s_{ijmin}^{el} and s_{ijmax}^{el} in the Y_{ij} plane.

Third, global elastic analysis is performed on the structure using the modified elasticity matrix of suction M' and initial strains $(\frac{1}{h} \cdot Y_{ij})$, leading to the residual suction field ρ_{ij}, inelastic displacement field u_i^{ine} and inelastic strain field ϵ_{ij}^{ine}.

Finally, the plastic strain field ϵ_{ij}^{p} is known by the given transformed structural parameter and the residual suction field.

The algorithm of previously proposed shakedown method is summarised in Figure 4.4 which will be implemented in the finite element code CAST3M to perform numerical calculations. In this algorithm, we use the criterion $(\Delta y_{ij} \geq 0)$ for all (i, j) to replace the one proposed for metallic materials by Gatt (1993) that considered some elastic points in the structure even though plastic shakedown occurs. As a matter of fact, no point violates this criterion in our modeling, because we suppose a very small yield surface and there is no elastic deformation for expansive soils when wetting and drying cycles are applied.

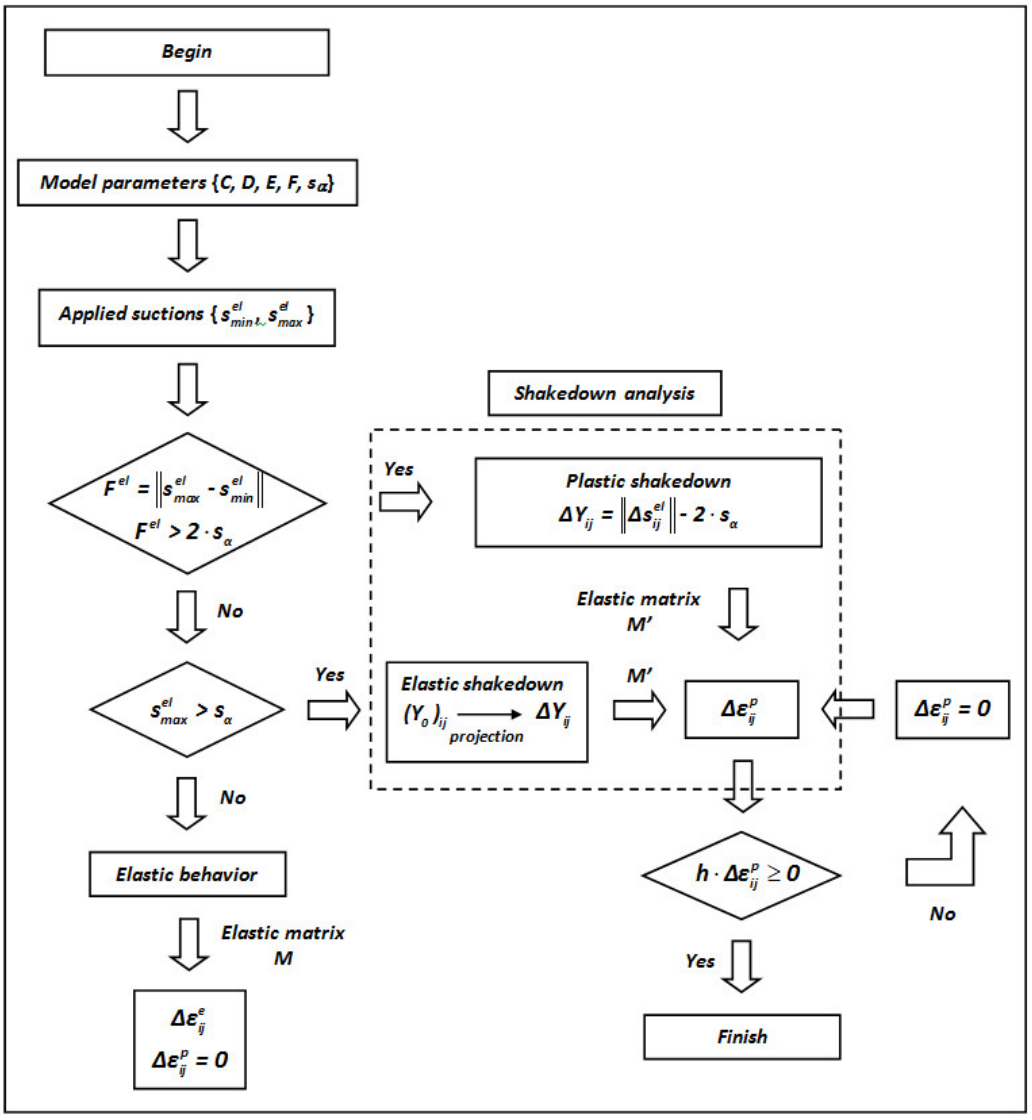

FIGURE 4.4: Algorithm of shakedown modeling for 3D structure.

4.4 Numerical validation of the proposed model

In this section, the plastic strain field and its related fields of an elasto-plastic structure are going to be calculated after several wetting and drying cycles due to the variation of the climatic conditions. We use a finite element code CAST3M to implement the proposed shakedown-based model. The finite element code CAST3M is briefly introduced at first and then three numerical tests are performed on different initial states of an expansive soil, defined in the previous chapter.

4.4.1 Finite element code CAST3M

• CAST3M presentation

The CEA (Commisariat à l'Energie Atomique) is a french government-funded technological research organisation, which has developed a dedicated toolbox in the past twenty years for finite element computations, called Cast3M. The toolbox contains the essential elements in order to perform a finite element computation. Its main application area is mechanics including elasticity, elasto-visco-plasticity material behavior and analysis adapted for equilibrium, buckling, vibration or dynamics problems. Other application areas include thermal, hydraulic or elactromagnetic analysis. Its modular character permits to program in an easy and comfortable manner, which make the tool adapted for coupled multi-physics analysis.

The website (http://www-cast3m.cea.fr/)[121]contains a general presentation of the code, example files, online services and downloadable documentations. Downloading of the computer code is available for a non-commercial usage of the program and the source code can also be recovered after a previous acceptance by the CEA, which are accessible for the majority of engineers and researchers.

• Cast3M language

From the programming point of view, Cast3M differentiates two levels of programming:

- a compiled low level language: ESOPE. This language is invisible for the normal user and it is the language of the creators of Cast3M. As explained in the software manual, it is just a derivation of the classical FORTRAN language enriched with operations for the manipulation of specific objects (creation, copy, removal, ... of data structure).

- a high level interpreted language: GIBIANE, formed by a lexicon of operation which permits an easy usage of the code and it is the language of the normal user as exemplified in the software manual.

In this way, ESOPE for CAST3M is the language of the developer, while GIBIANE is the language of the user.

• Finite element modeling

Any general analysis using the finite element method can be divided into three successive phases and each of them is able to be subdivided in a series of elementary processes. These typical stages of FEM analysis can be listed below:

Phase 1. Pre-processing

- construct the parts in a solid modeler and combine the multiple parts into an assembly;

- defeature the assembly and select the element type for meshing;

- define the material properties, boundary conditions and the type of analysis, such as plane strains or stresses, axisymetry. . . ;

Phase 2. Solving

- calculate the stiffness and mass matrix of each finite element;

- assemble the stiffness and mass matrix to the complete structure;

- apply the external loadings and the boundary conditions;

- solve the linear equilibrium equations;

Phase 3. Post-processing

The post-processing provides impressive color displays, or graphs, of the solution and its related information, such as the displacement, the stress field, the strain field, or from the global quantities, the strain energy, etc. Today, a second post-processing of the recovered derivatives can offer error estimations that show where the study needs the improvement.

All these characteristics of FEM make it possible for users to program their own codes to resolve the self-defined problems.

4.4.2 Numerical simulation: the structure of an expansive soil

The proposed analytical shakedown model presented in chapter 3, is implemented into CAST3M to perform the numerical simulations of an elaso-plastic structure. Figure 4.5 shows the geometry, mechanical loadings, boundary conditions and the finite element mesh, being used for the numerical simulations. In this figure, the studied model 600 cm $\times$ 200 cm, is made up of an expansive soil whose three initial states (loose, dense and intermediate) are separately used in the following simulations. In these simulations, the geometry is discretized into 4-node quadrilateral elements and 4800 elements have been used to analyse a 2-D plane strain problem.

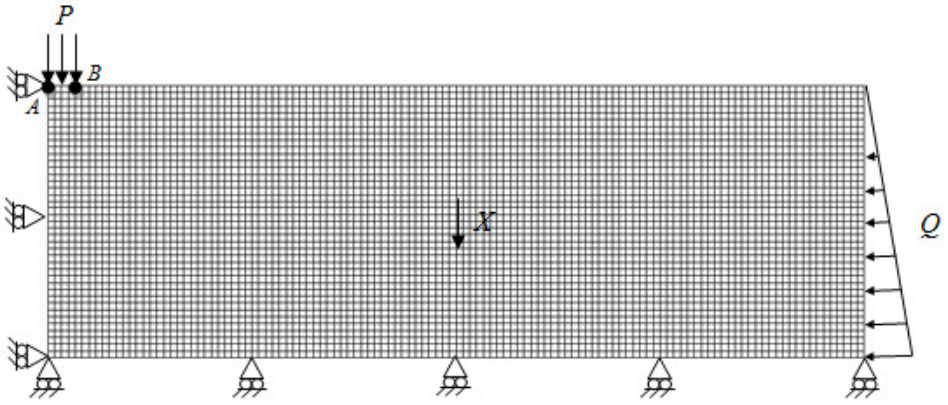

FIGURE 4.5: Finite element model for a 2-D plane strain simulation.

Before shakedown calculation, the in-situ geostatic analysis of the expansive soils is performed where the gravity and lateral stresses are applied to the model (Figure 4.5). This geostatic stresses are determined by the initial dry density of the soil γ_d (presented in chapter 3) and the lateral stress coefficient K_0, taken 0.5 in all the simulations.

Except for the geostatic stress, a series of vertical loads P are also applied on the top of the geometry between AB in Figure 4.5 (the length of AB is 30 cm): 15, 30, 60 kPa and the limit stress of 67.85 kPa. The limit stress is 67.85 kPa produces the maximum net mean stress of 60 kPa in the finite element model. Since we obtained the evolution law of shakedown model between 15 and 60 kPa for all the studied materials, the net mean stress values beyond 60 kPa are not taken into account in the numerical modeling.

In this way, the mechanical analysis is performed with the consideration of finite element model presented in Figure 4.5, where the gravity, the lateral stress and the external load are applied. Three Young moduli: 14, 18, 18 MPa for loose, dense, intermediate soils and Poisson ratio 0.2 for all different initial state soils are also used in this elastic mechanical analysis.

As to the suction range due to climate change, we consider a linear variation of suction with depth as described in Figure 4.6 in the dry season, while the soil is fully saturated (suction zero) in the wet season. Then, the finite element calculation of the limit state is performed for the wetting and drying cycles between these two extreme conditions under different vertical loads.

Figure 4.7 presents the distribution of net mean stress for three initial state soils under limit load 67.85 kPa. Here, we only take the mechanical analysis for the limit load as an example. From this figure, it is easy to say that the influence of vertical load on the distribution of net mean stress is predominate, compared with the gravity and the lateral stress.

For the given net mean stress p, the resilient modulus E_r as well as the hardening modulus h can be finally estimated according to the Equations 3.33 and 3.34 where the parameters C, D, E and F are reported in Tables 3.2, 3.4, 3.5 and 3.6.

Figure 4.8 shows the plastic strains on the soil surface (y=0 m) after several wetting and drying cycles under a series of vertical stresses for different samples. It can be observed that the vertical stress mainly influences the plastic strain field between AB. For the soils at loose initial state, shrinkage deformations are occurred and for the soils at dense initial state, swelling deformations are observed. On the contrary, for the intermediate soils the swelling plastic strains are produced at the vertical stresses of 15 and 30 kPa, while the accumulated shrinkage deformations are occurred for the higher vertical stresses. Outside AB, the swelling plastic strain reaches its maximum value because of null external loads.

Figure 4.9 presents the inelastic displacement field of the geometry surface (y=0 m) after wetting and drying cycles under a series vertical stresses for different initial state soils. Between AB, only settlement for loose soils and heave for dense soils can be observed. For the intermediate soils, no settlement happens after the wetting and drying cycles and the heaving deformation decreases with the increase of the vertical pressures. All these findings can be related to the residual stress field in the studied geometry (see Equation 4.10).

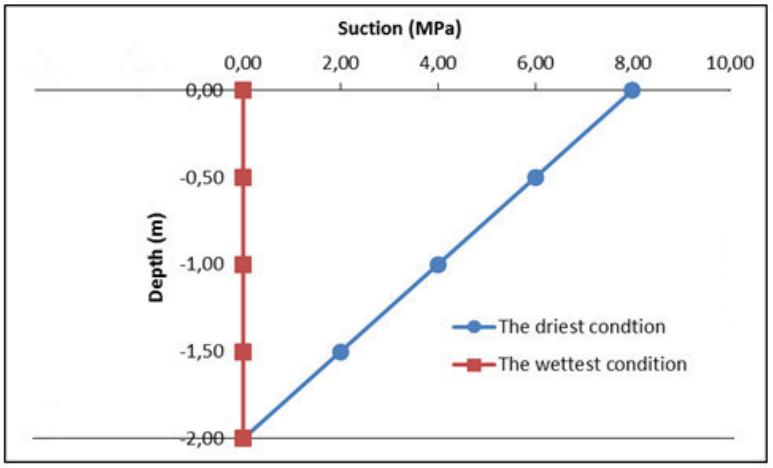

FIGURE 4.6: Suction profile at the driest and the wettest conditions for 2-D plane strain simulation.

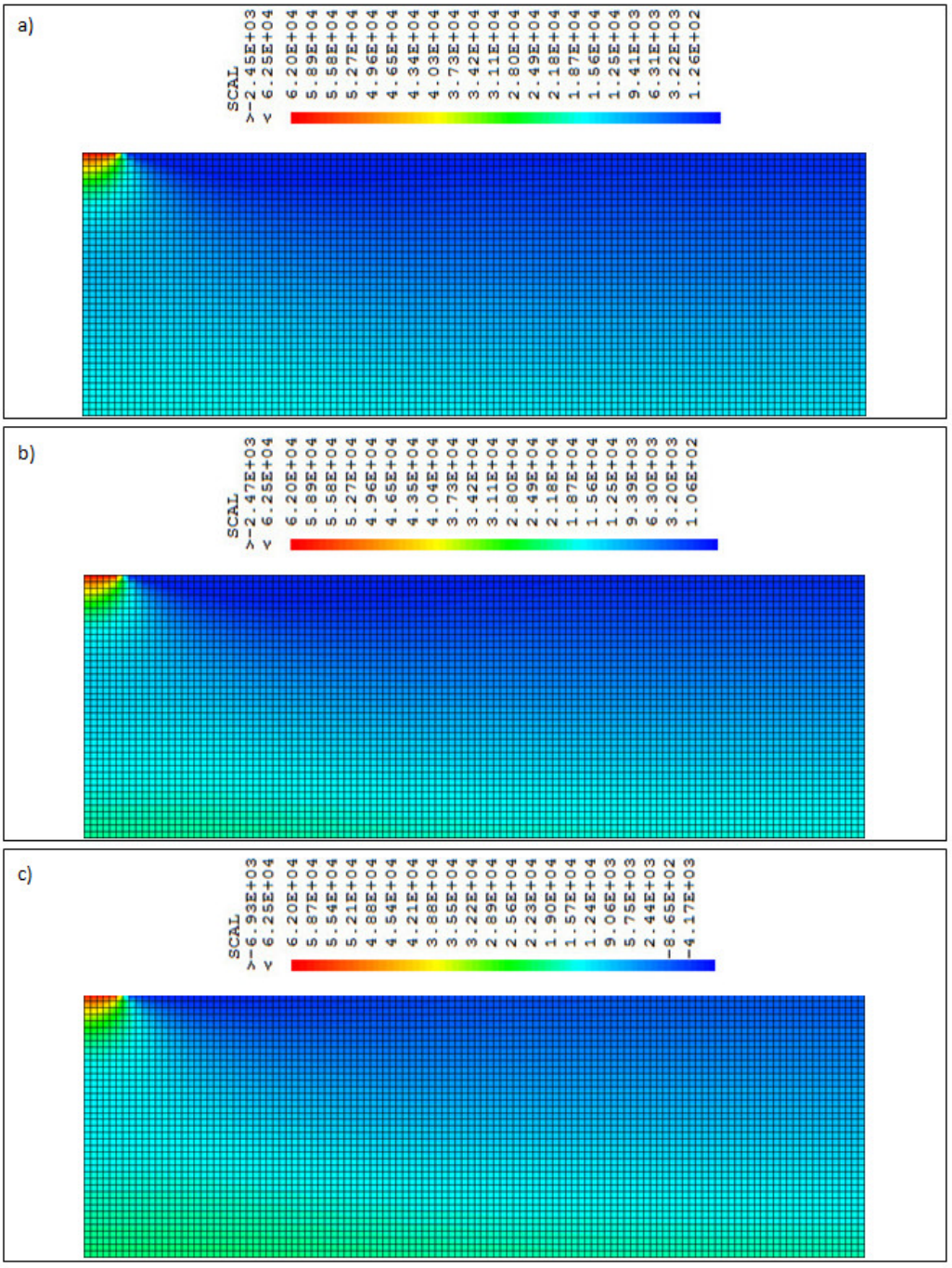

FIGURE 4.7: Distribution of net mean stress of 2D simulation under the limit load: a) loose soil; b) dense soil; c) intermediate soil.

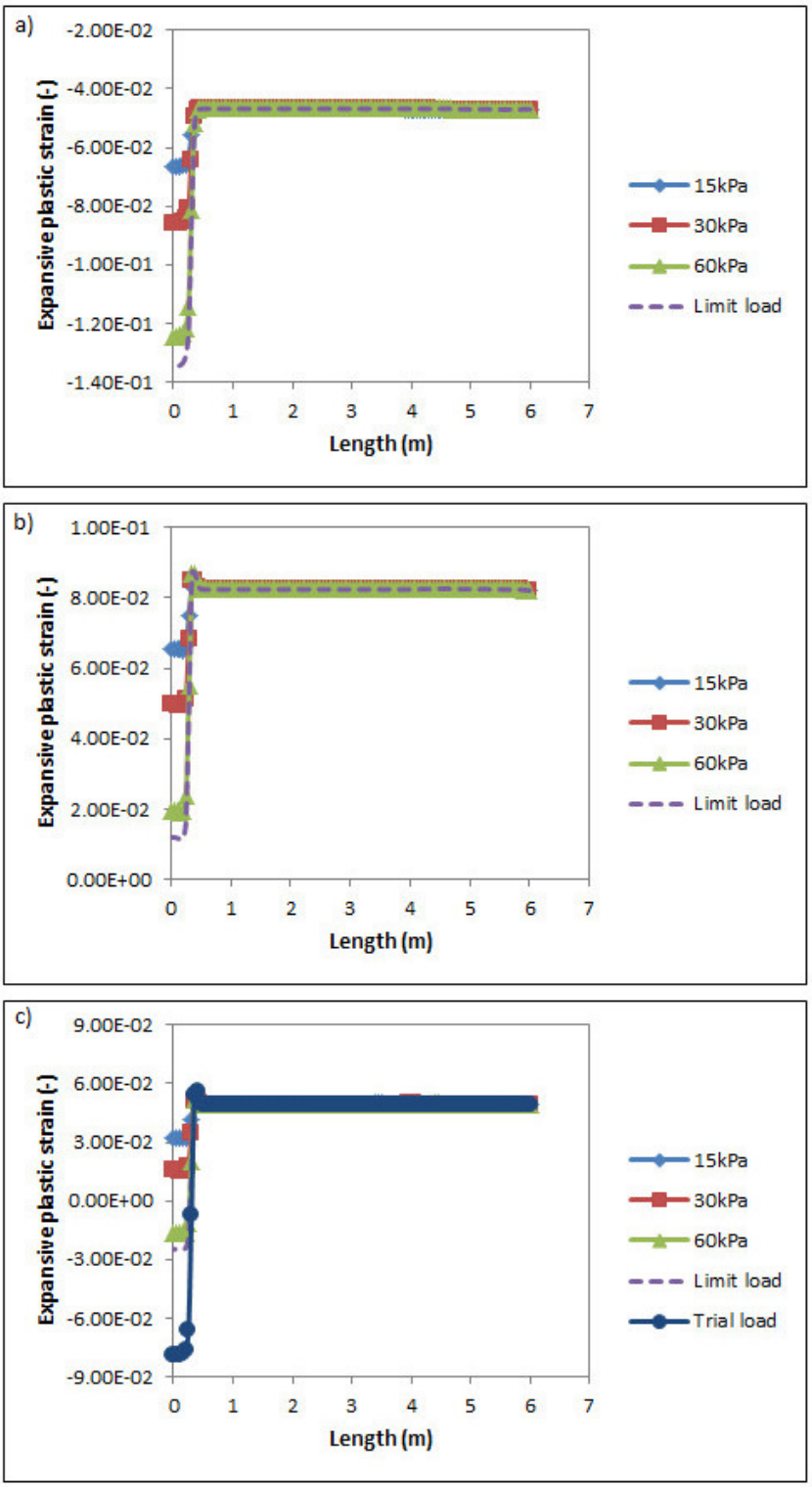

FIGURE 4.8: Numerical calculation of plastic strain on the surface (y=0 m): a) loose soil; b) dense soil; c) intermediate soil.

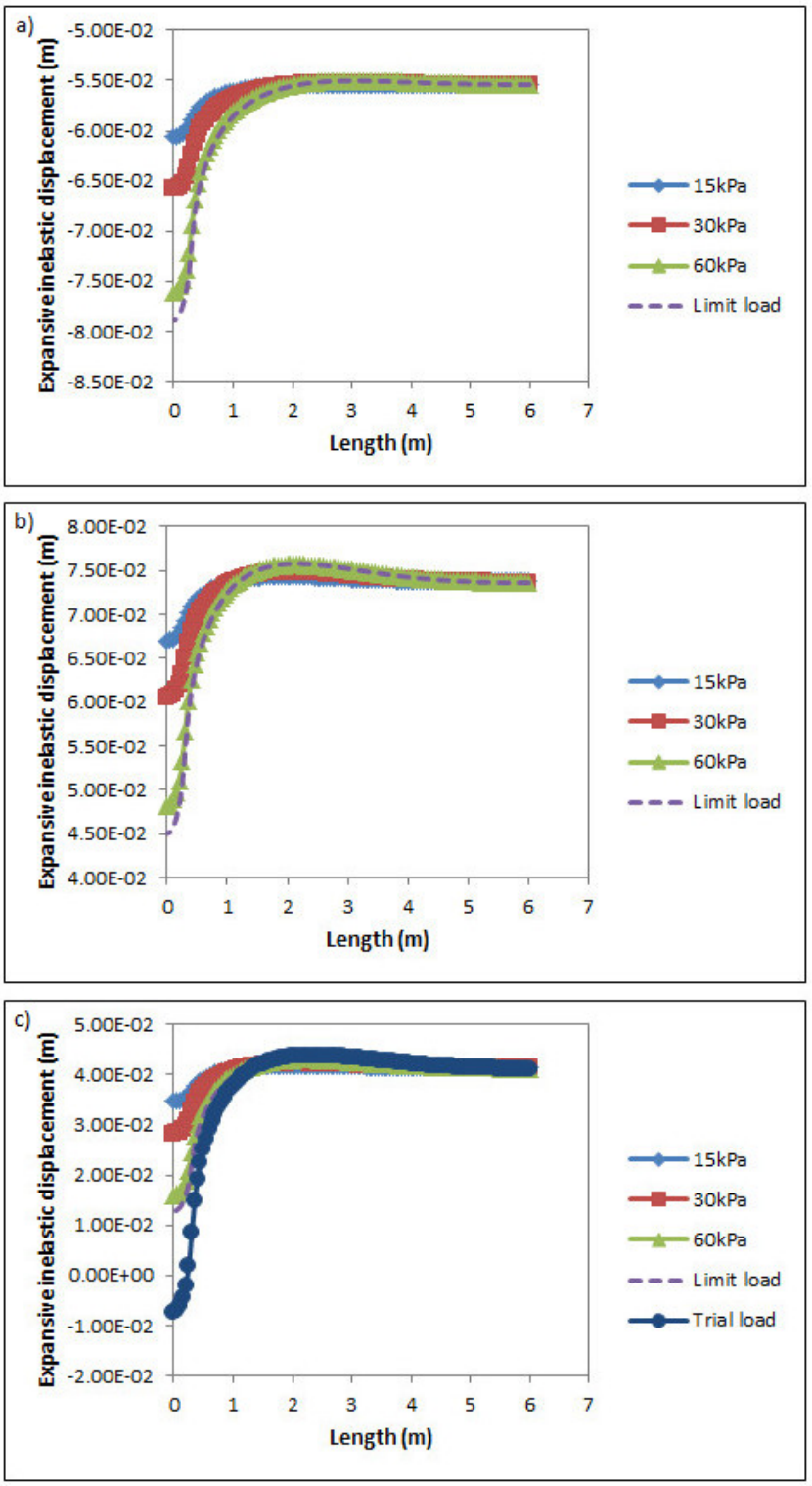

FIGURE 4.9: Numerical calculation of displacement on the surface (y=0 m): a) loose soil; b) dense soil; c) intermediate soil.

To predict the heave and settlement at the same time, we impose a trial stress of 120 kPa on the boundary AB of the finite element model, made up of the intermediate initial state soil. For the intermediate soil, there is no collapse phenomenon during wetting and drying cycles when the trial stress of 120 kPa is applied, because this trial stress is always inside the elastic region of preconsolidation stress.

The results of these simulations are also presented in Figure 4.8 and Figure 4.9. In Figure 4.9, the settlement is observed between AB after the wetting and drying cycles when the trial load 120 kPa is applied. This proves that our code is able to predict the heave for intermediate soils under the lower level of vertical pressure, meanwhile the settlement can also be generated when the vertical pressure is large enough.

4.5 Conclusion

The finite element equations have been firstly extended for a structure from the proposed analytical shakedown model presented in chapter 3. Subsequently, these equations have been implemented in the finite element code CAST3M to perform the numerical simulations. In these simulations, three different initial states of an expansive soils are used for shakedown analysis.

From the modeling results, we can observe that shrinkage deformations are occurred for loose soils and swelling deformations are accumulated for dense soils, while for the intermediate soils the swelling plastic strains are produced at lower level of the vertical stress and the accumulated shrinkage deformations are generated at the higher vertical stresses.

On the other hand, during wetting and drying cycles only settlement for loose soils and heave for dense soils can be observed. For the intermediate soils, no settlement occurs within the limit load after the wetting and drying cycles and the heaving deformation decreases with the increase of the vertical pressures. All these findings can be explained by the existence of the residual stress field in the studied geometry. Under the trial stress of 120 kPa, the settlement is finally observed for the intermediate state soil during wetting and drying cycles.

Chapter 5

Application of Shakedown Theory to Heavily Dense Expansive Soils

5.1 Introduction

Experimental evidence in the literatures shows a slightly hydraulic hysteresis during a wetting and drying path for heavily dense expansive soils, because of the absence of macro-pores in these materials. When heavily dense expansive soils experience several wetting and drying cycles, the hydraulic hysteresis will completely disappear, leading to a linearly elastic equilibrium state. However, this linearly elastic equilibrium state can not be explained by the previously developed shakedown-based model, because it only considers a kinematic hardening plasticity (i.e. a constant width of the rectangular yield surface) and the theory of plastic shakedown is finally used to estimate the accumulated plastic strain during suction cycles.

Consequently, a modified shakedown-based model with the combined hardening mechanism including kinematic hardening and isotropic hardening should be developed. The focus of this chapter is to complete the modeling of unsaturated expansive soils based on shakedown theory with a combined hardening mechanism. The modified model with the combined hardening plasticity is calibrated by the experimental results of heavily dense expansive soils to demonstrate its capacity.

5.2 Modified shakedown theory for heavily dense expansive soils

The purpose of this section is first to present a modified shakedown-based model with a more complex hardening mechanism to improve means of representing hardening behavior in materials under cyclic loadings. Then this modified shakedown theory is used to model the hydromechanical behavior of heavily dense expansive soils.

5.2.1 Water retention curves for heavily dense expansive soils

A conceptual model for the evolution of water retention curves during suction cycles on heavily dense expansive soils is presented in Figure 5.1. Before wetting and drying cycles, a slight hysteresis of water retention curve can be observed. With the increase of cycle numbers, the retention loop becomes smaller and finally it can be considered as a straight line, leading to a linearly elastic state at the end of several suction cycles where elastic shakedown is occurred. Therefore, we consider a linearly elastic equilibrium state (elastic shakedown behavior) for heavily dense expansive soils at the end of wetting and drying cycles.

However, the proposed shakedown-based model in chapter 3 can not explain the linearly elastic equilibrium state of heavily dense expansive soils after several wetting and drying cycles. Consequently, the modified shakedown model with a combined hardening plasticity should be developed to model the hydromechanical behavior of heavily dense expansive soils.

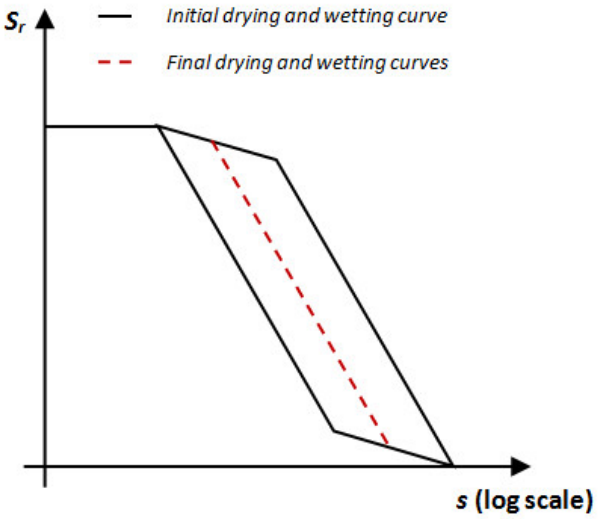

FIGURE 5.1: Evolution of the water retention curves with suction cycles for heavily dense expansive soils.

5.2.2 Modified shakedown method with a combined hardening

In the case of 1-dimensional elasto-plastic problem, the elastic behavior of the material can be supposed linear, independent of temperature. Thus, the mechanical problem can be solved as follows:

$$\epsilon(x,t) = \frac{1}{E} \cdot \sigma(x,t) + \epsilon^p(x,t) + \epsilon^I(x,t) \tag{5.1}$$

in which, $\sigma(x,t)$ is the stress, $\epsilon(x,t)$ the strain, $\epsilon^p(x,t)$ the plastic strain, E the elastic modulus, and $\epsilon^I(x,t)$ the initial strain.

The yield surface equation for perfect plasticity can be written as:

$$f = |\sigma| - \sigma_\alpha \tag{5.2}$$

where σ_α is the yield stress.

• An elementary model for isotropic hardening plasticity

To illustrate the mathematical structure of strain-hardening plasticity, we consider the simplest situation illustrated in Figure 5.2a. In this model, the hardening is assumed to obey two conditions:
a. The hardening is isotropic in the sense that at any state of loading, the center of the convex remains at the origin;
b. The hardening is linear in the amount of plastic flow. The first condition leads

to a yield criterion of the form,

$$f(\sigma, \alpha) = |\sigma| - (\sigma_\alpha + K \cdot \alpha) \tag{5.3}$$

where, α is an internal hardening variable and K is often called plastic modulus, its interpretation presented in Figure 5.2b.

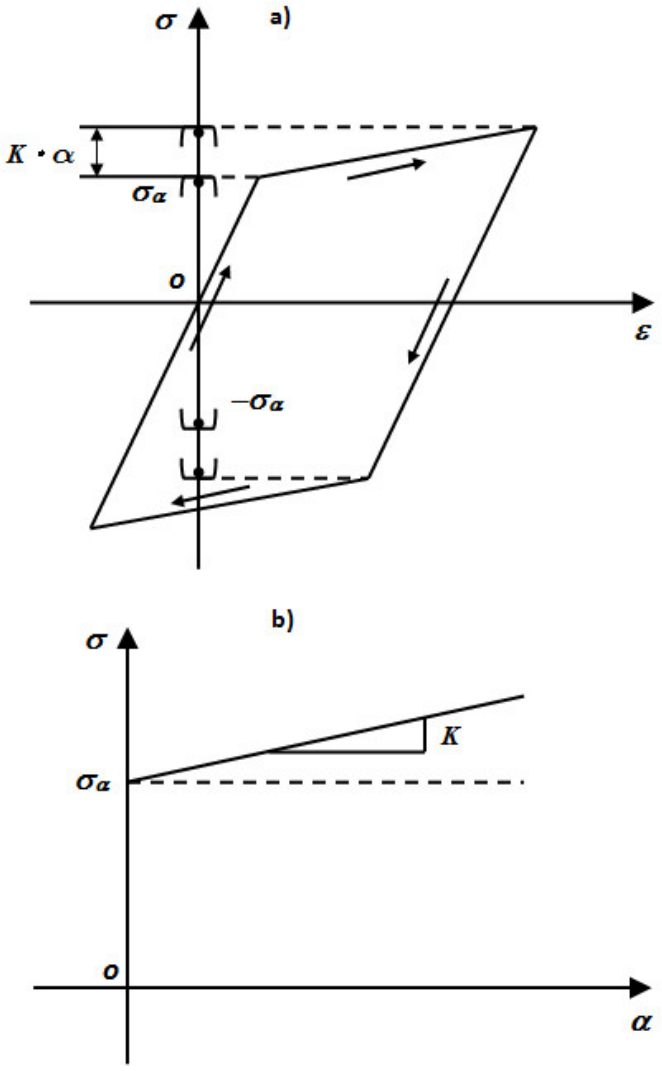

FIGURE 5.2: a) response of isotropic hardening model in a closed cycle; b) the interpretation of plastic modulus.

Here, we denote $\Delta\sigma_\alpha$ as the size variation of yield surface and it can be written as:

$$\Delta\sigma_\alpha = K \cdot \Delta\alpha \tag{5.4}$$

where, $\Delta\alpha$ is the plastic strain variation, controlling the yield surface change.

• Further refinements of the hardening law

In many engineering materials (such as metals) subjected to cyclic loading, it is experimentally observed that the center of the yield surface experiences a motion in the direction of the plastic flow. Figure 5.3 gives an idealized illustration of this hardening behavior closely related to a phenomenon known as the Bauschinger effect.

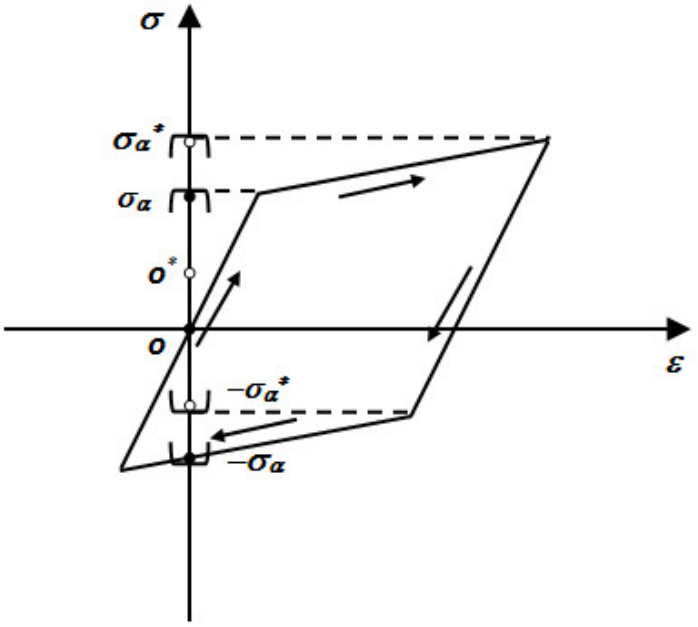

FIGURE 5.3: Response of kinematic hardening model in a closed cycle.

A simple model that captures the aforementioned effect is constructed by introducing an additional internal variable, denoted by y_α and called back stress, which defined the location of the center of the yield surface.

This hardening law defines a yield equation to the form,

$$f(\sigma, \alpha) = |\sigma - y_\alpha| - \sigma_\alpha \tag{5.5}$$

The evolution of the back stress (y_α) is related to the plastic strain (ϵ^p) in a linear relation,

$$y_\alpha = h \cdot \epsilon^p \tag{5.6}$$

where, h is the hardening modulus.

Finally, the yield condition with the combined hardening is modified to the form:

$$f(\sigma, \alpha) = |\sigma - y_\alpha| - (\sigma_\alpha + K \cdot \alpha) \tag{5.7}$$

This combined hardening is used when the yield surface not only expands (or contracts) but also translates in the stress space and these two purely linear hardenings are widely accepted and applied to model strain-hardening materials.

• Modified shakedown method

In this section, the isotropic hardening plasticity is added to modify the classical Zarka shakedown method. The convex is able to translate and expand (or contract) at the same time in the transformed internal parameter plane. The modified shakedown method is showed in Figure 5.4.

Figure 5.4 shows that the convex moves with the applied loading (σ) and the linear elastic behavior, elastic shakedown and plastic shakedown are defined in the transformed internal parameter plane according to the amplitude of applied loading (see figure 5.4a-5.4e):

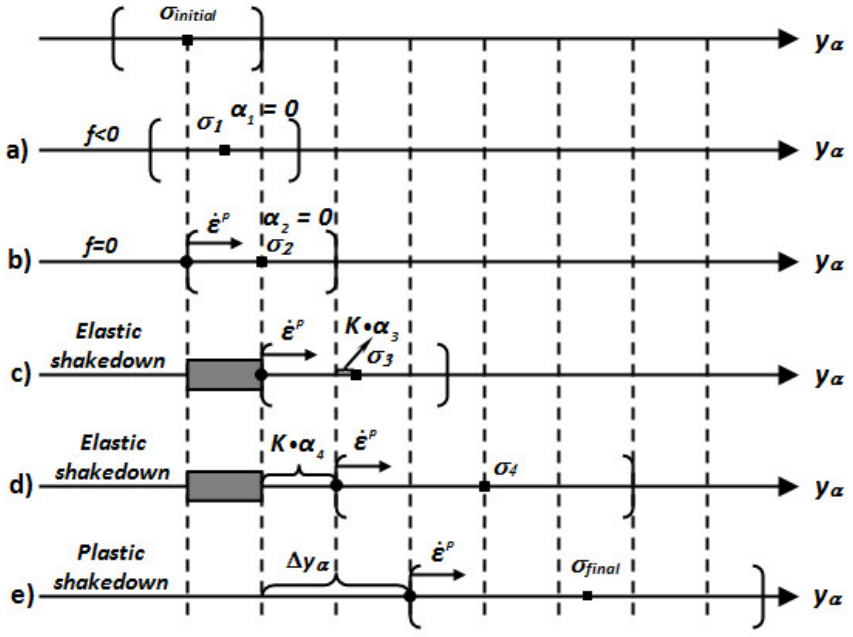

FIGURE 5.4: Transformed internal parameter plane for: a) elastic behavior; b)plastic mechanism; c and d) elastic shakedown; e) plastic shakedown.

(1) Linear elastic behavior. The material firstly presents linear elastic behavior when the applied stress (σ) is inside the convex (see Figure 5.4a). In this case,

there is no yield surface expansion because of $f < 0$ and the purely elastic strain is given by:

$$\Delta\epsilon^e = \frac{\Delta\sigma}{E} \tag{5.8}$$

where, E is the Young modulus.

(2) Elastic shakedown theory. Continuing loading, applied stress (σ) is beyond the yield stress (σ_α) where plastic strain is generated and the yield surface starts to expand (see Figure 5.4b). When plastic mechanism is activated ($f = 0$), the initial yield equation (Equation 5.7) can be written as the following form:

$$y_\alpha = \sigma - (\sigma_\alpha + K \cdot \alpha) \tag{5.9}$$

This equation means that the convex, centered in applied stress (σ) with a convex radius of ($\sigma_\alpha + K \cdot \alpha$), translates in the transformed internal parameter plane (y_α) plane.

Here, we define that elastic shakedown occurs when convex translation is going through two phases presented in Figure 5.4c and 5.4d:

Case 1. If the two extreme positions of the convex, taking into account a combined hardening plasticity, have an intersection showed in Figure 5.3c, elastic shakedown behavior is obtained after a number of cycles. For this, elastic shakedown depends on whether there is an intersection between two extreme positions of the convex, the same as the Zarka method.

Case 2. If there is no a common part between the extreme positions of the yield surface, elastic shakedown behavior can also be obtained when the applied stress σ is small,

$$\sigma \leq 2 \cdot (\sigma_\alpha + K \cdot \alpha) \tag{5.10}$$

In this case, the elastic region expands, because of isotropic hardening plasticity. The prerequisite of elastic shakedown is Equation 5.10 to guarantee the purely elastic response of materials after cyclic loadings.

Therefore, elastic shakedown occurs if Equation 5.10 is met and the plastic strain during cyclic loading is defined:

$$\Delta\epsilon^p = \frac{\Delta\sigma' - \Delta\sigma_\alpha}{h} \tag{5.11}$$

where, $\Delta\sigma' = \Delta(\sigma - \sigma_\alpha)$ and $\Delta\sigma_\alpha$ is calculated by Equation 5.4.

(3) Plastic shakedown theory. When the applied loading becomes large enough, Zarka proves that a stationary limit state is reached. For this, we define that plastic shakedown occurs (see Figure 5.4e) and the plastic strain during cyclic loadings can be written as:

$$\Delta\epsilon^p = \frac{\Delta y_\alpha}{h} \tag{5.12}$$

in which, h is the kinematic hardening modulus and Δy_α is defined in Figure 5.4e.

5.2.3 Elastic shakedown modeling of heavily dense expansive soils

In Figure 5.5, the convex translates along y_α axis from $s_{initial}$ to s_{final} and the material firstly shows purely elastic behavior because the suction changes very small ($f < 0$) (see Figure 5.5a). Continuing wetting the heavily dense expansive soils, the plastic mechanism is activated and the yield surface starts to expand due to isotropic hardening mechanism (see figure 5.5b). When applied suction reaches the final value presented in Figure 5.5c, elastic shakedown is eventually obtained because the final yield surface has an intersection with the initial yield surface.

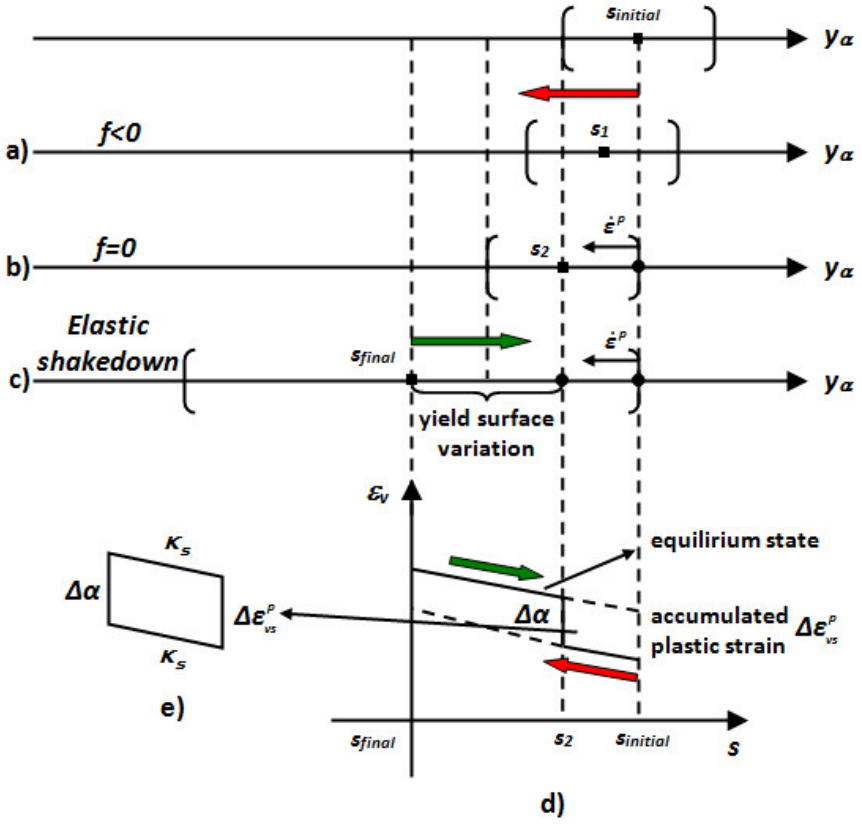

FIGURE 5.5: Elastic shakedown behavior of heavily dense expansive soils during suction cycles.

In the suction-volumetric strain plane presented in figure 5.5d, heavily dense expansive soils demonstrate elastic behavior when suction variation is small and plastic flow is followed when applied suction is outside the convex. After several suction cycles, the plastic strain is accumulated and the final equilibrium state is achieved where only elastic behavior can be observed because the yield surface expands to cover the whole range of suction variations. Moreover, the colored arrows in figure 5.5 represent convex movements where the red arrow presents the first cycle that elastic and plastic deformation coexist while the green arrow defines the reversible elastic deformation at the linearly elastic equilibrium state after suction cycles.

The accumulated plastic strain $\Delta\epsilon^p_{vs}$ in figure 5.5d corresponds to the total plastic strain during suction cycles between $s_{initial}$ and s_{final} while plastic strain $\Delta\alpha$ corresponds to the isotropic hardening plasticity during cyclic loadings because point A in Figure 5.5c represents the size variation of the yield surface during suction cycles.

Figure 5.5e shows the relation of the plastic strains ($\Delta\epsilon^p_{vs}$ and $\Delta\alpha$). This relation considers the simplest evolutionary equation for α to define the isotropic hardening plasticity, namely,

$$\Delta\alpha = \Delta\epsilon^p_{vs} \tag{5.13}$$

Therefore, the total plastic strain ($\Delta\epsilon^p_{vs}$) during suction cycles is replaced by the plastic strain ($\Delta\alpha$) because ($\Delta\alpha$) is easily determined from elastic shakedown modeling if initial and final size of the yield surfaces are given.

For heavily dense expansive soils, the initial size of the yield surface is supposedly small and the final size of the yield surface is known due to linear elasticity at the equilibrium state (see figure 5.5d). Therefore, elastic shakedown is used to model the behavior of heavily dense expansive soil subjected to suction cycles and the total plastic strain during suction cycles can be defined by the following equation:

$$\Delta\alpha = \frac{\Delta s_\alpha}{K} \tag{5.14}$$

where, Δs_α is the yield surface variation during suction cycles.

When the modified shakedown method is applied to model the behavior of heavily dense expansive soils, the combined hardening plasticity evolves into a unique

isotropic hardening during suction cycles. For this special case, the modified shakedown model only needs the plastic modulus to calculate the plastic strain, instead of the kinematic hardening modulus (see chapter 3).

5.2.4 Elastic behavior at the equilibrium state

The linear variation of the elastic volumetric strain with the suction can be found at the equilibrium state where demonstrates the reversible elastic behavior (see figure 5.5d). It can be written as:

$$\Delta\epsilon_{vs}^{e} = \frac{1}{E_r} \cdot \Delta s \tag{5.15}$$

where, E_r is the resilient modulus that can be calibrated from the linearly elastic equilibrium state at the end of cyclic suction-controlled odometer tests. In the study, we use the same definition for E_r as the description in chapter 3 that the inverse of this value is linearly change with the net mean stress.

In Figure 5.6, the total volumetric strain during suction cycles can be determined by the accumulated plastic strain from elastic shakedown analysis and the elastic volumetric strain at the equilibrium state. Then, it can be written as:

$$\Delta\epsilon_{vs} = \Delta\epsilon_{vs}^{e} + \Delta\epsilon_{vs}^{p} \tag{5.16}$$

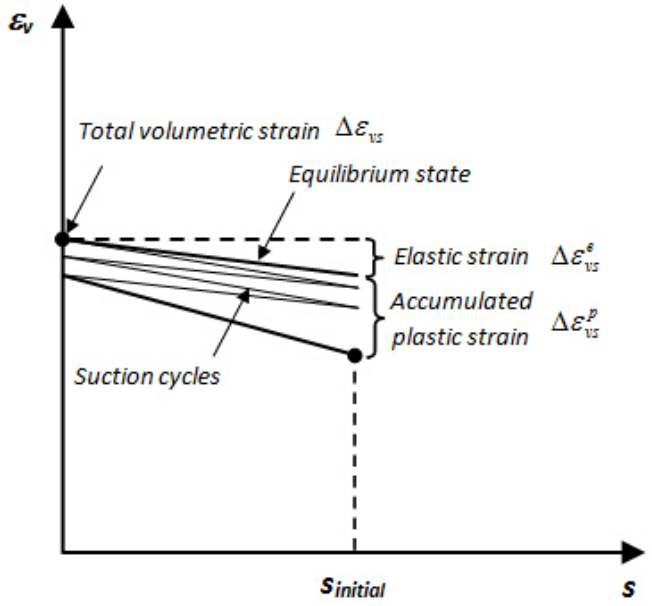

FIGURE 5.6: Variation of the volumetric strain with suction during the suction cycles.

For the modified shakedown model for heavily dense expansive soils, it requires to calibrate the model parameters: resilient modulus, plastic modulus and the threshold value of elastic limit for suction variation. Finally, the framework of one-dimensional modified shakedown model for heavily dense expansive soils is summarized in Figure 5.7 which can be extended to the 2-Dimensional (or 3-Dimensional) algorithm to conduct finite element modeling in future. With the framework of the modified model, kinematic hardening modulus is replaced by plastic modulus to carry out the shakedown analysis, that keeps identical number of model parameters but not the same model parameters.

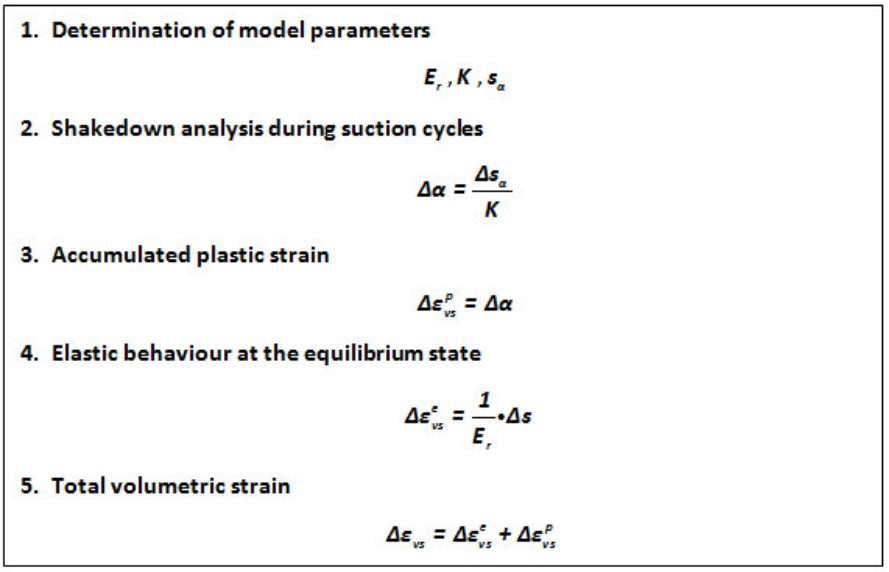

FIGURE 5.7: 1-Dimensional algorithm of the modified shakedown model for heavily dense expansive soils.

5.3 Calibration of the modified shakedown model

In the following section, the studied materials for model calibration, hydraulic tests during a wetting and drying path and the cyclic suction-controlled oedometer tests on the studied materials are presented. Finally, the model calibration is carried out to show the modeling capacity of the modified shakedown method by comparing model calculations with experimental results.

5.3.1 Test description

• Studied materials

The studied heavily dense expansive soil comes from a depth between 5.20 and 5.70 m of a core sample near Le Deffend, which is located approximately 4 km southeast of Poitiers (France). These clayey soils had a liquid limit of 65%, a plastic index of 25%, a specific gravity of 2.62 and a clay content of 52%. The remolded samples were compacted with an initial water content of 10% to form dense state samples under the compaction pressure of 1500 kPa, and the initial dry densities is 1.75 Mg·m^{-3} for the heavily dense samples.

• Hydraulic tests during a wetting and drying path

Figure 5.8 shows the measured water retention curve for heavily dense expansive soils[65]. The soil sample experiences a wetting path from the initial state to a fully saturated state, then it is dried from the fully saturated state to the suction of 287.9 MPa. In this curve, it is obvious to find a slightly hydraulic hysteresis during the wetting and drying path and this can be explained by the absence of macro-pores in heavily dense expansive soils. When these soils experience wetting and drying cycles, the hydraulic hysteresis will decrease and then completely disappear after several suction cycles, leading to a linearly elastic equilibrium state.

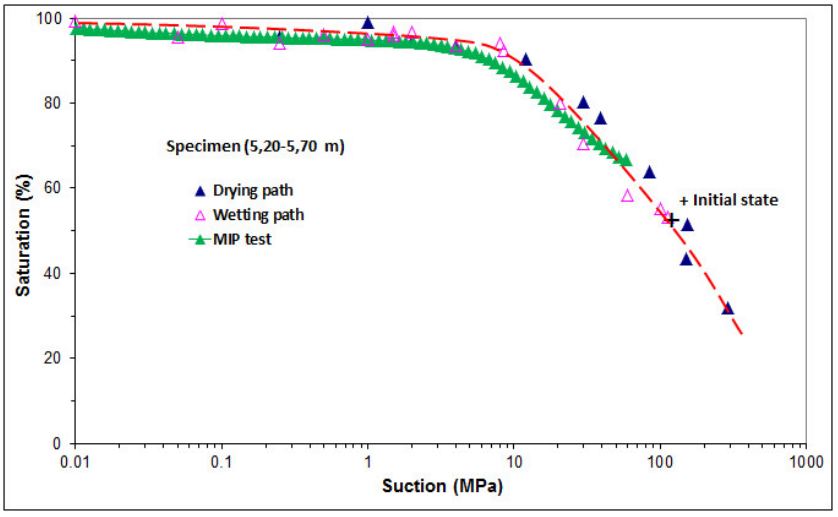

FIGURE 5.8: Measured water-retention curve of heavily dense expansive soil (Nowamooz and Masrouri, 2010).

• Cyclic suction-controlled tests

The hydromechanical behavior of heavily dense expansive soils associated with wetting and drying cycles was studied by Nowamooz and Masrouri[119]. The loading program of the oedometer tests on heavily expansive soil presented in Appendix 3. In all the tests, the considered initial states are represented by point A and point B represents the suction of 8 MPa at an initial vertical pressure of 10 kPa. Thereafter, three different vertical stresses 15, 30 and 60 kPa were applied to the heavily dense samples. In the end, several successive wetting and drying cycles were applied between 8 MPa and 0 MPa to the studied materials.

The void ratio variation versus suction of the heavily dense samples is presented in Figure 5.9 for different applied stresses: 15, 30 and 60 kPa. During the successive wetting and drying cycles, the studied material shows the accumulated swelling strains and the volumetric strains converge to an equilibrium state at the end of suction cycles. In these tests, we note that one or two additional suction cycles are still necessary for the studied materials to reach the final equilibrium state, but in this study we suppose the equilibrium state has already been achieved. This result will be used in model calibration.

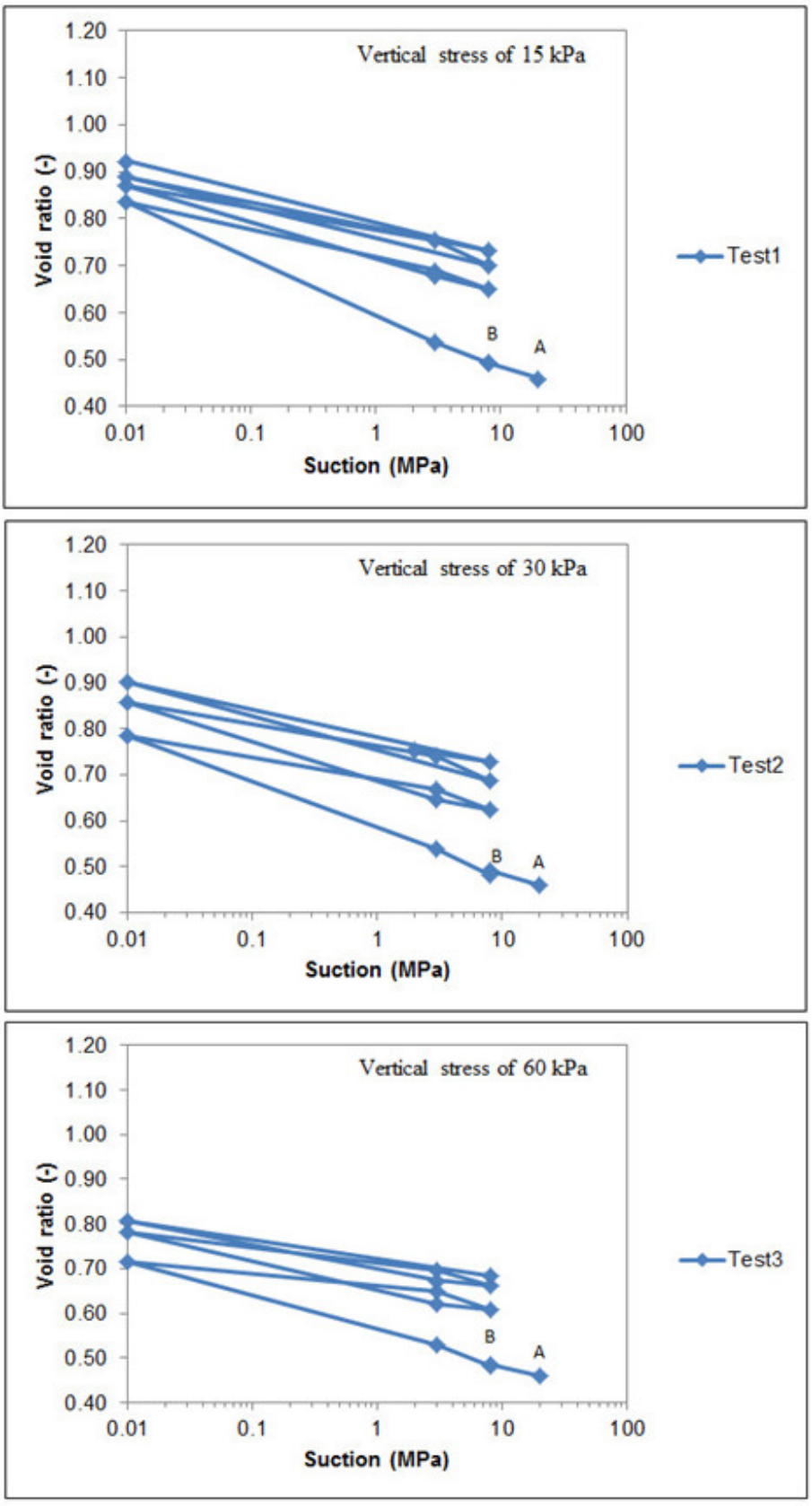

FIGURE 5.9: Cyclic oedometer tests on heavily dense expansive soils at the constant vertical pressure of 15, 30, 60 kPa

5.3.2 Elasticity parameters

The determination of the elasticity parameters can be conducted by the elastic strain at the equilibrium state at the end of wetting and drying cycles. Table 5.1 summarises the resilient modulus E_r value of heavily dense samples for the different net mean stresses 15, 30 and 60 kPa.

TABLE 5.1: Calibrated resilient modulus for the heavily dense expansive soil

Net mean stress (kPa)	15	30	60
E_r value (MPa)	62	68	96

With the given value of resilient modulus, the same evolution law for resilient modulus, described in section 3.4.2 in chapter 3, can be used in this section and Figure 5.10 plots this evolution law in terms of net mean stresses. In this figure, the inverse of resilient modulus decreases with a increase of net mean stress that represents larger loading pressure, smaller elastic strain at the end of wetting and drying cycles. Thereafter, model parameters C and D are summarised in Table 5.2.

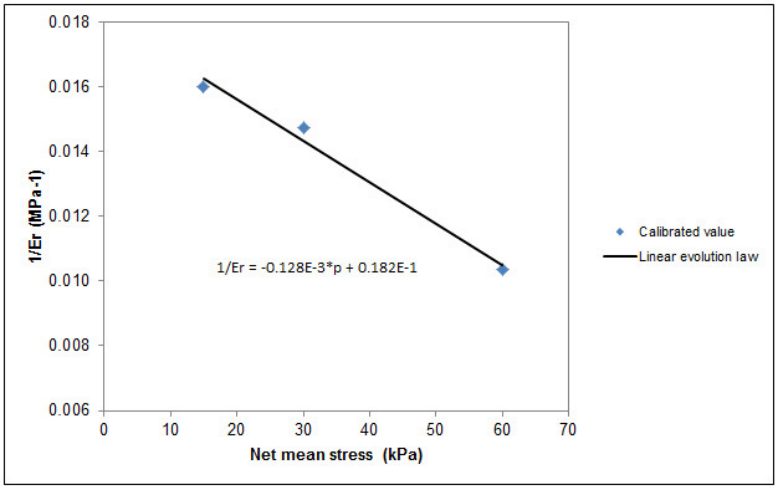

FIGURE 5.10: Linear evolution of the inverse of the resilient modulus ($1/E_r$) with the net mean stress for heavily dense samples.

TABLE 5.2: Variations of the parameters C and D for the heavily dense expansive soil

Parameters	$C(\mathrm{MPa}^{-2})$	$D(\mathrm{MPa}^{-1})$
Heavily dense(γ_d=1.75 Mg·m^{-3})	-0.128	0.182E-1

5.3.3 Plasticity parameters

Plasticity parameters of the modified shakedown-based model include the plastic modulus and the threshold value of elastic limit for suction variation. Here, we suppose that the initial threshold value of elastic limit for suction variation (s_α) is small, equal to zero, while the final size of yield surface is easily determined because of the linear elasticity at the equilibrium state.

As to plastic modulus (K), it can be deduced according to Equation 5.14, since we know the yield surface variation during wetting and drying cycles (Δs_α) as well as the accumulated plastic deformation ($\Delta\epsilon_{vs}^p$) at a given net mean stress. Table 5.3 presents these calibrated plastic modulus for heavily dense expansive soils.

TABLE 5.3: Calibrated hardening modulus for the heavily dense expansive soil

Net mean stress (kPa)	15	30	60
K value (MPa)	-50	-49	-59

Figure 5.11 illustrates the evolution of the inverse of the plastic modulus ($1/K$) with the net mean stress (p). Eventually, we propose additionally a linear variation of the inverse of the plastic modulus ($1/K$) with the net mean stress (p):

$$1/K = G \cdot p + H \tag{5.17}$$

where, G and H are constant parameters, can be related to the initial dry density of expansive soils, given in Table 5.4.

TABLE 5.4: Variations of the parameters G and H for the heavily dense expansive soil

Parameters	$G(\mathrm{MPa}^{-2})$	$H(\mathrm{MPa}^{-1})$
Heavily dense(γ_d=1.75 Mg·m^{-3})	0.760E-1	-0.219E-1

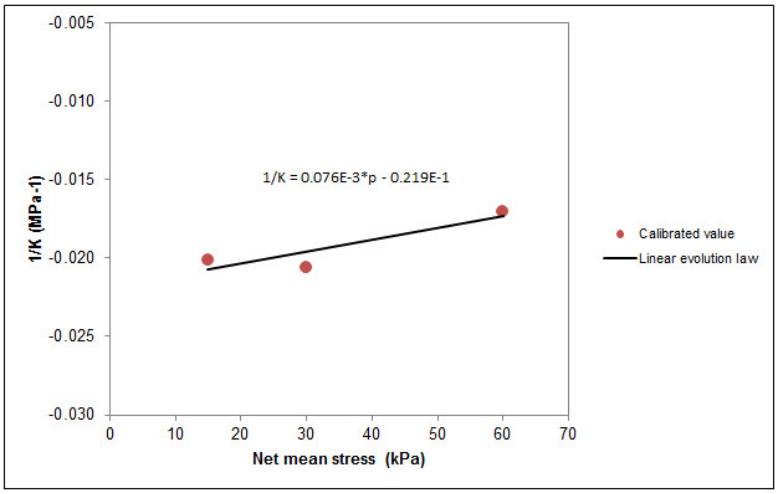

FIGURE 5.11: Linear evolution of the inverse of the plastic modulus (1/K) with the net mean stress for heavily dense samples.

5.3.4 Model calibration

Based on two proposed linear evolution laws of resilient modulus and plastic modulus, the model calibration can be carried out. Figure 5.12 shows the comparison of test results with model calibration at the net mean stress of 15, 30 and 60 kPa, where the accumulated plastic strain of unsaturated expansive soils during suction cycles is calculated from shakedown analysis and elastic volumetric strain is determined from the linear elastic equilibrium state. Furthermore, the model calibrations for heavily dense samples demonstrate a pretty good agreement with the test results.

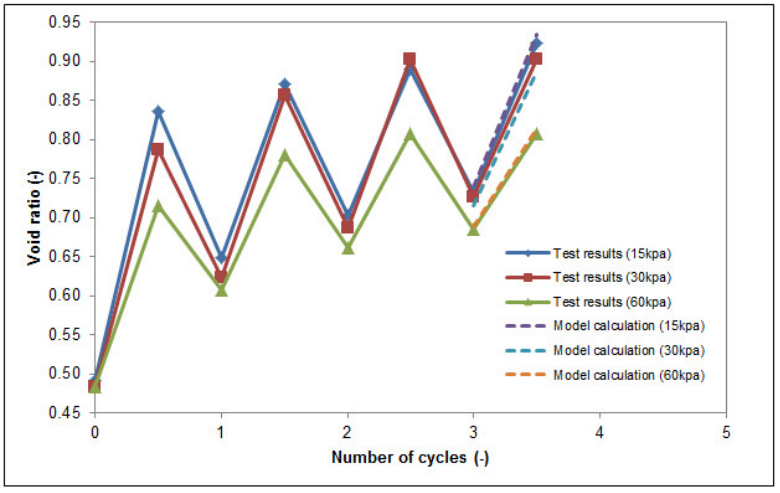

FIGURE 5.12: Comparison of test results with the model calibration at different net mean stresses.

5.4 Conclusion

In this chapter, a modified shakedown-based method is firstly developed by taking into account two linear hardening mechanisms. This modified method is then used to model the behavior of heavily dense expansive soils subjected to wetting and drying cycles.

Elastic shakedown is investigated by the transformed internal parameter plane and it occurs for heavily dense expansive soils at the end of wetting and drying cycles because of an intersection between two extreme positions of convex. Eventually, the combined hardening plasticity becomes a unique isotropic hardening and elastic shakedown theory explains the linearly elastic behavior at the equilibrium state.

Elasticity and plasticity parameters of the proposed shakedown-based model require to be determined by suction-controlled experiments. Parameters C, D for the evolution law of the resilient modulus (E_r) are determined from the elastic equilibrium state at the end of suction cycles. Parameters G, H for the evolution law of the plastic modulus (K) are determined from the accumulated strains during wetting and drying cycles. For the sake of simplicity of modeling, the initial threshold value of elastic limit for suction variation (s_α) is also taken small, equal to 0 MPa.

Finally, the comparison of tests with model calibrations is carried out for heavily dense expansive soils. These model simulations demonstrate that the modified shakedown-based method is able to simulate the hydromechanical behavior of heavily dense expansive soils subjected to suction cycles with the same number of model parameters as the proposed model presented in chapter 3.

Conclusions and perspectives

Previous studies have suggested that the behavior of unsaturated expansive soils is fundamentally different to that of unsaturated non-expansive soils. These soils can cause differential ground movements due to seasonal cyclic alterations that damages the buildings, the roads and the light infrastructures constructed on them. The developed constitutive models for unsaturated expansive soils need numerous parameters and classic incremental calculations lead to unrealistic calculation time when a large number of cycles are applied. In this context, the simple shakedown-based model for the simulation of the hydromechanical behavior of expansive soils subjected to wetting and drying cycles has been developed in this study.

This additional chapter covers the main conclusions of this study, together with the perspectives for the future work on modeling the behavior of unsaturated expansive soils. They are summarised as follows:

• Analytical modeling of expansive soils with shakedown concept

A new shakedown-based model for unsaturated expansive soils is developed and it requires five parameters:

- Parameters C and D, for the linear variation of the inverse of resilient modulus ($1/E_r$) with net mean stress (p), are determined from the equilibrium state of suction-controlled oedometer tests;
- Parameters E and F, for the linear evolution law of the inverse of hardening modulus ($1/h$) with net mean stress (p), are calibrated by the accumulated plastic strains during suction cycles from suction-controlled oedometer tests;
- The last plasticity parameter is the threshold value of elastic limit for suction variation (s_α), we take it equal to 0 MPa in this study.

Apart from the shakedown-based model, the coupling law between suction cycles and mechanical behavior is also developed. To determines the translation of

PLC (Pseudo Loading Collapse) during suction cycles, four parameters should be calibrated:

- Parameters A and B, controlling the slope and the intercept of the PLC curve, are determined by the compression oedometer tests under different constant suctions at the end of suction cycles;
- Parameter $\lambda(0)$ and κ are considered as constants, determined by the equilibrium state of compression oedometer tests on expansive soils with the application of suction cycles.

The model validations are performed by comparing the model predictions with the corresponding tests on an expansive soil compacted at intermediate initial state and these comparisons show the modeling capacity of the proposed models.

At the end of the analytical modeling, the sensitivity study of model parameters in the shakedown-based model is carried out to study the influence of shakedown parameter on model response:

- The influence of parameter C and E on model outputs increase with the net mean stress while parameters D and F are relatively stable;
- The influence of parameter s_α on plastic deformation is always negligible.

• Finite element modeling of in-situ behavior of expansive soils

With the implementation of the analytical shakedown model into a finite element code CAST3M, a series of numerical simulations on a two-dimensional plan strain model are carried out. From these simulations, we observe:

- The influence of vertical load on the distribution of net mean stress is more important, compared with the gravity and the lateral stress. Therefore, light infrastructures are damaged seriously when the expansions occurred;
- The shrinkage deformations during suction cycles are occurred for loose soils and swelling deformations are accumulated for dense soils. For the intermediate soils, the swelling plastic strains are produced at smaller vertical stresses and the shrinkage deformations are generated at higher vertical stresses;
- Under different vertical loads, only settlement during suction cycles for loose soils and heave for dense soils can be observed. For the intermediate soils, there is no settlement within the limit load and this can be explained by the existence of the residual suction field in the model;
- Considering a trial load of 120 kPa, the settlement during suction cycles is

finally observed for the intermediate state soil. It shows that our code is able to predict the settlement and the heave at the same time.

• Application of shakedown theory to heavily dense expansive soils

To apply shakedown theory to heavily dense expansive soils, a combined hardening plasticity including isotropic hardening and kinematic hardening is considered. This model needs five model parameters to be determined from the suction-controlled oedometer tests and no kinematic hardening:

- Parameters C, D for the evolution law of $(1/E_r)$ are determined from the elastic equilibrium state at the end of suction cycles;
- Parameters G, H for the evolution law of $(1/K)$ are decided from the accumulated strains during wetting and drying cycles;
- The initial threshold value of elastic limit for suction variation (s_α) is taken as 0 MPa and the final value of this parameter is easily to be determined according to the linear elastic behavior at the equilibrium state;
- Model calibration shows that the modified shakedown method is able to simulate the behavior of heavily dense expansive soils.

• Perspectives on future modeling

The research in this thesis has resulted in a better understanding of the behavior of unsaturated expansive soils. However, many questions are not answered and the future research is required:

- The coupling model between suction cycles and mechanical behavior should be implemented in the previously developed code to simulate subsequent mechanical behavior of expansive soils with the application of wetting and drying cycles;
- The finite element framework has to be used to extend the modified shakedown model, to take into account a combined hardening plasticity. Implementing these equations in the finite element code is necessary to simulate the behavior of a geotechnical structure, made up of a heavily dense expansive soil;
- More experimental points at the equilibrium state for expansive soils should be added to take into account the hydraulic hysteresis. The consideration of water retention curve is able to precisely describe the mechanical behavior during wetting and drying cycles;
- The results of suction-controlled test with a triaxial stress state should be considered to model the behavior of expansive soils subjected to wetting and

drying cycles under a fixed shear and confining state, it will improve the understanding of the soil behavior;

∘ Suction distributions due to climate change should be determined by nonlinear Darcy's law considering water flows in the soil, instead of a linear assumption with the depth. This choice will better simulate the real suction cycle range, leading to a satisfactory prediction on the hydromechanical behavior of expansive soils.

Appendix A

Oedometer Device for Cyclic Suction-controlled Tests

The experimental results on expansive soils used in this study are obtained from the suction-controlled odometer tests (Nowamooz, 2007, 2008, 2009, $\cdots$). The schematic representation of this oedometer device is presented in Figure A.1. In this figure, the pump allows to circulate a solution of PEG (*polyethylene glycol*), at a given concentration. This solution passes through the grooved base of the oedometer, which is designed for the circulation of fluid to through the whole bottom surface of the sample. Between the sample and the PEG solution, a semi-permeable membrane is introduced to prevent PEG macromolecules from passing towards the sample.

For the illustrated suction-controlled oedometer device, the maximum imposed suction was 8.5 MPa (imposed suction range between 0 and 8.5 MPa). The diameter of the sample is 7 cm and its initial height is about 1 cm. When a given suction was applied, approximately ten days are required for a stable equilibrium deformation. The mechanical loading is made in the same manner in a typical oedometer test and about two days are needed to reach a stable deformation for a given stress path.

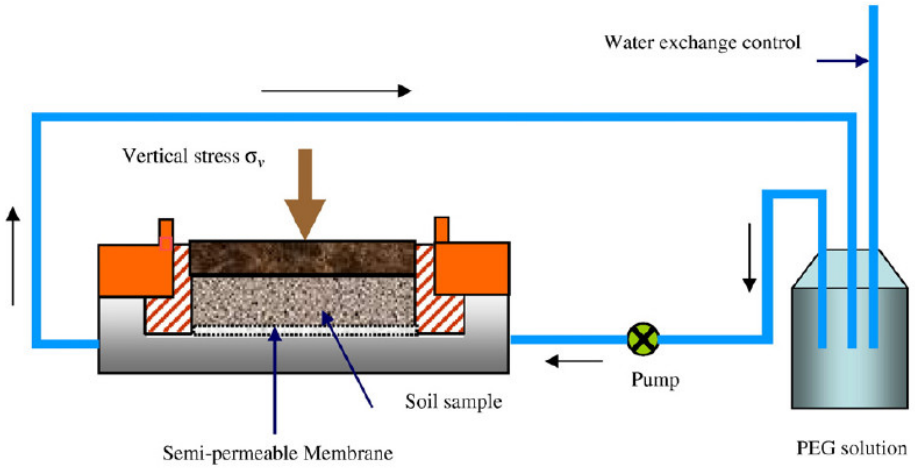

FIGURE A.1: Schematic of the suction-controlled oedometer device using osmotic solutions (Nowamooz and Masrouri, 2008).

Appendix B

Loading Programs of Oedometer Tests on Compacted Soils

Three series tests were performed using the oedometer device on the loose samples (L1, L2, L3), intermediate samples (I1, I2, I3) and dense samples (D1, D2, D3), respectively. The stress paths for these three groups of tests are illustrated in Figure B.1 and Table B.1. The considered initial state is represented by point A in Figure B.1, which corresponds to the sample inserted in the odometers starting with the same initial water content. Point B represents the suction of 8 MPa at an initial vertical pressure of 10 kPa for all tests. Thereafter, a successive wetting and drying cycle were applied between 8 and 0 MPa under three different vertical pressures 15, 30 and 60 kPa. At the end of the successive suction cycles, a loding/unloading cycle was carried out to these samples under three constant suction 0, 2 and 8 MPa. The maximum applied vertical stress was about 1000 kPa for loose samples and 3000 kPa for intermediate samples as well as dense samples.

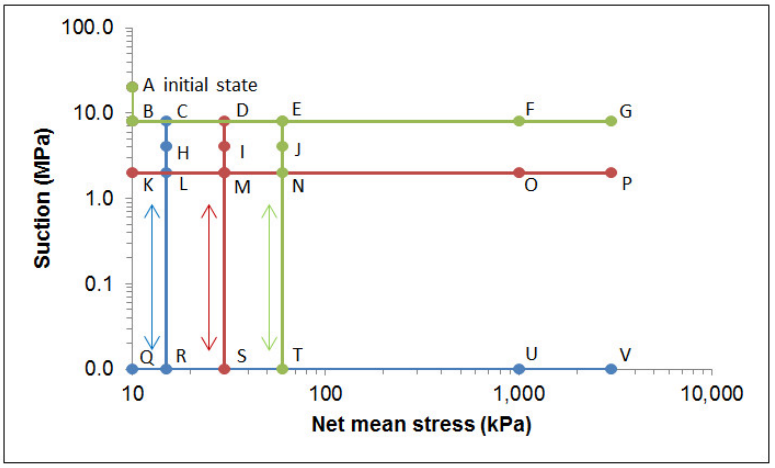

FIGURE B.1: Stress paths in $\sigma_v - s$ plane for suction-controlled tests on compacted expansive soils.

TABLE B.1: Stress paths of suction-controlled oedometer tests on compacted expansive soils

Tests	Stress paths
L1	A-B-C-R-C-R-C-R-C-R-C-R-U-R
L2	A-B-D-S-D-S-D-S-D-S-D-M-O-L
L3	A-B-E-T-E-T-E-T-E-F-C
I1	A-B-C-H-R-H-C-H-R-H-C-R-V-Q
I2	A-B-D-I-S-I-D-I-S-I-D-M-P-K
I3	A-B-E-J-T-J-E-J-T-J-E-G-B
D1	A-B-C-L-R-L-C-L-R-L-C-L-R-L-C-L-R-V-Q
D2	A-B-D-M-S-M-D-M-S-M-D-M-S-M-D-M-P-K
D3	A-B-E-N-T-N-E-N-T-N-E-N-T-N-E-G-B

Appendix C

Loading Programs of Oedometer Tests on Heavily Dense Expansive Soils

The loading program of the cyclic suction-controlled oedometer tests on heavily dense expansive soil is presented in Figure C.1 and Table C.1. The samples were remolded with an initial water content of 10%. Under the compaction pressure of 1500 kPa, the heavily dense expansive states were formed with a dry density of 1.75 $Mg{\cdot}m^{-3}$. The considered initial states are represented by point A in Figure C.1 and point B represents the suction of 8 MPa at an initial vertical pressure of 10 kPa for all tests. Thereafter, three different vertical stresses 15, 30 and 60 kPa were applied to the heavily dense samples. In the end, several successive wetting and drying cycles were applied between 8 MPa and 0 MPa to the heavily dense expansive soils.

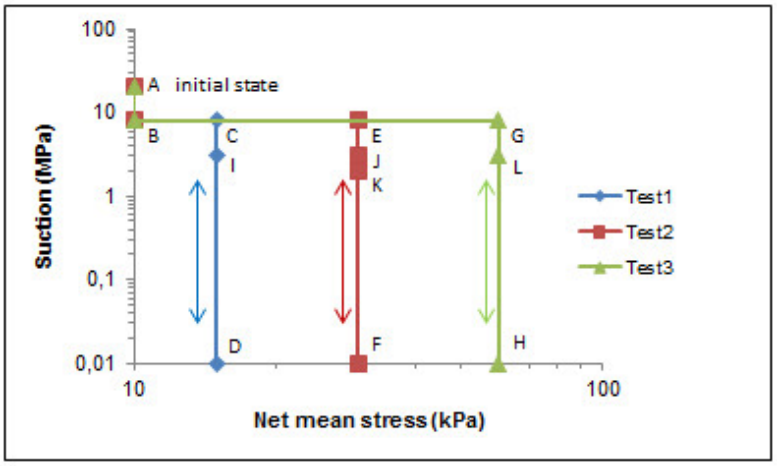

FIGURE C.1: Stress paths in $\sigma_v - s$ plane for suction-controlled tests on heavily dense expansive soils.

TABLE C.1: Stress paths of suction-controlled oedometer tests on heavily dense expansive soils

Test number	Loading paths
Test1	A-B-C-I-D-I-C-I-D-I-C-D-C-D
Test2	A-B-E-J-F-J-E-J-F-J-E-F-E-K
Test3	A-B-G-L-H-L-G-L-H-L-G-L-H-G

Appendix D

Calibration of Shakedown Model on Bentonite-sand Mixture

The capacity of our proposed shakedown model is also investigated for the experimental results published by Alonso *et al.*(2005)[46]. Cyclic wetting and drying cycles between 130 and 4 MPa under three constant net vertical stresses of 98, 196 and 396kPa were performed on a compacted mixture of bentonite-sand with an initial dry density of 1.5 $Mg{\cdot}m^{-3}$. The differences between two successive wetting and drying paths become smaller as the number of cycles increases and the shrinkage strain is accumulated. Eventually, the soil tends towards an elastic state at the end of suction cycles.

Table D.1 summarizes the required parameters of the proposed shakedown model for the mixture of bentonite and sand: parameters C and D are for the linear evolution law of $1/E_r$, calibrated from the elastic equilibrium state at the end of suction cycles; parameters E and F are for the linear evolution law of $1/h$, determined by the accumulated plastic strain during suction cycles; s_α is supposed negligible for the studied material. Based on these model parameters, the calibration of shakedown-based model is carried out. Figure D.1 presents the comparison between test result and model calibration at a given net mean stress (196kPa). This figures shows that the proposed shakedown model is able to reproduce the accumulated plastic strains during the suction cycles at a constant net mean stress.

TABLE D.1: Required shakedown model parameters for bentonite-sand mixture

Parameters	$C(\mathrm{MPa}^{-2})$	$D(\mathrm{MPa}^{-1})$	$E(\mathrm{MPa}^{-2})$	$F(\mathrm{MPa}^{-1})$	s_α(MPa)
Studied material	0.595E-4	0.465E-3	0.262E-3	0.294E-3	negligible

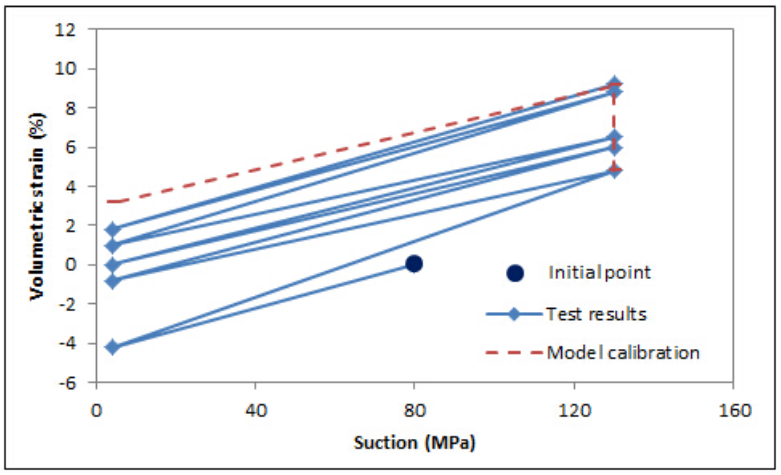

FIGURE D.1: Comparison of test result with model calibration for bentonite-sand mixture at the net mean stress of 196kPa.

Bibliography

[1] Fredlund D. G. and Rahardjo H. Soil mechanics for unsaturated soils. *A Wiley-Interscience Publication, JOHN WILEY and SONS, INC.*, 1993.

[2] Fredlund D. G. and Morgenstern N.R. Stress state variables for unsaturated soils. *Jounal of the Geotechnical Engineering Division*, 103:447–466, May 1977.

[3] Fredlund D. G. Morgenstern N.R. and Widger R.A. Shear strength of unsaturated soils. *Canadian Geotechnical Journal*, 15:313–321, 1978.

[4] Gan J.K.M. Fredlund D.G. and Rahardjo H. Determination of the shear strength parameters of an unsaturated soil using the direct shear test. *Canadian Geotechnical Journal*, 25:500–510, 1988.

[5] Escario V. and Juca V. Shear strength and deformation of partly saturated soils. *12th International Conference on Soil Mechanics and Foundation Engineering*, 2:43–46, 1989.

[6] Childs E.C. An introduction to the physcial basis of soil water phenomena. *A Wiley-Interscience Publication, JOHN WILEY and SONS, INC.*, 1969.

[7] Sharma R.S. Mechanical behavior of unsaturated highly expansive clays. *Doctoral Thesis, University of Oxford, UK*, 1998.

[8] Dineen K. The influence of soil suction on compressibility and swelling. *Doctoral Thesis, University of London (Imperial College of Science, Technology and Medicine), England*, 1997.

[9] Brooks R.H. and Corey A.T. Hydraulic properties of porous media affecting fluid flow. *Journal of Irrigation and Drainage Engineering*, 92:61–88, 1964.

[10] Brutsaert W. Probability for pore-size distribution. *Soil Science*, 101:400–404, 1966.

[11] van Genuchten M.Th. A closed-form equation for predicting the hydraulic conductivity of unsaturated soils. *Soil Science*, 44:892–898, 1980.

[12] Gardner W.R. Some steady state solution of the unsaturated moisture flow equation with application to evaporation from a water table. *Soil Science*, 85:228–232, 1985.

[13] Pereira J.H.F. and Fredlund D.G. Volume change behaviour of collapsible compacted gneiss soil. *Journal of Geotechnical and Geoenvironmental Engineering*, 126(10):907–916, 2000.

[14] Bolt G.H. Analysis of validity of the gouy-chapman theory of the electric double-layer. *Journal of Colloid Science*, 10:206–218, 1955.

[15] Jennings J.E. and Knight K. The prediction of total heave from the double oedometer test. *Transaction of the South African Insitution of Civil Engineers*, 7(9):13–19, 1967.

[16] Gromko G.J. Review of expansive soils. *Journal of Geotechnical Engineering*, pages 667–689, June 1974.

[17] Gens A. and Alonso E.E. Determination of the shear strength parameters of an unsaturated soil using the direct shear test. *Canadian Geotechnical Journal*, 29(6):1013–1032, 1992.

[18] Fookes P.G. and Parry R.H.G. Engineering characteristics of arid soils. *1st International Symposium on Engineering Characteristics of Arid Soils*, July 1993.

[19] Mitchell J.K. Fundamentals of soil behavior. *Wiley, New York.*, 1993.

[20] Yong R.N. Soil suction and soil-water potentials in swelling clays in engineered clay barriers. *Engineering Geology*, 54:3–13, 1999.

[21] Alonso E.E. Vaunat J. and Gens A. Modeling the mechanical behavior of expansive clays. *Engineering Geology*, 54:173–183, 1999.

[22] Low P.F. The swelling of clay: Ii montmorillonites. *Soil Science Society of America Journal*, 44:667–676, 1980.

[23] Sridharan A. and Jayadeva M.S. Double layer theory and compressibility of clays. *Geotechnique*, 32:133–144, 1982.

[24] Alonso E.E. Loret A. Gens A. and Yang D.Q. Experimental behavior of highly expansive double structure clay. *1st International Conference on Unsaturated Soils, Paris*, 1:11–16, 1995.

[25] Barshad I. Adsorption and swelling properties of clay-water systems. *California Department of Natural Resources*, 169:77–90, 1955.

[26] Parham W.E. and Austin G.S. Clay mineralogy, fabric and industrial uses of the shale of the decorah formation, southeastern minnesota. *Minnesota Geological Survey Report of Investigations*, 10:32P, 1969.

[27] Baser O. Stabilization of expansive soils using waste marble dust. *Master of Science Thesis Submitted to Civil Engineering Department, Middle East Technical University*, 2009.

[28] Mokhtari M. and Dehghani M. Swell–shrink behavior of expansive soils, damage and control. *Electronic Journal of Geotechnical Engineering*, 17: 2673–2682, 2012.

[29] Yilmaz I. Relationships between liquid limit, cation exchange capacity and swelling potentials of clayey soils. *Eurasian Soil Science*, 37(5):588–595, 2004.

[30] Panjaitan N.H. Rifai A. and Psumardi A.D.A. Experimental study of cation exchange on expansive clay with electrokinetics process. *International Journal of Civil and Environmental Engineering*, 13(2):29–34, 2013.

[31] Sudjianto A.T. Suryolelono K.B. Rifai A. and Mochtar I.B. The effect of water content change and variation suction in behavior swelling of expansive soil. *International Journal of Civil and Environmental Engineering*, 11(3): 29–34, 2011.

[32] van der Merwe D.H. The prediction of heave from the plasticity index and percentage clay fraction of soils. *Civil Engineers in South Africa*, 6(6):103–107, 1964.

[33] Nayak N.V. and Christensen R.W. Swelling characteristics of compacted expansive soils. *Clays and Clay Minerals*, 19:251–261, 1970.

[34] Armstrong C.P. Effect of fabric on the swelling of highly plastic clays. *Master Thesis, Department of Civil Engineering, The University of Texas at Austin, United States of America*, 2014.

[35] Nowamooz H. Jahangir E. and Masrouri F. Volume change behaviour of a swelling soil compacted at different initial states. *Engineering Geology*, 153 (3-4):25–34, 2013.

[36] Sabnis A.K. Impact of moisture variation on strength and deformation of clays. *ETD Collection for University of Taxas, EI Paso*, 1993.

[37] Mitchell P.W. Clamate change effects on expansive soil movements. *18th International Conference on Soil Mechanics and Geotechnical Engineering, Paris*, pages 1159–1162, 2013.

[38] Driscoll R. The influence of vegetation on the swelling and shrinking of clay soils in britain. *Geotechnique*, 33(2):93–105, 1983.

[39] Fredlund D.G. and Hung V.Q. Prediction of volume change in an expansive soil as a result of vegetation and environmental changes. *ASCE Conference on Expansive Clay Soils and Vegetative Influences on Shallow Foundaiongs, Texas*, pages 24–43, 2001.

[40] Cui Y.J. Sultan N. and Delage P. A thermal-mechanical model for saturated clays. *Canadian Geotechnical Journal*, 37(3):607–620, 2000.

[41] Tang A.M. Cui Y.J. and Barnel N. Thermal-mechanical behavior of a compacted swelling clay. *Geotechnique*, 58(1):45–54, 2008.

[42] Wheeler S.J. Sharma R.S. and Buisson S.R. An elasto-plastic critical state framework for unsaturated soil. *Geotechnique*, 45:35–53, 2003.

[43] Baser O. Geotechnical aspects of buildings on expansive soils in kibaha, tanzania: Preliminary study. *Licentiate Thesis Submitted to Department of Civil and Architectural Engineering, Royal Institute of Technology*, 2006.

[44] Ahmad R. Engineering properties and mineralogical composition of expansive clays in al-qatif area. *Master Thesis, Saudi Arabia: University of Petroleum and Minerals Dhahran*, 1988.

[45] Lucian C. Geotechnical aspects of buildings on expansive soils in kibaha, tanzania. *Licentiate Thesis, Department of Civil and Architectural Engineering, Royal Institute of Technology, Stockholm, Sweden*, 2011.

[46] Alonso E.E. Romero E. Hoffmann C. and Garcia-Escudero E. Expansive bentonite-sand mixtures in cyclic controlled-suction drying and wetting. *Engineering Geology*, 81(3):213–226, 2005.

[47] Cuisinier O. and Masrouri F. Hydromechanical behavior of a compacted swelling soil over a wide suction range. *Engineering Geology*, 81(3):204–212, 2005.

[48] Wheeler S.J. and Sivakumar V. An elasto-plastic critical state framework for unsaturated soil. *Geotechnique*, 45(1):35–53, 1995.

[49] Alonso E.E. Gens A. and Hight D.W. Special problem soils, general report. *9th European Conference on Soil Mechanics and Foundation Engineering, Balkema Dublin*, 3:1087–1146, 1987.

[50] Vicol P.T. Comportement hydraulique et mechanique d'un sol fin non sature: Application a la modelisation. *These de Doctorat, Ecole Nationale des Ponts et Chaussee, Paris*, 1990.

[51] Cui Y.J. Etude du comportement d'un limon compacte non sature et de sa modelisation dans un cadre elasto-plastique. *These de Doctorat, Ecole Nationale des Ponts et Chaussee, Paris*, 1993.

[52] Futai M.M. de Almeida M.S.S. Conciani W. and Silva Fiho F.C. Experimental and theoretical evaluation of plate load test in collapsible soil, unsaturated soils. *3rd International Conference on Unsaturated Soils, UNSAT*, 2: 721–726, 2002.

[53] Kogho Y. Asano I. and Tagashira H. Modelling of state surfaces of unsaturated soils. *Clay Science for Engineering*, 9:467–474, 2001.

[54] Zhan L.T. and Ng C.W.W. Shear strength characteristics of an unsaturated expansive clay. *Canadian Geotechnical Journal*, 43(7):751–763, 2006.

[55] Miao L. Liu S. and Lai Y. Research of soil water characteristic and shear strength of naniang expansive soil. *Engineering Geology*, 65:261–267, 2002.

[56] Ye W.M. Zhang Y.W. Chen B. Zhou X.H. and Xie Q. Shear strength of an unsaturated weakly expansive soil. *Journal of Rock Mechanics and Geotechnical Engineering*, 2(2):155–161, 2010.

[57] Chu T.Y. and Mou C.H. Volume change characteristics of expansive soils determined by controlled suction tests. *3rd International Conference of Expansive soils, Haifa*, 2:177–185, 1973.

[58] Pousada E. Deformabilidad de arcillas expansivas bajo succion controlada. *Doctoral Thesis, Universidad Politecnica de Madrid, Spain*, 1984.

[59] Dif A.E. and Bluemel W.F. Expansive soils under cyclic drying and wetting. *Geotechnical Testing Journal*, 14:96–102, 1991.

[60] Day R.W. Swell-shrink behavior of compacted clay. *Journal of Geotechnical Engineering*, 120:618–623, 1994.

[61] Al-Homoud A. Basma A.A. Husein Malkawi A.I. and Al-Bashabsheh M.A. Cyclic swelling behavior of clays. *Journal of Geotechnical Engineering*, 121: 562–565, 1995.

[62] Basma A.A. Al-Homoud A. Husein Malkawi A.I. and Al-Bashabsheh M.A. Swelling-shrinkage behavior of natural expansive clays. *Applied Clay Science*, 11:211–227, 1996.

[63] Subba R.K. Rao S.M. and Gangadhara S. Swelling behavior of a desiccated clay. *Geotechnical Testing Journal*, 23(2):193–198, 2000.

[64] Tripathy S. Cyclic swellshrink behaviour of a compacted expansive soil. *Geotechnical and Geological Engineering*, 27(1):89–103, 2009.

[65] Nowamooz H. and Masrouri F. Influence of suction cycles on the soil fabric of compacted swelling soil. *Comptes Rendus Geoscience*, 342(12):901–910, 2010.

[66] Chen R. and Ng C.W.W. Impact of wettingdrying cycles on hydro-mechanical behavior of an unsaturated compacted clay. *Applied Clay Science*, 86:38–46, 2013.

[67] Nowamooz H. and Masrouri F. Hydromechanical behaviour of an expansive bentonite/silt mixture in cyclic suction-controlled drying and wetting tests. *Engineering Geology*, 101(3-4):154–164, 2008.

[68] Alonso E.E. Gens A. and Josa A. A constitutive model for partially saturated soils. *Géotechnique*, 40:405–430, 1990.

[69] Lloret A. Villar M.V. Sanchez M. Gens A. Pintado X. and Alonso E.E. Mechanical behavior of heavily compacted bentonite under high suction changes. *Geotechnique*, 53:27–40, 2003.

[70] Terzaghi K. The shear resistance of saturated soils and the angle between the planes of shear. *1st International Conference on Soil Mechanics and Foundation Engineering*, 1:22–26, June 1936.

[71] Rendulic L. A fundamental law of clay mechanics and its experimental verification. *Bauingenieur*, 18:459–467, 1936.

[72] Bishop A.W. and Eldin G. Undrained triaxial tests on saturated soils and their significance in the general theory of shear strength. *Geotechnique*, 2: 13–32, 1950.

[73] Laughton A.S. The compaction of ocean sediments. *Ph.D. Thesis, University of Cambridge*, 1955.

[74] Skempton A.W. Effective stress in soils, concrete and rocks. *Pore Pressure and Suction in Soils, Butterworths, London*, page P4, 1961.

[75] Bishop A.W. The principle of effective stress. *Teknisk Ukeblad*, 106(39): 859–863, 1959.

[76] Aitchison G.D. Relationships of moisture stress and effective stress functions in unsaturated soils. *Pore Pressure and Suction in Soils*, pages 47–52, March 1961.

[77] Jennings J.E. A revised effective stress law for use in the prediction of the behavior of unsaturated soils. *Pore Pressure and Suction in Soils*, pages 26–30, March 1961.

[78] Jennings J.E. and Burland J.B. Limitations to the use of effective stress in partly saturated soils. *Geotechnique*, 12(2):125–144, 1962.

[79] Richards B.G. Moisture flow and equilibria in unsaturated soils for shallow foundations. *Permeability and Capillarity of Soils*, pages 4–34, 1967.

[80] Aitchison G.D. The quantitative description of the stress-deformation behavior of expansive soils. *3rd International Conference of Expansive soils, Haifa Israel*, 2:79–82, 1973.

[81] Houlsby G.T. The work input to an unsaturated granular material. *Geotechnique*, 47(1):193–196, 1997.

[82] Cui Y.J. Delage P. and Sultan N. An elasto-plastic model for compacted soils. *1st International Conference on Unsaturated Soils, Paris*, 2:703–709, 1995.

[83] Romero E. and Vaunat J. Experimental evidence and theoretical approaches in unsaturated soils. *International Workshop on Unsaturated Soils, Netherlands*, pages 91–106, 2000.

[84] Buisson M.S.R. and Wheeler S.J. Inclusion of hydraulic hysteresis in a new elastoplastic framework for unsaturated soils. *Workshop on Unsaturated Soils, Trento, Italy*, 2000.

[85] Jommi C. and Di Prisco C. Un semplice approccio teorico per la modellazione del comportamento meccanico dei terreni granulari parzialmente saturi (in italian). *In Atti Convegno Sul Tema: Il Ruolo deiFluidi nei Problemi di Ingegneria Geotecnica, Mondovi*, pages 167–188, 1994.

[86] Abou bekr N. Modelisation du comportelent mecanique et hydraulique des sols partiellement satures. *Ph.D. Thesis, Ecole centrale Paris*, 1995.

[87] Bolzon G. Schrefler B.A. and Zienkiewicz O.C. Elasto-plastic soil constitutive laws generalized to partially saturated states. *Geotechnique*, 46:279–289, 1996.

[88] Sun W.J. and Sun D.A. Coupled modeling of hydromechanical behavior of unsaturated compacted expansive soils. *International Journal for Numerical and Analytical Methods in Geomechanics*, 36(8):1002–1022, 2012.

[89] Melan E. Zur plastizitat des raumlichen kontinuums. *Ingenieur Archiv*, 9: 116–125, 1938.

[90] Koiter W.T. General theorems for elastic-plastic solids. *Progress in Solid Mechanics*, 1:167–221, 1960.

[91] Bleich H. Uber die bemessung statisch unbestimmter stahltragwerke unter berucksichtigung des elastisch-plastischen verhaltens des baustoffes. *Bauingenieur*, 19-20:261, 1932.

[92] Symonds P.S. Shakedown in continuous media. *Journal of Applied Mechanics*, 18:85, 1951.

[93] Symonds P.S. and Neal B.G. Recent progress in the plastic methods of structural analysis. *Journal Franklin Institute*, 252:383–407, 1951.

[94] Neal B.G. Plastic collapse and shakedown theorems for structures of strain-hardening material. *Journal of the Aeronautical Sciences*, 17:297, 1950.

[95] Maier G. Plastic collapse and shakedown theorems for structures of strain-hardening material. *International Symposium on Foundations of Plasticity, Warsaw*, 1:213, 1972.

[96] Maier G. A general shakedown theorem for inelastic materials. *3rd International Conference on Structural Mechanics in Reactor Technology*, L5/2, 1975.

[97] Konig J.A. Shakedown criteria in the case of loading and temperature variations. *Journal of Theoretical and Applied Mechanics*, 21:99–108, 1982.

[98] Konig J.A. On exactness of the kinematical approach in the strucutre shakedown and limit analysis. *Ingenieur Archiv*, 52:318–326, 1982.

[99] Zarka J. and Casier J. Elastic-plastic response of structure to cyclic loading: Practical rules. *Mechanics Today*, 6:93–198, 1979.

[100] Sharp R. and Booker J. Shakedown of pavements under moving surface loadelastic-plastic response of structure to cyclic loading: Practical rules. *Journal of Transportation Engineering*, 6:1–14, 1984.

[101] Raad L. Weichert D. and Najim W. Stability of multilayer systems under repeated loads. *Transportation Research Reccord*, 1207:181–186, 1988.

[102] Raad L. Najim W. Weichert D. and Gross weege J. Shakedown of shell-like structures allowing for certain geometrical non-linearities. *Journal of Applied Mathematics and Mechanics*, 69:T366, 1989.

[103] Radovsky R.S. and Murashina N.V. Shakedown of subgrade soil under repeated loading. *Transportation Research Reccord*, 1547:82–88, 1996.

[104] Yu H.S. and Hossain M.Z. Lower bound shakedown analysis of layered pavements using discontinuous stress fields. *Computer Methods in Applied Mechanics and Engineering*, 167:209–222, 1998.

[105] Shiau S.H. and Yu H.S. Shakedown of three-layered pavements. *7th International Conference on Structural Failure and Plasticity, Melbourne, Australia*, 1999.

[106] Yu H.S. Three-dimensional analytical solutions for shakedown of cohesive frictional materials under moving surface loads. *Proceedings of the Royal Society*, 461:1951–1964, 2005.

[107] Wang J. and Shu H.S. Three-dimensional shakedown solutions for anisotropic cohesive-frictional materials under moving surface loads. *International Journal for Numerical and Analytical Methods in Geomechanics*, 38(4):331–348, 2014.

[108] Collins I.F. and Cliffe P.F. Shakedown in frictional materials under moving surface loads. *International Journal for Numerical and Analytical Methods in Geomechanics*, 11(4):409–420, 1987.

[109] Collins I.F. and Boulbibane M. Geomechanical analysis of unbound pavements based on shakedown theory. *Journal of Geotechnical and Geoenvironmental Engineering*, 126(1):50–59, 2000.

[110] Chen H.F. and Ponter A.R.S. Integrity assessment of a 3d tube plate using the linear matching method, part 1 shakedown reverse plasticity and ratchetting. *International Journal of Pressure Vessel Technology*, 82:85–94, 2005.

[111] Li H.X. and Yu H.S. Integrity assessment of a 3d tube plate using the linear matching method, part 1 shakedown reverse plasticity and ratchetting. *International Journal of Solids and Structures*, 43:6597–6614, 2006.

[112] Habiballah T. and Chazallon C. An elastoplastic model based on the shakedown concept for flexible pavements unbound granular materials. *International Journal for Numerical and Analytical Methods in Geomechanics*, 29: 577–596, 2005.

[113] Allou F. Chazallon C. and Hornych P. A numerical model for flexible pavements rut depth evolution with time. *International Journal for Numerical and Analytical Methods in Geomechanics*, 33:1–22, 2007.

[114] Chazallon C. Allou F. Hornych P. and Mouhoubi S. Finite element modeling of the long term behavior of a full scale flexible pavement with the shakedown theory. *International Journal for Numerical and Analytical Methods in Geomechanics*, 33:45–70, 2009.

[115] Chazallon C. Koval G. and Mouhoubi S. A two-mechanism elastoplastic model for shakedown of unbound granular materials and dem simulations. *International Journal for Numerical and Analytical Methods in Geomechanics*, 33:1847–1868, 2012.

[116] Moreau J.J. Rafle par un convexe variable. *Seminaire unilaterale, Universite de Montpellier*, 1971.

[117] Nowamooz H. Retrait/gonflement des sols argileux compactes et naturels. *Doctoral Thesis, Institut National Polytechnique de Lorraine, France*, 2007.

[118] Romero E. Gens A. and Lloret A. Water permeability, water retention and microstructure of unsaturated boom clay. *Engineering Geology*, 54:117–127, 1999.

[119] Nowamooz H. and Masrouri F. Density-dependent hydromechanical behaviour of a compacted expansive soil. *Engineering Geology*, 106(3-4):105–115, 2009.

[120] Nowamooz H. and Masrouri F. Shrinkage/swelling of compacted clayey loose and dense soils. *Comptes Rendus Mecanique*, 337(11-12):781–790, 2009.

[121] CAST3M. Cast3m is a research fem environment and its development is sponsored by the french atomic energy commission, http://www-cast3m.cea.fr/.

Modélisation du Comportement Hydromécanique des Sols Gonflants Basée sur la Théorie de L'état Limite

Doctorant : Kai LI

Directeur de Thèse : Bernard Migault

Equipe Génie Civil et Energétique, Laboratoire ICube

24 Boulevard de la Victoire, 67084, Strasbourg, France

Résumé étendu

- **Contexte**

En Génie Civil, les phénomènes de retrait-gonflement des sols gonflants et des formations géologiques argileuses induisent des tassements différentiels qui se manifestent par des désordres affectant pricipalement les structures construites en surface et les ouvrages enterrés. Depuis 1989, ce sont près 8 000 communes françsises, reparties dans 90 départements de France métroplitaine qui ont été reconnues au moins une fois en état de catastrophe naturelle vis à vis du retrait-gonflement, ce qui traduit parfaitement l'ampleur du phénomène. Il est donc important d'appréhender le comportement hydromécanique de ces matériaux afin de mieux maîtriser leur utilisation.

Différents modèles élastoplastiques ont été développés pour décrire le comportement des sols non saturés. Alonso *et al*. (1990) ont proposé un modèle élastoplastique pour les sols non saturés non gonflants BBM (Barcelona Basic Model). Ce modèle est une extension du modèle de Cam-clay modifié dans le domaine des sols non saturés, il a été révisé pour les sols gonglants sous l'appellation BExM (Barcelona Expansive Model) (Alonso *et al*. 1999). L'introduction des surfaces de charge SD et SI permet de reproduire le gonflement ou le retrait irréversible lors d'une humidification ou d'un séchage. De même, il autorise la modélisation des variations de volume enregistrées au cours de cycles hydriques successifs en intégrant l'influence de la charge verticale. Cependant, ce modèle présente de nombreux paramètres, i.e. l'expression de couplage entre la micro- et la macrostructure. La calibration de ces paramètres a besoin de plusieurs essais expérimentaux qui prennent du temps pour caractériser le comportement des sols gonflants.

Le concept d'état limite a été développé par Zarka et Casier (1979) pour les structures métalliques soumises à un chargement cyclique. Chazallon *et al*. (2005, 2007, ...) ont appliqué cette méthode pour décrire le comportement sous un grand nombre de cycles des matériaux granulaires de chaussées lors d'essais triaxiaux à chargements répétés. Ils ont introduit les variables internes transformées structurelles pour caractériser le comportement mécanique et ensuite construit les géométries locales dans le plan des variables internes transformées structurelles afin d'estimer l'état stabilisé et les déformations relatives. Cette approche est une méthode simplifiée qui permet de déterminer directement l'état limite et requiert moins de paramètres de modélisation. Surtout, cette méthode est capable de remplacer le calcul pas à pas et de gagner du temps quand un grand nombre de cycles de succion sont appliqués.

Dans ce contexte, un modèle basé sur la méthode de Zarka est proposé pour modéliser le comportement hydromécanique de sols gonflants soumis à des cycles de succion sous différentes charges vericales constantes et la validation de ce modèle simplifié est realisé par la comparaison entre les résultats du modèle et les résultats obtenus lors d'essai oedométrique sur sol gonflant.

- **Plan du mémoire**

Le contexte et les objectifs de la thèse étant fixés, ce mémoire est découpé en cinq chapitres avec un bref résumé des conclusions et perspectives :

Le chapitre 1 : "Introduction" présente les objectifs de cette étude et la structrue de cette thèse.

Le chapitre 2 : "Bibliographie relative au sol gonflant non saturé" contient quatre parties. La première partie introduit les définitions principales et les concepts généraux de la mécanique des sols non saturés. La deuxième partie résume la nature des sols gonflants, les facteurs affectant le retrait/gonflement, les dommages aux structures et le contrôle du comportement de retrait/gonflement. La troisième partie examine les résultats expérimentaux typiques sur le comportement hydromécanique des sols gonflants pour mieux comprendre le comportement du sol. A la fin, la quatrième partie examine plusieurs modèles représentatifs de sols gonflants, présentant l'état de compréhension actuelle sur les sols gonflants.

Le chapitre 3 : "Modélisation analytique des sols gonflants avec la théorie de l'état limite", tout d'abord présente la théorie de l'état limite et développe un modèle basé sur cette méthode pour modéliser les sols gonflants non saturés soumis à des cycles de succion sous différentes charges vericales constantes. Les paramètres du modèle

simplifié sont calibrés par les résultats de l'essai oedométrique sur les sols gonflants compactés lâches et denses (Nowamooz 2008, 2013). Par la suite, le modèle proposé est validé pour le sol gonflant compacté intermédiaire par la comparaison entre la prédiction de modèle et les résultats expérimentaux. Dans le même temps, un modèle de couplage entre les cycles de succion et les comportements mécaniques est dévelopé, la validation de ce modèle est également effectuée en montrant les comparaisons des calculs du modèle avec les résultats expérimentaux. Finalement, l'analyse de sensibilité des paramètres du modèle est effectuée pour étudier l'influence des paramètres du modèle sur sa réponse.

Le chapitre 4 : "Modélisation numérique du comportement in situ des sols gonflants", présente la formulation éléments finis pour une structure élastoplastique soumise à des cycles de succion entre des conditions extrêmement sèches et humides. Ensuite, le modèle simplifié est implanté dans un code aux éléments finis CAST3M et trois exemples bidimensionnels sont simulés pour étudier le comportement in situ des sols gonflants soumis à des cycles de succion sous différentes charges vericales. Pour étudier l'influence de la contrainte verticale, une série de contraintes verticales sont appliquées au modèle dans ces simulations.

Le chapitre 5 : "Application de la théorie de l'état limite au sol gonflant extrêmement dense", contient une modification de la théorie classique développée par Zarka, avec la plasticité combinée de l'écrouissage cinématique et de l'écrouissage isotrope. Par la suite, cette méthode modifiée est utilisée pour modéliser les sols gonflants extrêmement denses soumis à des cycles de succion sous différentes charges vericales constantes. A la fin, le modèle modifié est calibré en comparant le calcul du modèle avec les résultats expérimentaux (Nowamooz, 2009).

Un chapitre supplémentaire : "Conclusions et perspectives", contient un résumé des conclusions de cette étude et propose plusieurs recommandations relatives à l'analyse de l'état limite et les études futures potentielles.

- **Modélisation analytique des sols gonflants avec la théorie de l'état limite**

La relation entre la teneur en eau du sol et la succion correspondante est appelée courbe de rétention de l'humidité du sol (Soil Water Retention Curve). Cette courbe peut être obtenue par drainage, séchage d'un sol initialement saturé ou bien par humidification, mouillage d'un sol initialement sec. La Figure 1 montre l'évolution théorique de la courbe de rétention au cours des cycles de succion.

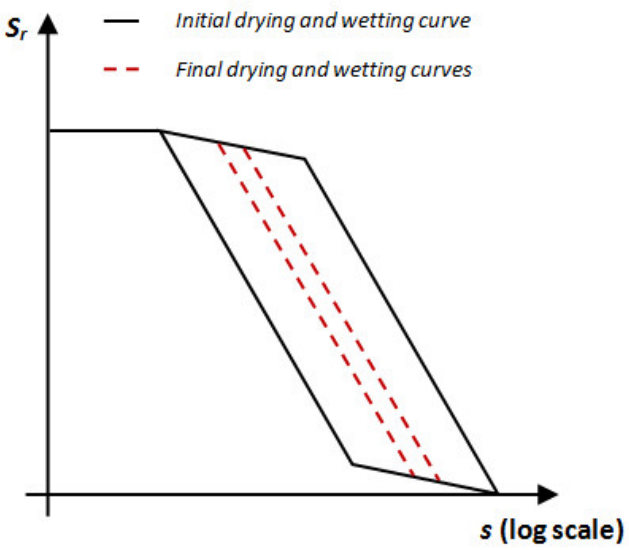

Figure 1. Evolution théorique de la courbe de rétention au cours des cycles de succion.

Dans cette figure, il y a un phénomène évident d'hystérésis lors des cycles de succion. L'hystérésis devient plus faible avec les cycles successifs suivants. Cependant, il ne peut pas être complètement éliminé, même si l'état d'équilibre est attendu après quelques cycles de succion. Ce comportement hydraulique indique que le cas de l'accommodation a lieu au cours des cycles de succion. En d'autres termes, la théorie de l'accommodation devrait être utilisée pour modéliser le comportement hydromécanique des sols gonflants lorsque les cycles de succion sont appliqués.

Le modèle basé sur la théorie de l'accommodation est développé dans le plan du paramètre interne transformé—contrainte moyenne nette avec une surface de charge de forme rectangulaire. Les paramètres élasitiques du modèle sont déterminés lors de l'état d'équilibre obtenu au moyen de l'essai oedométrique, en plus, les paramètres plastiques sont calibrés à partir des déformations plastiques cumulées pendant les cycles de succion lors de l'essai oedométrique. Dans cette étude, on suppose que la valeur de la limite élastique de succion est petite, égale à 0 MPa.

En dehors du modèle d'accommodation, le modèle de couplage entre les cycles de succion et le comportement mécanique est également développé pour illustrer la translation de la surface de chargement-effondrement (PLC : Pseudo loading collapse). Les paramètres du modèle de couplage sont déterminés par les essais de compressibilité à succion contrôlée des sols gonflants. Par la suite, les comparaisons des résultats

expérimentaux avec les calculs du modèle sont réalisées pour montrer la capacité du modèle proposé.

A la fin de cette partie, l'analyse de sensibilité des paramètres du modèle est réalisée. Selon l'analyse, on trouve que toutes les variations de réponse du modèle sont moins importantes que les variations des paramètres d'entrée du modèle, et ceci est particulièrement vrai pour le paramètre de limite élastique de succion.

- **Modélisation numérique du comportement in situ des sols gonflants**

Dans cette partie, la formulation aux éléments finis du modèle a été tout d'abord développée pour résoudre le problème structurel . Ensuite, ces équations ont été implantés dans un code de calcul aux éléments finis CAST3M. La Figure 2 est le modèle d'éléments finis pour simuler le comportement in situ des sols gonflants.

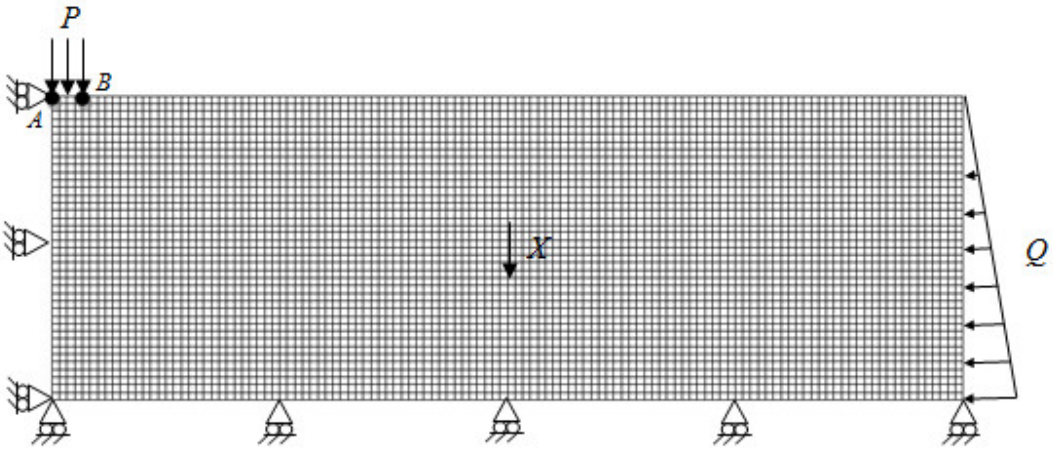

Figure 2. Maillage et conditions aux limites du modèle d'éléments finis

Le modèle d'éléments finis est considéré élastoplastique. La force massique ***X*** ainsi que la pression latérale ***Q*** sont définies dans ce modèle. Une contrainte verticale ***P*** est appliquée à la surface AB et les cycles de succion sont ensuite imposés dans le volume du modèle. Finalement, les simulations numériques sont réalisées par le modèle proposé basé sur la théorie de l'état limite.

Dans ces simulations, trois états initiaux d'un sol gonflant (lâche, intermédiaire et dense) sont utilisés. D'après les résultats, on peut observer que les déformations de retrait sont cumulées pour le sol lâche et les déformations de gonflement sont cumulées pour le sol dense. Cependant, les déformations de gonflement pour le sol intermédiaire sont

produites avec une intensité inférieure à celle du sol dense et les déformations de retrait sont produites avec une intensité supérieure à celle du sol lâche.

En plus, on trouve un unique tassement pour le sol lâche et un unique gonflement pour le sol dense à la fin des cycles de succion. Pour le sol intermédiaire, il n'y a pas de tassement après les cycles de succion et le gonflement diminue avec l'augmentation des contraintes verticales. Tous ces résultats peuvent s'expliquer par l'existence du champ de contraintes résiduelles dans la structure étudiée.

- **Application de la théorie de l'état limite au sol gonflant possédant une grande densité**

L'evolution théorique de la courbe de rétention au cours des cycles de succion pour le sol gonflant ayant une grande densité est présentée dans la Figure 3. Lors des cycles de succion, une légère hystérésis est observée pour le sol gonflant extrêmement dense. Avec les cycles de succion, la boucle de rétention devient négligeable et il peut être considéré comme une ligne droite, ce qui conduit à un état élastique linéaire à la fin des plusieurs cycles où l'adaptation a lieu. Par conséquent, on peut considérer un état d'équilibre élastique linéaire (le cas de l'adaptation) pour le sol gonflant extrêmement dense à la fin des cycles de succion.

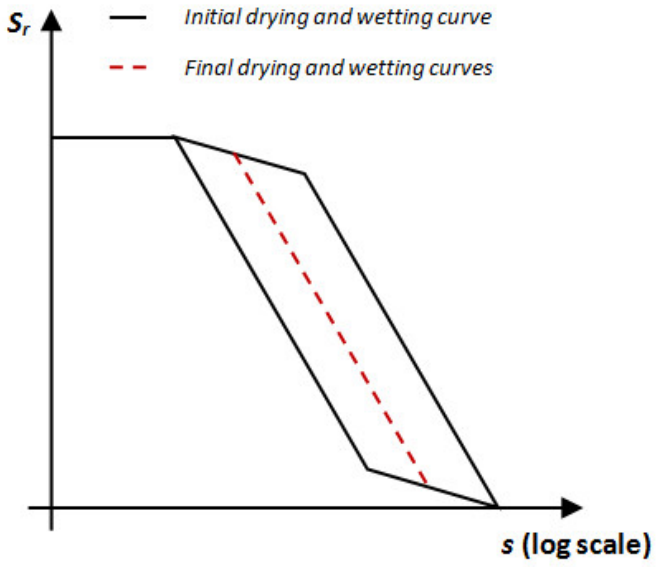

Figure 3. L'evolution théorique de la courbe de rétention au cours des cycles de succion pour le sol gonflant extrêmement dense.

Cependant, le modèle proposé ne peut pas expliquer l'état d'équilibre élastique linéaire des sols gonflants extrêmement dense après plusieurs cycles de succion. Donc, il faut modifier la théorie de l'état limite avec une plasticité combinée pour modéliser le comportement mécanique du sol gonflant extrêmement dense.

Dans cette partie, on a tout d'abord modifié la théorie classique de l'état limite avec l'écrouissage isotrope. Ensuite, cette méthode modifiée est utilisée pour modéliser le comportement hydromécanique du sol gonflant etrêmement dense. Le modèle modifié a besoin de cinq paramètres à calibrer : deux paramètre élastiques sont déterminés par l'état équilibre de l'essai oedométrique et deux paramètres plastiques sont calibrés par les déformations plastiques cumulées pendant les cycles de succion de l'essai oedométrique. Pour le dernier paramètre (la limite élastique de succion), on a fait l'hypothèse qu'il est petit, égale à 0 MPa. Finalement, la calibration du modèle modifié est présentée à partir des résultats expérimentaux de l'essai oedométrique.

- **Conclusions et perspectives**

Dans cette étude, on a tout d'abord examiné les résultats expérimentaux typiques et plusieurs modèles représentatifs pour mieux comprendre le comportement du sol gonflant. Ensuite, un modèle basé sur la théorie classique de l'état limite est développé pour modéliser les sols gonflants non saturés soumis à des cycles de succion sous différentes charges vericales constantes. La validation de ce modèle proposé est réalisée en comparant les calculs du modèle aux résultats expérimentaux des essai oedométriques. La formulation du modèle dans le cadre des éléments finis a été développée, d'après le modèle analytique proposé pour simuler le comportement in situ des sols gonflants. Les résultats de la modélisation numérique d'une structure sous des cycles de succion, montrent des résultats encourageants avec un temps de calcul réduit. Pour appliquer la théorie de l'état limite au sol gonflant extrêmement dense, un modèle modifié est proposé pour modéliser ses comportements hydromécaniques. A la fin, la calibration du modèle modifié est présentée en comparant les calculs du modèle aux résultats experimentaux des 'essais oedométriques.

Les résultats obtenus dans cette thèse ont donnés une meilleure compréhension du comportement des sols gonflants non saturés en présentant un modèle possédant un nombre de paramètre réduit.

- **Bibliographie**

[1] Alonso EE, Gens A, Josa A, A constitutive model for partially saturated soils. Geotechnique 1990; 40: 405-430.

[2] Alonso EE., Vaunat J, Gens A. Modeling the mechanical behavior of expansive clays. Engineering Geology 1999; 54: 173-183.

[3] Zarka J, Casier J. Elastic plastic response of structure to cyclic loading: practical rules. In: Nemat-Nasser S, editor. Mechanics Today, vol. 6. Pergamon Press: Oxford; 1979, p. 93-198.

[4] Habiballah T, Chazallon C. An elastoplastic model based on the shakedown concept for flexible pavements unbound granular materials. International Journal for Numerical and Analytical Methods in Geomechanics 2005; 29: 577-596.

[5] Allou F, Chazallon C, Hornych P. A numerical model for flexible pavements rut depth evolution with time. International Journal for Numerical and Analytical Methods in Geomechanics 2007; 33: 1-22.

[6] Nowamooz H, F,Masrouri. Hydromechanical behavior of an expansive bentonite/silt mixture in cyclic suction-controlled drying and wetting tests. Engineering Geology 2008; 101: 154-164.

[7] Nowamooz H, Jahangir E, Masrouri F. Volume change behavior of a swelling soil compacted at different initial states. Engineering Geology 2013; 153: 25-34.

[8] Nowamooz H, F,Masrouri. Shrinkage/swelling of compacted clayey loose and dense soils. Comptes Rendus Mécanique 2009; 337 (11-12): 781-790.

- **Publications principles**

1. Li Kai, Nowamooz Hossein, Chazallon Cyrille, Migault Bernard. Numerical modeling of unsaturated expansive soils subjected to wetting and drying cycles based on shakedown theory. *Computers and Geotechnics*. (Soumis, Novembre 2014, 35 pages)

2. Li Kai, Nowamooz Hossein, Chazallon Cyrille, Migault Bernard. Modeling of dense expansive soils subjected to wetting and drying cycles based on shakedown theroy. *11th World Congress on Computational Mechanics (WCCM XI)*. 2014.7. (11 pages)

3. Li Kai, Nowamooz Hossein, Chazallon Cyrille, Migault Bernard. An elasto-plastic model for unsaturated expansive soils based on shakedown concept. *XII International Conference on Computational Plasticity*. 2013.9. (10 pages)

Kai LI

MODELISATION DU COMPORTEMENT HYDROMECANIQUE DES SOLS GONFLANTS BASEE SUR LA THEORIE DE L'ETAT LIMITE

Résumé

Les matériaux argileux sont soumis aux chemins complexes de succion/contrainte qui se manifestent par des désordes affectant pricipalement les structures construites en surface et les ouvrages enterrés. Dans ce contexte, il est important d'appréhender le comportement hydromécanique de ces matériaux afin de mieux maîtriser leur utilisation. Le comportement hydromécanique complexe des matériaux argileux est directement relié à leur strucuture interne qui a été le principal sujet de plusieurs études sur la micro- et macrostructure des sols. Ces études ont conduit aux développements des modèles élastoplastiques pour sols gonflants. Les modèles existants sont capables de simuler le comportement principal de sol gonflant non saturé, mais ils présentent un grand nombre de paramètres, ce qui prend du temps pour le calcul. Par conséquence, on propose une méthode simplifiée pour modéliser le comportement hydromécanique des sols gonflants basée sur la théorie de l'état limite. Ce modèle est tout d'abord validé par les résultats de l'essai oedométrique. Ensuite, il est implanté dans un code aux éléments finis (CAST3M) pour simuler le comportement in situ des sols gonflants. Enfin, l'application de la théorie de l'état limite au sol gonflant avec une grande densité est effectuée par la combinaison de l'écrouissage cinématique et l'écrouissage isotrope.

Mots clés: sols gonglants non saturés; théorie de l'adaptation; théorie de l'accommodation; modélisation par éléments finis

Abstract

Clayey materials are often subjected to the complex suction/stress paths, causing many problems in both surface structures and buried structures built on them. In this context, it is important to study the hydromechanical behavior of these materials in order to better control their use in civil engineering. The complex hydromechanical behavior of clay materials is basically connected to their fabric which has been the main subject of several studies on the micro- and macrostructure of soils. These studies have led to the development of elastoplastic models for expansive soils. The existed models are able to simulate the basic behavior of unsaturated expansive soil, but present a large number of model parameters, leading to a time-consuming calculation. Therefore, we propose a simplified method to model the hydromechanical behavior of expansive soils based on shakedown concept. This model is first validated by the experimental results of cyclic suction-controlled oedometer tests. Then, it is implemented in a finite element code (CAST3M) to simulate the in-situ behavior of expansive soils. Finally, the application of shakedown theory to heavily dense expansive soils is carried out by considering a combined hardening plasticity.

Key words: unsaturated expansive soils; elastic shakedown; plastic shakedown; Finite element modeling